

DECEMBER 2015

Ph.D. in Mechanical Engineering

CEYHUN YILMAZ

**UNIVERSITY OF GAZIANTEP
GRADUATE SCHOOL OF
NATURAL & APPLIED SCIENCES**

**THERMOECONOMIC DESIGN AND OPTIMIZATION OF
GEOHERMAL ENERGY USE IN HYDROGEN
PRODUCTION AND LIQUEFACTION**

**Ph.D. THESIS
IN
MECHANICAL ENGINEERING**

**BY
CEYHUN YILMAZ**

DECEMBER 2015

**Thermoeconomic Design and Optimization of Geothermal
Energy Use in Hydrogen Production and Liquefaction**

Ph.D. Thesis

in

Mechanical Engineering

University of Gaziantep

Supervisor

Prof. Dr. Mehmet KANOĞLU

by

Ceyhun YILMAZ

December 2015

© 2015 [Ceyhun YILMAZ]

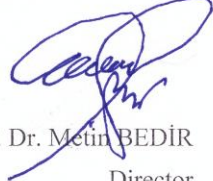
REPUBLIC OF TURKEY
UNIVERSITY OF GAZİANTEP
GRADUATE SCHOOL OF NATURAL & APPLIED SCIENCES
MECHANICAL ENGINEERING DEPARTMENT

Name of the thesis: Thermoeconomic Design and Optimization of Geothermal Energy Use in Hydrogen Production and Liquefaction

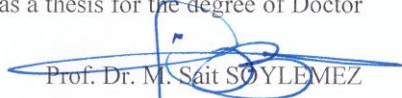
Name of the student: Ceyhun YILMAZ

Exam date: 23.12.2015

Approval of the Graduate School of Natural and Applied Sciences


Prof. Dr. Metin BEDİR
Director

I certify that this thesis satisfies all the requirements as a thesis for the degree of Doctor of Philosophy.


Prof. Dr. M. Sait SOYLEMEZ
Head of Department

This is to certify that we have read this thesis and that in our consensus opinion it is fully adequate, in scope and quality, as a thesis for the degree of Doctor of Philosophy.


Prof. Dr. Mehmet KANOĞLU
Supervisor

Examining Committee Members:

Prof. Dr. Mehmet KANOĞLU

Assoc. Prof. Dr. Önder KAŞKA

Assoc. Prof. Dr. Ayşegül ABUŞOĞLU

Assoc. Prof. Dr. Emrah ÖZAHİ

Asst. Prof. Dr. Ertaç HÜRDOĞAN

Signature


.....

.....

.....

.....

.....

I hereby declare that all information in this document has been obtained and presented in accordance with academic rules and ethical conduct. I also declare that, as required by these rules and conduct, I have fully cited and referenced all material and results that are not original to this work.



Ceyhun YILMAZ

ABSTRACT

THE THERMOECONOMIC DESIGN AND OPTIMIZATION OF GEOTHERMAL ENERGY USE IN HYDROGEN PRODUCTION AND LIQUEFACTION

YILMAZ, Ceyhun

Ph.D. in Mechanical Engineering

Supervisor: Prof. Dr. Mehmet KANOĞLU

December 2015, 125 pages

Six models are developed for the use of geothermal energy in hydrogen production and liquefaction and thermoeconomic analysis and optimization of these models are performed. The aim is to use geothermal energy in hydrogen production by appropriate combination of systems at optimum operating conditions. Optimum operating conditions that minimize the unit hydrogen cost are obtained. A liquid geothermal resource at 200°C with a flow rate of 100 kg/s is considered. Among the models involving hydrogen production, the minimum exergetic cost of hydrogen production is obtained in Model 2 with a value of 1.088 US\$/kg H₂. In Model 2, the power generated from a combined flash-binary geothermal power plant is supplied to an electrolysis unit for hydrogen production, and geothermal water at the exit of the power plant is used to preheat electrolysis water. In the models involving hydrogen liquefaction, the minimum exergetic cost occurs in Model 4 with a value of 1.114 US\$/kg H₂. In this model, geothermal heat is used for absorption cooling of hydrogen gas and geothermal electricity is used to supply power to a liquefaction unit. In Model 6, in which geothermal energy is used for both hydrogen production and liquefaction, the exergetic cost is calculated as 1.993 US\$/kg H₂, which is 9.5% less than the sum of the values in Model 2 and Model 4. Parametric studies indicate that unit cost of hydrogen decreases by an increase in geothermal resource temperature.

Keywords: Hydrogen, geothermal energy, hydrogen production, hydrogen liquefaction, thermoeconomics, exergy, energy, optimization.

ÖZET

JEOTERMAL ENERJİNİN HİDROJEN ÜRETİLMESİ VE SIVILAŞTIRILMASINDA KULLANIMININ TERMOEKONOMİK TASARIMI VE OPTİMİZASYONU

YILMAZ, Ceyhun

Doktora Tezi, Makina Mühendisliği Bölümü

Tez Yöneticisi: Prof. Dr. Mehmet KANOĞLU

Aralık 2015, 125 sayfa

Tezin amacı, hidrojen üretimi ve sıvılaştırmasında jeotermal enerjinin kullanımı için geliştirdiğimiz altı modelin kapsamlı bir şekilde termoeconomik yöntemler yardımıyla incelenmesi ve optimizasyon analizlerinin yapılmasıdır. 200°C sıcaklıkta ve 100 kg/s debide sıvı bir jeotermal kaynak için termoeconomik optimizasyon maliyeti analizine göre hidrojenin üretimi ile ilgili modellerde en düşük hidrojen üretim maliyeti Model 2’de gerçekleşmektedir (1.088 US\$/kg H₂). Bu modelde elektroliz suyunun ön ısıtması ile gerekli olan iş miktarının düşürülmesinin termoeconomik avantajı ortaya çıkmaktadır. Model 6’da sıvılaştırma eklenmesi termodinamik olarak avantaj sağlamakta ama buna karşılık ekserjetik maliyet 1.993 US\$/kg’a çıkmaktadır. Hidrojenin sıvılaştırılması ile ilgili modellerde en düşük ekserjetik maliyet Model 4’te gerçekleşmektedir (1.114 US\$/kg H₂). Jeotermal enerjinin hem üretim hem de sıvılaştırmada kullanıldığı Model 6’da gerçekleşen 1.993 US\$/kg H₂’lik ekserjetik maliyet Model 2’deki (1.088 US\$/kg H₂) ve Model 4’deki (1.114 US\$/kg H₂) maliyetlerin toplamı olan 2.202 US\$/kg H₂ değerinden %9.5 daha düşüktür. Böylece hidrojenin hem üretilip hem sıvılaştırıldığı Model 6’nın hidrojenin sadece üretildiği ve sadece sıvılaştırıldığı en ekonomik modellere göre daha avantajlı olduğu ortaya çıkmaktadır. Tüm modeller için yapılan parametrik çalışmalarda jeotermal kaynak sıcaklığı arttıkça birim maliyetin düştüğü görülmektedir.

Anahtar Kelimeler: Jeotermal enerji, hidrojen üretimi, hidrojen sıvılaştırılması, enerji, ekserji, termoeconomik, optimizasyon.

ACKNOWLEDGEMENT

I would like to thank my supervisor Prof. Dr. Mehmet Kanođlu for giving me the opportunity to study under his supervision and do my dissertation in this field. Without his continuous interest and guidance, the completion of this thesis would not have been possible.

I appreciate educational and academic support of all my teachers starting from elementary school to the university. Without their dedicated teachings, I could not be at this point now.

I would love to thank my family for their endless support.

This study is sponsored by The Scientific and Technological Research Council of Turkey (TUBITAK) under the project 113M207. This support is greatly appreciated.

TABLE OF CONTENTS

ABSTRACT.....	vi
ÖZET	vii
ACKNOWLEDGEMENTS	viii
LIST OF FIGURES	xii
LIST OF TABLES	xv
NOMENCLATURE	xviii
CHAPTER 1: INTRODUCTION	1
1.1 Motivation	1
1.2 Objectives of Thesis	3
1.3 Summary of Approach and Rationale	4
1.4 Outline of Thesis	4
1.5 Literature Review	5
CHAPTER 2: HYDROGEN PRODUCTION AND LIQUEFACTION MODELS	11
2.1 Introduction	11
2.2 Short Description of Models	11
2.3 System description of Model 1	13
2.4 System description of Model 2	15
2.5 System description of Model 3	16
2.6 System description of Model 4	18
2.7 System description of Model 5	19
2.8 System description of Model 6	20
CHAPTER 3: THERMODYNAMIC ANALYSIS	22
3.1 Energy and Exergy Analyses	22
3.2 Fuel-Product Approach for Exergy Analysis	24

3.3 Thermodynamic Analysis of Combined Flash-Binary Geothermal Plant	26
3.4 Thermodynamic Analysis of Electrolysis Unit	28
3.5 Thermodynamic Analysis of Absorption Refrigeration Cycle	32
3.6 Thermodynamic Analysis of Claude Liquefaction Cycle	35
3.7 Thermodynamic Analyses Results of Models	40
3.7.1 Model 1	40
3.7.2 Model 2	41
3.7.3 Model 3	47
3.7.4 Model 4	59
3.7.5 Model 5	59
3.7.6 Model 6	61
CHAPTER 4: THERMOECONOMIC ANALYSIS	63
4.1 Introduction	63
4.2 Economic Analysis.....	64
4.3 Specific Exergy Cost (SPECOC) Method	66
4.3.1 Model 1.....	69
4.3.2 Model 2.....	74
4.3.3 Model 3.....	75
4.3.4 Model 4.....	76
4.3.5 Model 5.....	77
4.3.6 Model 6.....	78
4.4 Thermo-economic Analyses Results of Models	78
CHAPTER 5: THERMOECONOMIC OPTIMIZATION	80
5.1 Introduction	80
5.2 Thermo-economic Optimization of Model 1	85
5.3 Thermo-economic Optimization of Model 2	87

5.4 Thermoeconomic Optimization of Model 3	89
5.5 Thermoeconomic Optimization of Model 4	91
5.6 Thermoeconomic Optimization of Model 5	93
5.7 Thermoeconomic Optimization of Model 6	95
5.8 Thermoeconomic Optimization Results	97
CHAPTER 6: GENERAL RESULTS AND CONCLUSIONS.....	98
6.1 Parametric Studies	97
6.2 Results, Discussion, and Conclusions	108
6.3 Validation.....	110
REFERENCES	114
BIOGRAPHICAL SKETCH.....	123

LIST OF FIGURES

Figure 2.1:	Thermodynamic models for the use of geothermal energy for hydrogen production and liquefaction	13
Figure 2.2:	In Model 1, electricity is produced from a combined flash binary geothermal power plant and used in the electrolysis unit for hydrogen production.....	14
Figure 2.3:	In Model 2, electricity is produced in a combined flash binary geothermal power plant and water is heated by the used geothermal water before the electrolysis unit	16
Figure 2.4:	In Model 3, geothermal heat is used in an absorption refrigeration process to precool hydrogen gas before the gas is liquefied in a liquefaction cycle (Claude cycle)	18
Figure 2.5:	In Model 4, hydrogen is cooled in an absorption cycle, power is produced in a binary geothermal power plant, and hydrogen is liquefied in the Claude cycle	19
Figure 2.6:	In Model 5, electricity is produced in a geothermal power plant and used in the Claude cycle	20
Figure 2.7:	In Model 6, part of geothermal power is used for the electrolysis process and the remaining part for liquefaction	21
Figure 3.1:	Combined flash-binary geothermal power plant	27
Figure 3.2:	Schematic of a water electrolysis process operating at T and P.....	28
Figure 3.3:	Water-ammonia refrigeration cycle used to precool the hydrogen gas in the liquefaction models.....	33
Figure 3.4:	Claude hydrogen gas liquefaction cycle is used in the models.....	36
Figure 3.5:	Temperature-entropy (T - s) diagram of the Claude liquefaction cycle.....	37
Figure 3.6:	Exergy flow diagram of Model 1.....	45

Figure 3.7:	Exergy flow diagram depicting the exergy destructions in the components of absorption refrigeration cycle.....	51
Figure 3.8:	Optimum compression pressure of Claude liquefaction cycle.....	52
Figure 3.9:	Exergy flow diagram depicting the exergy destructions in the Claude liquefaction cycle.....	56
Figure 3.10:	Exergy flow diagram of the overall system based on fuel-product approach.....	57
Figure 3.11:	Various exergy input and output parameters in the integrated system.....	58
Figure 4.1:	Exergy costing configuration of geothermal powered hydrogen production system (Model 1).....	71
Figure 5.1:	Working principle of the Genetic algorithm optimization technique.....	81
Figure 5.2:	Schematic of the contributions of fuel cost and capital cost to the total product cost, as a function of the exergetic efficiency and the sum of exergy destruction and exergy loss.....	84
Figure 6.1:	Variation of the energy and exergy efficiencies with the geothermal water temperature in Model 1.....	98
Figure 6.2:	Variation of the energy and exergy efficiencies with the geothermal water temperature in Model 2.....	99
Figure 6.3:	Variation of the precooling temperature of hydrogen with the geothermal water temperature.....	100
Figure 6.4:	Variations of liquefaction mass fraction and liquefaction work as a function of cooled hydrogen gas temperature.....	101
Figure 6.5:	Variations of the overall exergy efficiency and overall COP as a function of the geothermal water temperature in Model 3.....	102
Figure 6.6:	Variation of utilization energy efficiency and exergy efficiencies of the overall system with geothermal water temperature in Model 4.....	102
Figure 6.7:	Variation of the energy and exergy efficiencies with the geothermal water temperature in Model 5.....	103
Figure 6.8:	Variation of the energy and exergy efficiencies with the geothermal water temperature in Model 6.....	104

Figure 6.9:	Variation of the unit exergetic cost of hydrogen and electricity with respect to geothermal water temperature in Model 1.....	105
Figure 6.10:	Variation of unit exergetic cost of hydrogen and electricity with respect to geothermal water temperature in Model 2.....	105
Figure 6.11:	Variation of unit exergetic cost of hydrogen liquefaction with respect to geothermal water temperature in Model 3.....	106
Figure 6.12:	Variation of unit exergetic cost of hydrogen liquefaction with respect to geothermal water temperature in Model 4.....	106
Figure 6.13:	Variation of unit exergetic cost of electricity and hydrogen liquefaction with respect to geothermal water temperature in Model 5.....	107
Figure 6.14:	Variation of unit exergetic cost of hydrogen production and electricity with respect to geothermal water temperature in Model 6.....	107
Figure 6.15:	Variation of unit exergetic cost of hydrogen with geothermal water temperature in all models.....	109

LIST OF TABLES

Table 3.1:	Enthalpy, entropy and Gibbs free energy of formation and standard chemical exergy for electrolysis.....	31
Table 3.2:	Thermodynamic analysis results of Model 1.....	41
Table 3.3:	Mass, energy, and exergy relations for the components of Model 2.....	42
Table 3.4:	System data, thermodynamic properties, and exergies with respect to state points in Fig. 2.3.....	44
Table 3.5:	Thermodynamic analysis results for Model 2.....	46
Table 3.6:	Exergy analysis results for Model 2.....	47
Table 3.7:	Mass, energy, and exergy relations for the components of the ammonia-water absorption refrigeration cycle.....	48
Table 3.8:	System data, thermodynamic properties, mass flow rates, and exergy data in the system with respect to the state points of the ammonia-water absorption refrigeration cycle in Fig. 2.4.....	50
Table 3.9:	Mass, energy and exergy relations for the components of the Claude liquefaction cycle.....	53
Table 3.10:	System data, thermodynamic properties, mass flow rates, and exergy data in the system with respect to the state points of the Claude liquefaction cycle.....	54
Table 3.11:	Thermodynamic analysis results of Model 3.....	58
Table 3.12:	Thermodynamic analysis results of Model 3.....	59
Table 3.13:	Thermodynamic analysis results of Model 5.....	60
Table 3.14:	Thermodynamic analysis results of Model 6.....	61
Table 4.1:	Aspen Plus assumptions for the economic analysis of system.....	64
Table 4.2:	Purchased equipment cost and cost rates of each system component.....	70

Table 4.3:	Cost balance equations and auxiliary equations for the exergy costing of system.....	71
Table 4.4:	Exergetic and exergoeconomic analyses results of the system states Model 1.....	72
Table 4.5:	Thermoeconomic analysis results of Model 1.....	74
Table 4.6:	Thermoeconomic analysis results of Model 2.....	75
Table 4.7:	Thermoeconomic analysis results of Model 3.....	76
Table 4.8:	Thermoeconomic analysis results of Model 4.....	76
Table 4.9:	Thermoeconomic analysis results of Model 5.....	77
Table 4.10:	Thermoeconomic analysis results of Model 6.....	78
Table 5.1:	Genetic algorithm optimization parameters.....	82
Table 5.2:	The base case and optimal case conditions of Model 1.....	85
Table 5.3:	Thermoeconomic optimization results of the exergetic and exergoeconomic analysis results for Model 1.....	86
Table 5.4:	Comparative results of the optimum case and the base case data of Model 1.....	87
Table 5.5:	The base case and optimal case conditions of Model 2.....	88
Table 5.6:	Comparative results of the optimum case and the base case of Model 2.....	89
Table 5.7:	The base case and optimal working conditions obtained by the genetic algorithm optimization of the system [69].....	90
Table 5.8:	Comparative results of the optimum case and the base case for Model 3.....	91
Table 5.9:	The base case assumptions and optimal working conditions.....	92
Table 5.10:	Comparative results of the optimum case and the base case of Model 4.....	93
Table 5.11:	The base case values and optimal working conditions based on optimization of Model 5.....	94
Table 5.12:	Comparative results of the optimum case and the base case of Model 5.....	94
Table 5.13:	The base case assumptions and optimal working conditions obtained by the optimization of Model 6.....	95

Table 5.14:	Comparative results of the optimum case and the base case of Model 6.....	96
Table 5.15:	Summary of thermoeconomic optimization results of the models.....	97
Table 6.1:	Total investment costs and exergetic costs.....	110

NOMENCLATURE

A	annuity (\$)
c	specific cost of exergy (\$/kJ)
C	equipment purchased equipment cost (\$)
\dot{C}	cost rate associated with exergy (\$/h)
\dot{C}_D	cost rate of exergy destruction (\$/h)
CRF	capital recovery factor
ex	specific exergy (kJ/kg)
$\dot{E}x$	exergy rate (kW)
h	specific enthalpy (kJ/kg)
\dot{m}	mass flow rate (kg/s)
P	pressure (kPa)
\dot{Q}	heat flow rate (kW)
s	specific entropy (kJ/kg K)
T	temperature (°C)
T_{vap}	vaporization temperature (°C)
T_{pp}	pinch-point temperature (°C)
\dot{W}	Power (kW)
ΔT_{pp}	pinch-point temperature difference (°C)
ΔH	total energy demand for electrolysis (kJ/kmol)
ΔG	Gibbs free energy (kJ/kmol)
ΔS	thermal energy demand (kJ/kmol K)
$V_{\text{T,P}}$	enthalpy voltage (Volt)
$E_{\text{T,P}}$	electrolysis voltage (Volt)
F	Faraday constant (C/mol)

C_p	heat capacity (kJ/kmol K)
J	current density (A/m ²)
M	molecular weight (kg/kmol)
LHV	lower heating value (kJ/kg)
US\$	United State Dollar (\$)
$y_{\text{dest},k}$	component exergy destruction over total exergy input
$y_{\text{dest},k}^*$	component exergy destruction over total exergy destruction
\dot{Z}^T	cost rate associated with the sum of capital investment and OMC (\$/h)
\dot{Z}^{CI}	cost rate associated with capital investment (\$/h)
\dot{Z}^{OMC}	cost rate associated with OMC (\$/h)

Greek Symbols

η	energy efficiency
ε	exergetic efficiency
τ	capacity factor of plant operation

Subscripts

0	dead states
CC	carrying charges (\$/yr)
D	destruction
e	exit state
ex	exergy
F	fuel
f	saturated liquid
g	gas
geo	geothermal fluid

i *i-th* stream
i inlet state
k *k-th* component
l liquid
L levelized cost (\$/yr)
n number of electron
OMC operating and maintenance cost
P product
pp pinch-point
th thermal
tot overall system

Superscripts

· time rate
CC carrying charge
CI investment cost
OMC operating and maintenance cost

CHAPTER 1

INTRODUCTION

1.1 Motivation

Renewable energies are increasing in their use throughout the world. This is motivated by the fact that fossil fuels are depleting and their combustion cause pollution and greenhouse emissions. The increase in utilization of renewable energy requires technical and infrastructural changes [1, 2].

Hydrogen is an alternative energy carrier and subject of a lot of research work [3]. The total cost of producing hydrogen depends on production, liquefaction, storage and distribution costs. Today approximately 9 billion kilograms of hydrogen are produced annually. More than 95% of the merchant hydrogen is used for industrial applications in the chemical, metals, electronics, and space industries [4]. Sustainable energy economy requires sustainable production of energy from renewable energy sources. Hydrogen is also a clean energy carrier for renewable energies. It stores and delivers energy in a usable form, but it must be produced from compounds that contain it [5]. Hydrogen can be produced using diverse, domestic resources including fossil fuels, such as coal and natural gas, nuclear and biomass and other renewable energy technologies, such as wind, solar, geothermal and hydroelectric power [6].

If hydrogen is to become the energy of the future, it must be produced using renewable energy sources and the technical and economic problems on its production, storage, transportation, and use should be solved. There are various methods used in hydrogen production. These methods may require both electricity and heat inputs, and renewable energy such as solar, wind, hydro and geothermal energy use are being investigated [7]. Hydrogen production via electrolysis is being pursued for renewable (wind, solar and geothermal) options. These pathways result in virtually zero greenhouse gas and pollutant emissions [8]. Geothermal based hydrogen production is a potential pathway for a future hydrogen economy.

Hydrogen can be produced by using electrolysis techniques. Electrolysis splits water electrochemically into hydrogen and oxygen molecules with the aid of electrical energy. There are three kinds of electrolysis techniques; alkaline, solid oxide and PEM (Proton Exchange Membrane) electrolysis [9]. Many establishments have been involved in the development of high efficiency, high security electrolyzers such as alkaline and PEM electrolyzers. In our models, we select an alkaline electrolysis unit mainly because it can operate over a temperature range and it is commonly selected in studies on commercial applications and renewable based hydrogen production.

Among renewable sources, geothermal energy has significant potential in hydrogen production. Electricity output from a geothermal power plant and direct geothermal heat or that resulting from power plants can be used in hydrogen production by means of water electrolysis process. The use of geothermal energy for hydrogen production with the electrolysis operation may prove to be an effective option in the future hydrogen structure. Power production from geothermal energy is well established and various thermodynamic systems such as single flash, double flash, binary, and combined flash/binary designs are commonly used. In this study, a flash-binary design geothermal power plant is selected since it is more efficient and a more commonly used design for liquid dominated and relatively high temperature geothermal resources. Both flash-binary geothermal power plant and alkaline electrolysis unit are common technologies and incorporating them with a heat exchange system can provide a viable option for geothermal powered hydrogen production technology. Hydrogen has a high energy content by mass (approximately three times that of gasoline) but low energy content by volume in gas state. Storage of hydrogen is a challenging task. Hydrogen can be stored as a compressed gas at high pressures; as a liquid which requires a cryogenic temperature of -253°C ; or combined with other compounds in a solid form like being absorbed in a metal hydride. Storage in gas state requires very large tanks; liquefaction requires large work input and super insulated storage tanks; and a metal hydride can only absorb a small amount of hydrogen [10]. The Claude liquefaction cycle is selected in this thesis for liquefaction of hydrogen. It is an efficient process for hydrogen liquefaction as it uses a turbine for producing work, thereby reducing work input in the cycle.

The expansion through an expansion valve is a highly irreversible process. In the Claude cycle, energy is removed from the gas stream by allowing it to do some work in a turbine. Compared to an isenthalpic expansion process in a throttling valve, a lower temperature is attained in a turbine exit [11]. Hydrogen liquefaction cycles have low efficiencies, between 20 to 30%, when the minimum work to actual work ratio is considered [12]. The liquefaction process requires energy input in the form of electricity. By getting this electricity from geothermal energy and using geothermal heat by means of an absorption cooling system, work consumption can be reduced and the process can be made more sustainable [13].

1.2 Objectives of Thesis

The aim of this thesis is thermoeconomic analyses and optimization of some models which have been developed for the use of geothermal energy in hydrogen production and liquefaction. As a result of this study, it is possible to use geothermal energy in hydrogen production by the best system and system combinations and at optimum operating conditions. Parametric studies will be performed at varying geothermal source temperatures while optimum operating conditions that minimize the unit hydrogen production and liquefaction cost are obtained in optimization studies. The models are considered to be simulated in EES and Aspen Plus programs and the analyses are performed to be using these programs.

Thermoeconomy is also called exergoeconomy. The methodology of thermoeconomics, as embodied in the specific exergy cost (SPECOC) methods, is used here to determine changes in the design parameters of the cycle that improve the cost effectiveness of the overall system. Thermoeconomy is becoming more important among other thermodynamic tools and in this method, the economic analysis and optimization are based on the second law. The first step of the thermoeconomic analysis is a comprehensive exergy analysis of the system based on the second law. This way, the costs of exergy destructions in all subsystems and components can be examined and the system can be designed and optimized in order to minimize losses.

In optimization, the genetic algorithm optimization technique is utilized to be which requires a minimum of available results and provides effective assistance in optimizing engineering systems, particularly in dealing with complex systems.

1.3 Summary of Approach and Rationale

In this thesis, various models of the hydrogen production and liquefaction are considered. Energy and exergy analyses are applied to calculate exergy related parameters particularly exergy destructions. Performance assessment parameters related to energy and exergy analyses are calculated. The system level design is then continued with engineering economic and thermoeconomic analyses to determine the cost of products. According to the results, some conclusions are drawn for the most feasible configuration based on exergetic costs.

There are three levels of modeling; which are thermodynamic component modeling, thermoeconomic modeling and thermoeconomic optimization modeling. This thesis mainly consists of two stages of approximations. In the first stage, a detailed modeling of hydrogen production and liquefaction systems is presented. Second, thermal design model of the overall systems is developed using energy, exergy, thermoeconomic and optimization analyses. Thermodynamic data are obtained from thermophysical property database of EES and Aspen Plus software. The analyses are performed using these softwares.

1.4 Outline of Thesis

This thesis is presented in six chapters as described below:

The second chapter provides descriptions of hydrogen production and liquefaction models. Basic definitions and working principles for thermodynamics of systems are outlined.

In the third chapter, thermodynamic analyses of hydrogen production and liquefaction models are performed. We provide thermodynamic analysis of the systems for the production and liquefaction of hydrogen driven by geothermal energy.

The fourth chapter demonstrates thermoeconomic analysis of the models. The results of the economic and thermoeconomic analyses of the models for hydrogen production and liquefaction, including estimates of exergetic cost of product are presented. Economic and thermoeconomic modeling of system simulation are accomplished using Aspen Plus. Exergy costing method is applied to combine the exergy and cost values and the calculation of useful exergoeconomic parameters.

The fifth chapter gives thermoeconomic optimization of the models. Thermoeconomic optimization procedure is applied by genetic algorithm method of EES software. The use of this optimization approach requires a comprehensive exergetic and exergoeconomic analyses of the systems. Thermoeconomic optimization procedure of the system is described and the procedure is used for obtaining cost-optimal exergetic efficiencies and related performance parameters. The objective functions of the hydrogen production and liquefaction system components are expressed for the optimization criterion as a function of dependent and independent variables. In addition, optimum performances are compared under the base assumptions of a typical system of hydrogen production and liquefaction models.

The sixth chapter includes the general results and discussion of the study. The validation of the simulation models and several parametric studies are also included in this section. Several parametric studies are presented especially at various geothermal temperatures. The cost performance of the models based on base and optimum conditions are examined. Third, the results of the thermodynamic and thermoeconomic optimization analyses of the models for hydrogen production and liquefaction are presented, including estimates of exergetic product cost. Fourth, general results of the models are evaluated and compared with each other. The conclusions derived from this thesis are presented and discussed, along with validations and some recommendations.

1.5 Literature Review

There are various methods used in hydrogen production. These methods may require both electricity and heat inputs, and renewable energy such as solar, wind, hydro and geothermal energy use are being investigated [14]. Hydrogen production via electrolysis is being pursued for renewable (wind, solar and geothermal) options [15].

Hydrogen provides the connecting point between renewable electricity production and transportation, stationary and portable energy needs. When the electricity from solar photovoltaic, wind, geothermal, ocean and hydro technologies are used to produce and store hydrogen, the renewable source becomes more valuable and can meet a variety of needs [16].

Although, there are a large number of studies in using solar, wind and nuclear energies for hydrogen production, limited number of studies exists on using geothermal energy. Next, we provide an overview of some of the more relevant studies in literature.

Kanoglu et al. [17] investigated energy, exergy, and exergoeconomic analysis of a geothermal assisted high temperature electrolysis process. Energy and exergy performance parameters such as heat transfer, power, exergy destruction, and exergy efficiencies were determined. Heat exchanger network and high temperature electrolysis unit are primarily responsible for exergy destructions in the system. Ahmadi et al. [18] developed a model for energy and exergy analyses of hydrogen production via an OTEC (ocean thermal energy conversion) system coupled with a solar-enhanced PEM (proton exchange membrane) electrolyzer. The energy and exergy efficiencies of the integrated OTEC system were determined to be 3.6% and 22.7%, respectively, and the exergy efficiency of the PEM electrolyzer was 56.5%. Esmaili et al. [19] analyzed low temperature electrolysis of a hydrogen production system using molybdenum oxo catalysts in the cathode and a platinum bared anode. A thermodynamic model was developed for the electrolysis process in order to predict and analyze the energy and exergy efficiencies. The new electrolysis system with molybdenum oxo catalysts consists of two half cells of PEM (proton exchange membrane) and alkaline electrolysis. The results were presented and compared with previous studies to demonstrate the promising performance of the system.

Kanoglu et al. [20] investigated three cases for the use of geothermal energy for hydrogen liquefaction. A binary geothermal power plant was considered for power production while the precooled Linde Hampson cycle was selected for hydrogen liquefaction. Kanoglu et al. [21] developed four models for the use of geothermal energy for hydrogen production. These models were studied thermodynamically, and both reversible and irreversible operations of the models were considered. Yilmaz [22] and Yilmaz et al. [23] considered seven models for hydrogen production and liquefaction by geothermal energy, and their thermodynamic and economic analyses were performed. The amount of hydrogen production and liquefaction per unit mass of geothermal water and the cost of producing and liquefying a unit mass of hydrogen were calculated for each model. The effect of geothermal water temperature on the cost of hydrogen production and liquefaction were also investigated. Yilmaz and Kanoglu [24] investigated thermodynamic energy and exergy analysis of a PEM water electrolyzer driven by geothermal power for hydrogen production. The first and second-law based performance parameters were identified for the considered system and the system performance was evaluated. The effects of geothermal water and electrolysis temperatures on the amount of hydrogen production were studied.

Balta et al. [25] and Balta et al. [26] investigated various geothermal based hydrogen production methods using energy and exergy methods. Ratlamwala and Dincer [27] focused on a comparative assessment of multi-flash geothermal power generating systems integrated with electrolyses through three definitions of energy and exergy efficiencies. According to Hand [28], when the electricity from geothermal technologies is used to produce hydrogen; the renewable source becomes more valuable and can meet a variety of needs.

Valdimar et al. [29] presented a feasibility study exploring the use of geothermal energy for hydrogen production. They investigated a HOT ELLY high temperature steam electrolysis process operating between 800 and 1000°C. Using the HOT ELLY process with geothermal steam at 200°C can reduce the hydrogen production cost by approximately 19%.

Árnason and Sigfússon [30] described a path towards a future hydrogen energy economy in Iceland. Sigurvinsson et al. [31] investigated the use of geothermal heat in high-temperature electrolysis (HTE) process. This HTE process includes heat exchangers and an electrolyser based on solid oxide fuel cell (SOFC) technology working in inverse, producing oxygen and hydrogen instead of consuming them. Using features related to the heat exchangers and the electrolyzers, a set of physical parameters was calculated using a techno-economic optimization methodology.

Conventional thermodynamic and economic evaluations of geothermal powered hydrogen production were previously investigated. This thesis extends this coverage by studying the thermoeconomic analysis and optimization of hydrogen production and liquefaction for various models. This is a unique contribution to the science of renewable based hydrogen production as it helps an enhanced thermoeconomic understanding of the process.

In 1895, Carl von Linde and William Hampson developed a cycle for the liquefaction of air. However, in 1966 Andrew Barron found that the Linde and Hampson cycle could also be used to liquefy hydrogen by incorporating a precooling process using liquid nitrogen. Similarly, the Claude cycle, invented in 1902 by Georges Claude, was developed to liquefy air but it can also be used to liquefy hydrogen. Using liquid nitrogen for precooling improves the cycle efficiency compared to a pre-cooled Linde-Hampson cycle [32, 33]. The liquefaction process requires energy input in the form of electricity. Generating this electricity from geothermal energy and using geothermal heat by means of an absorption cooling system can reduce work consumption and make the process more sustainable. An absorption system differs from a vapor-compression refrigeration unit in that the compressor of the vapor compression system is replaced by a rather complex system. In this process, the pressure of the working fluid is increased by a pump, which requires significantly less work input compared to a compressor. The main energy input comes from a heat source [34].

In our study, the heat input for the absorption system comes from hot geothermal water. Absorption systems have some disadvantages such as high capital cost and low coefficient of performance (COP) values. However, an inexpensive geothermal heat source can cancel out some of the disadvantages [35]. Kairouani et al. [36] developed and studied the possibility of using geothermal energy for an absorption system cascaded with conventional vapor compression system. Three working fluids (R717, R22, and R134a) are selected for the conventional vapor-compression system and the ammonia-water pair for the absorption system. The COP of this combined system is significantly higher than (37 to 54%) that of a single stage refrigeration system. Adewusi and Zubair [37] performed an experimental study on a water-lithium bromide absorption refrigeration system powered by geothermal energy in a hot spring. The results showed that a mass flow rate of 12.5 kg/s from the geothermal source at 60°C was sufficient for a cooling effect of 226 kW. When the mass concentrations of the strong and weak solutions in the generator and absorber were 44 and 48%, respectively, the maximum COP was obtained. Best et al. [38] showed experimentally that an ammonia water absorption cooler can be successfully operated using low enthalpy geothermal heat. A cooling capacity of 10.3 kW and a COP of 0.433 were obtained with a generator temperature of 91.5°C and an evaporator temperature of -13°C.

Nandi et al. [39] compared performances of precooled Linde-Hampson cycle, Claude cycle, and helium-hydrogen condensing cycle used in hydrogen liquefaction. These cycles were optimized for certain operating parameters. Wayne [40] performed a numerical analysis of a supercritical hydrogen liquefaction cycle, which used electricity from a grid. He studied the effects of component efficiencies on overall cycle efficiency. Krasae-in et al. [41] presented a comprehensive review for large-scale hydrogen liquefaction systems developed in the last century. Nandi et al. [42] compared efficiencies of precooled Linde-Hampson cycle and precooled Claude cycle, and showed that precooled Claude cycle is more efficient. Syed et al. [43] reported the results for the second law analysis of a hydrogen liquefier operating on the modified Collins cycle. They studied some modifications to the cycle and potential sites for improvements. Syed et al. [44] provided a cost evaluation of three common hydrogen liquefaction cycles, and found that energy costs have a dominant effect on the total liquefaction cost.

Previous studies on hydrogen liquefaction have primarily concentrated on performance assessment. There has also been some limited work on using geothermal heat to power hydrogen liquefaction. These studies were primarily on the thermoeconomic based performance assessment of certain liquefaction models. In this thesis, models consisting of an ammonia-water absorption refrigeration cycle for precooling of hydrogen gas and the Claude cycle for the liquefaction of hydrogen are analyzed primarily by the second law of thermodynamics. The equipment used in the absorption system and the Claude cycle are analyzed and their individual performances are assessed along with the assessment of the overall system. The defining liquefaction models are analyzed thermoeconomically and exergetic cost destructions and the unit exergetic cost of the liquefied hydrogen is determined.

CHAPTER 2

HYDROGEN PRODUCTION AND LIQUEFACTION MODELS

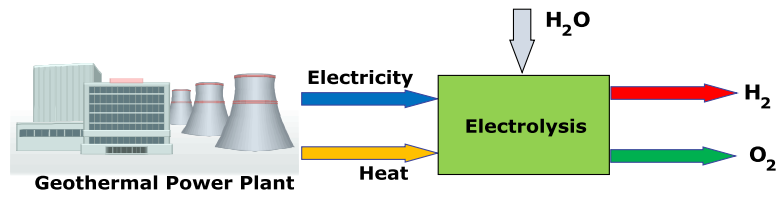
2.1 Introduction

In this thesis, the use of geothermal energy for hydrogen production and liquefaction is proposed, and six possible models are investigated for accomplishing such a task. The models are studied using thermoeconomic design, analysis, and optimization. These models are described next.

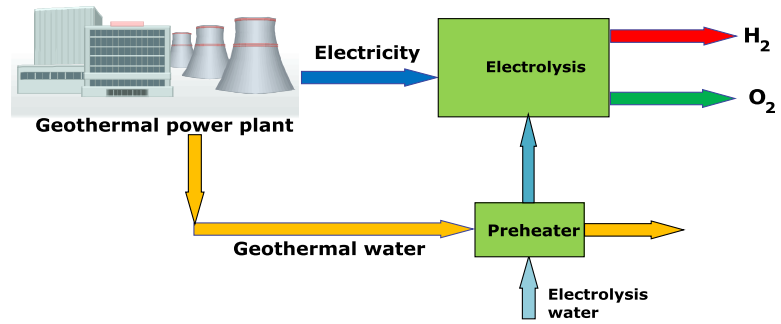
2.2 Short Description of Models

Figure 2.1 shows six models for the use of geothermal energy for hydrogen production and liquefaction.

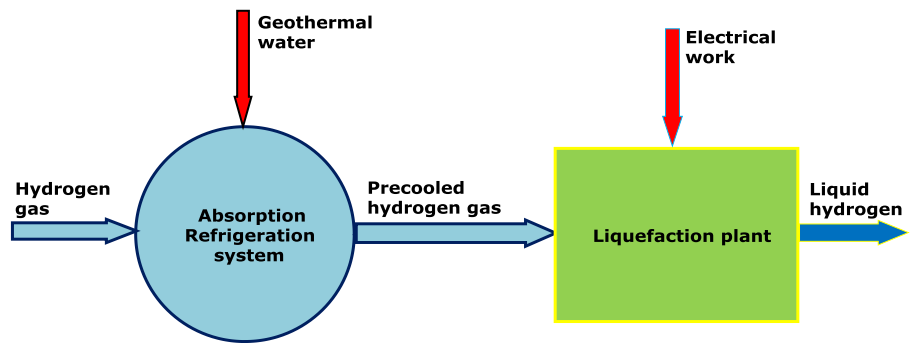
Model 1: Uses geothermal work output as the work input for an electrolysis process (Fig. 2.1a). Model 2: Uses part of geothermal heat to produce work for electrolysis process and part of geothermal heat in an electrolysis process to preheat the water (Fig. 2.1b). Model 3: Uses geothermal heat in an absorption refrigeration process to precool the gas before the gas is liquefied in a liquefaction cycle (Fig. 2.1c). Model 4: Uses part of the geothermal water heat for absorption refrigeration to precool the hydrogen gas and part of the geothermal water heat to produce work with a binary geothermal cycle (for low temperature geothermal water) and use it in a liquefaction cycle (Fig. 2.1d). Model 5: Uses geothermal work output as the electricity input for a liquefaction cycle (Fig. 2.1e). Model 6: Uses part of geothermal work for electrolysis and the remaining part for liquefaction (Fig. 2.1f).



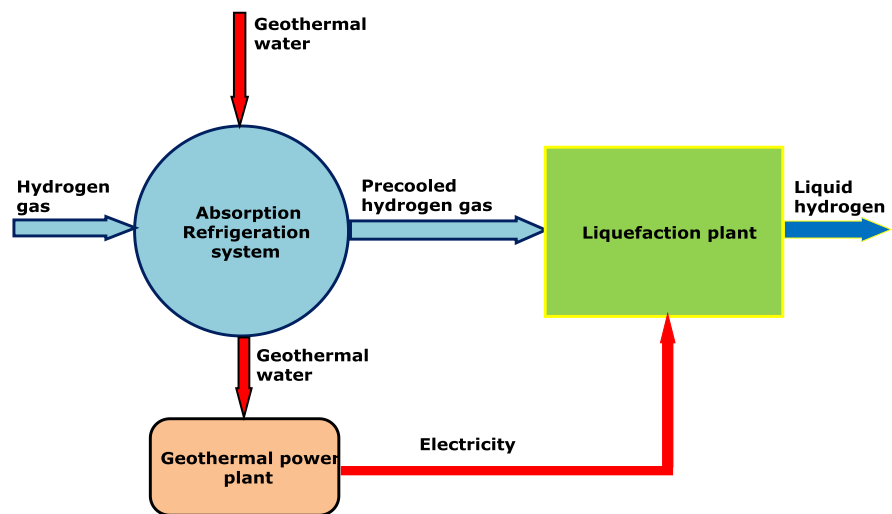
(a) Model 1

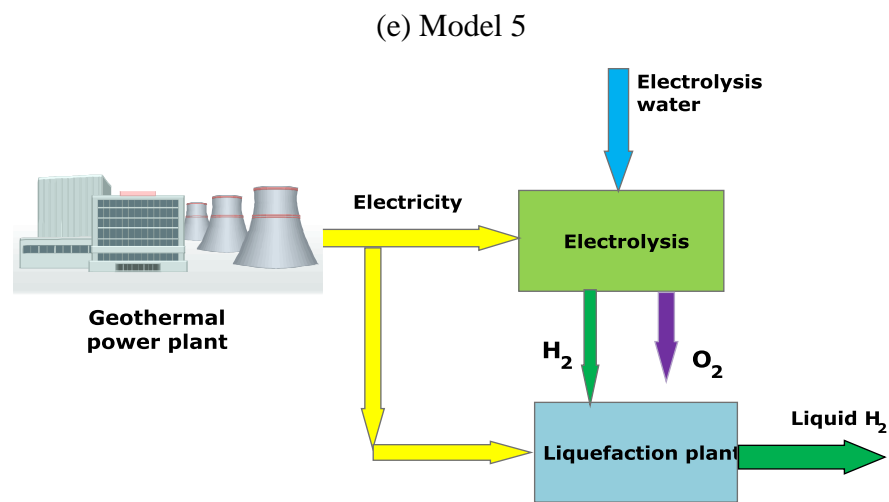
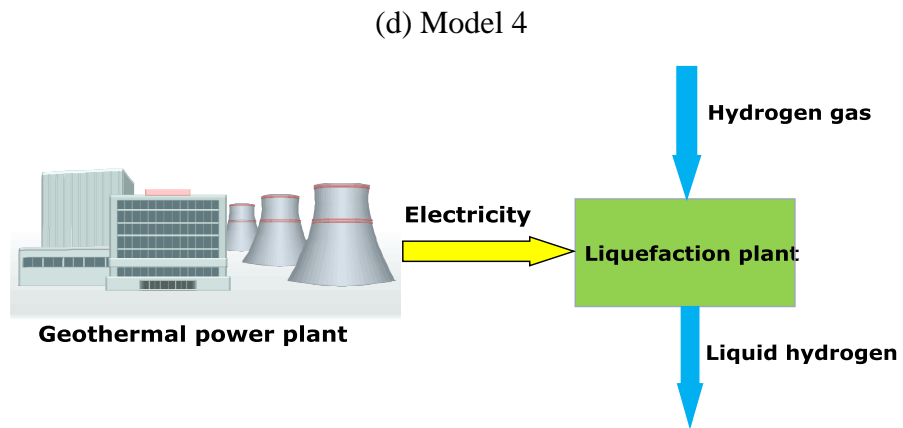


(b) Model 2



(c) Model 3





(f) Model 6: Figure 2.1. Thermodynamic models for the use of geothermal energy for hydrogen production and liquefaction.

For the analysis of hydrogen production and liquefaction models powered by geothermal energy, an environment temperature is taken as of 25°C and an atmospheric pressure as 100 kPa. Thermophysical properties of the working fluids (geothermal water, ammonia-water, air, and hydrogen) are obtained from EES software with built-in thermodynamic property functions. In the evaluation of all models, a liquid geothermal source is considered at a temperature of 200°C with a mass flow rate of 100 kg/s.

2.3 System description of Model 1

The detail of this model is given in Fig. 2.2. In this model, a combined flash-binary geothermal power plant is considered. Combined flash-binary geothermal power plants incorporate both a binary unit and a flashing unit to exploit the advantages associated

with both systems. The liquid portion of geothermal fluid serves as the heat input for the binary cycle and the steam portion of geothermal fluid drives a steam turbine to produce power. Geothermal liquid water coming out of the well is flashed to a lower pressure and resulting vapor is separated from the liquid. The vapor is expanded in a steam turbine, condensed, and reinjected. The liquid geothermal water from the separator is used as the heat source in the binary cycle. The working binary fluid is selected as isobutane. The working fluid is completely vaporized by the heat of geothermal water in the heat exchanger.

The vapor expands in the turbine, and then condenses in an air-cooled condenser before being pumped back to the heat exchanger to complete the cycle. The geothermal water leaving the heat exchanger is reinjected back to the ground. The power generated in the plant is used in a water electrolyses unit to produce hydrogen gas.

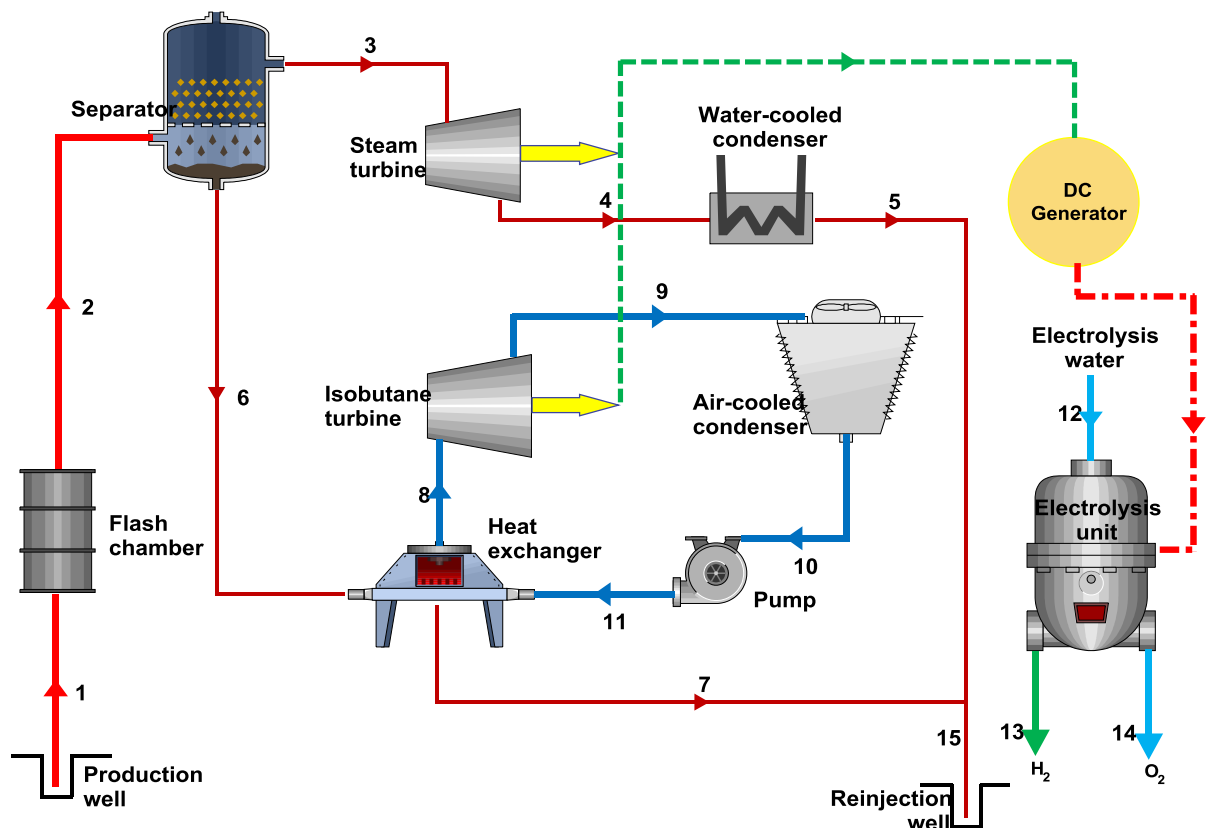


Figure 2.2. In Model 1, electricity is produced from a combined flash-binary geothermal power plant and used in the electrolysis unit for hydrogen production.

2.4 System description of Model 2

The detail of Model 2 is given in Fig. 2.3. The system is similar to Model 1 except that the electrolysis water is heated by geothermal water before the electrolyses process. A higher water temperature for the electrolysis process results in a reduction in electricity consumption in the electrolysis unit.

The system consists of an alkaline electrolysis unit, a water preheater for the electrolysis water, two steam turbines, a heat exchanger for energy transfer from the geothermal fluid to the binary cycle, a flash chamber to reduce geothermal fluid pressure, a separator for extracted water and steam from geothermal fluid, a water cooler condenser for the flash part of cycle, and an air cooler condenser for the binary cycle. In the geothermal plant, liquid is flashed to a lower pressure producing a mixture of steam and liquid. Steam is directed to the turbine while liquid is used as the heat input for the binary cycle.

Binary fluid isobutane is vaporized by geothermal water and runs through the turbine to produce power. Geothermal water leaving the heat exchanger of the binary cycle is used to heat fresh water of electrolysis in a preheater to reduce work requirement. Power outputs from the steam and isobutene turbines are used for the electrolysis process. The used geothermal water is reinjected back to the ground.

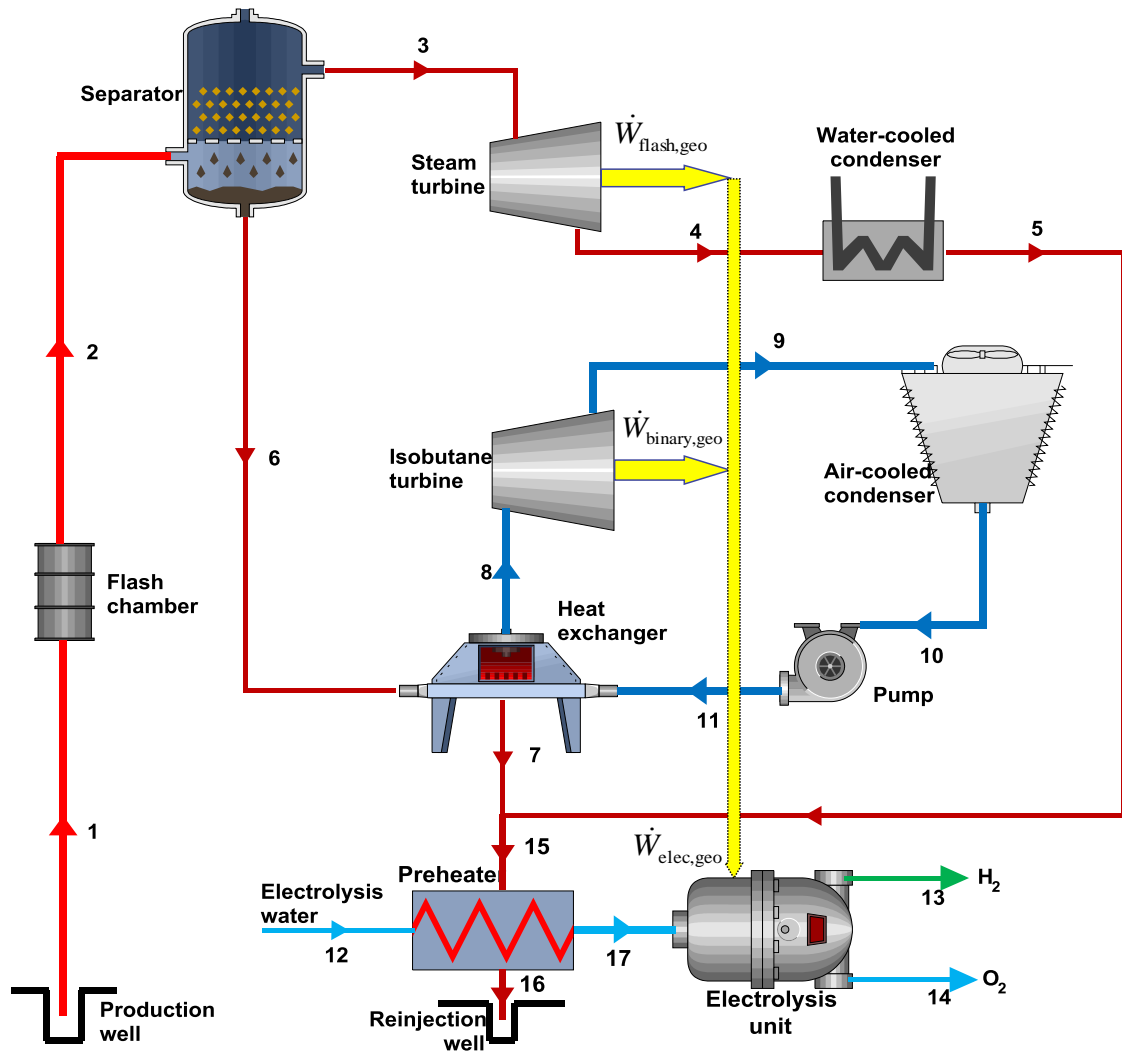


Figure 2.3. In Model 2, electricity is produced in a combined flash-binary geothermal power plant and water is heated by the used geothermal water before the electrolysis unit.

2.5 System description of Model 3

The detailed schematic of Model 3 is given in Fig. 2.4. Geothermal hot water provides the thermal energy requirement for the absorption refrigeration system. In order to reduce work input in the hydrogen liquefaction process, hydrogen gas is cooled in an ammonia-water absorption system before being liquefied in the Claude cycle.

Pure ammonia vapor leaving the evaporator is absorbed by water in the absorber. The solution in the absorber should be continuously cooled by a water stream to facilitate the absorption of ammonia. The ammonia-rich liquid solution is first heated in the regenerator by the returning stream with low ammonia fraction, and then pumped to the generator. In the generator, ammonia evaporates as a result of heat transfer from the hot geothermal water. Any remaining liquid in the ammonia is returned to the rectifier. The water-ammonia solution that is poor in ammonia is returned to the absorber by passing through the regenerator and expansion valve. Pure ammonia flows through the condenser where heat is removed from the cycle. The pressure of liquid ammonia is reduced to match the evaporator pressure in the expansion valve. As the liquid-vapor mixture of ammonia flows in the evaporator, it absorbs heat from cold hydrogen gas, and it leaves the evaporator as a vapor. The cooled hydrogen gas leaves the evaporator and enters the compressor of the Claude cycle.

The Claude hydrogen liquefaction cycle is shown on the right side of Fig. 2.4. The Claude cycle is an efficient process for hydrogen liquefaction as it uses a turbine for producing work, thereby reducing work input in the cycle. The expansion through an expansion valve is a highly irreversible process. In the Claude cycle, energy is removed from the gas stream by allowing it to do some work in a turbine. Compared to an isenthalpic expansion process in a throttling valve, a lower temperature is attained in the turbine exit.

In the Claude liquefaction cycle, the hydrogen gas is first compressed to a high pressure at state 13, and then passed through the first heat exchanger. It is further cooled by liquid nitrogen. Some of the gas is then diverted to a turbine; it is expanded in the turbine; and reunited with the return stream at state 18. The stream to be liquefied continues the second and third heat exchangers, and is finally expanded through an expansion valve to the liquid receiver.

The liquid hydrogen is collected as the product of the cycle. Cold hydrogen gas flows through the third heat exchanger to cool the high pressure gas. It then passes through the second and first heat exchangers. Finally, it mixes with precooled hydrogen gas from the absorption cycle and enters the compressor.

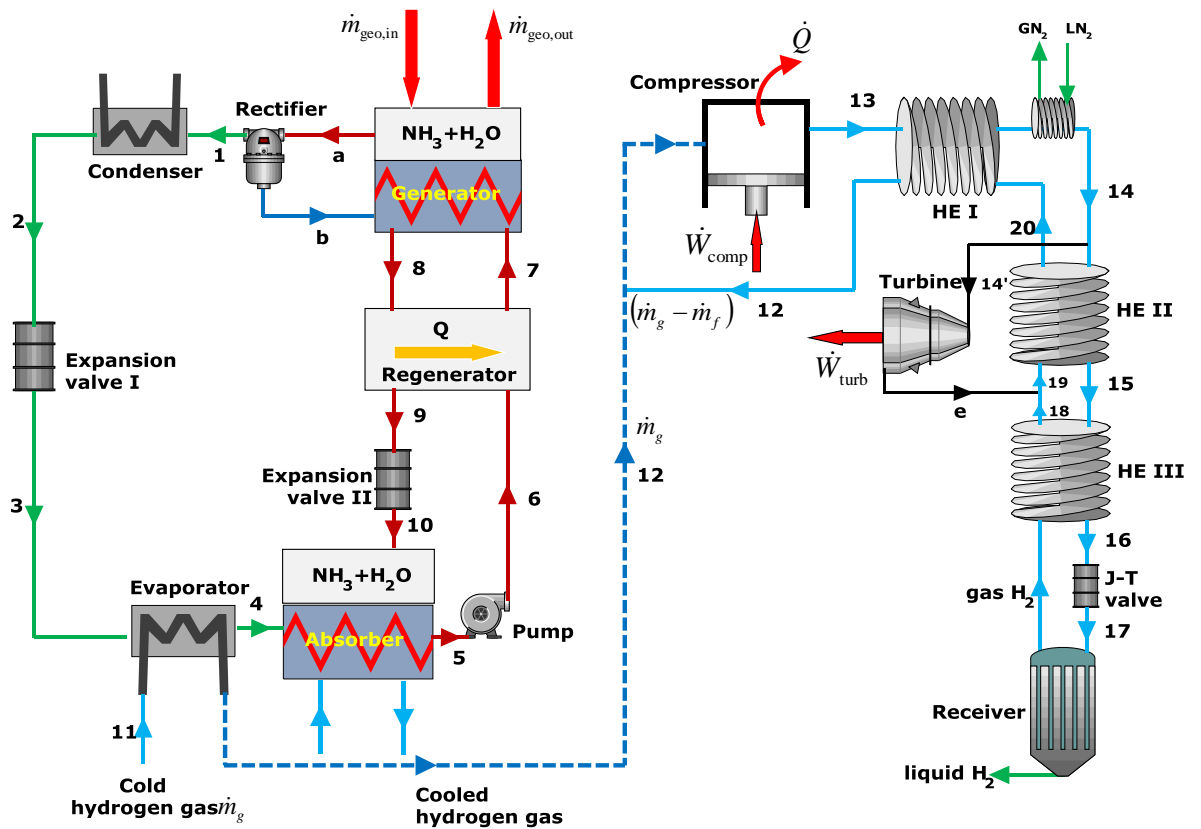


Figure 2.4. In Model 3, geothermal heat is used in an absorption refrigeration process to precool hydrogen gas before the gas is liquefied in a liquefaction cycle (Claude cycle).

2.6 System description of Model 4

The schematic of Model 4 is given in Fig. 2.5. This model is similar to Model 3 except that geothermal water leaving the absorption system is used to produce power in a binary geothermal power plant. The power output of the plant is used to provide compression work in the Claude cycle.

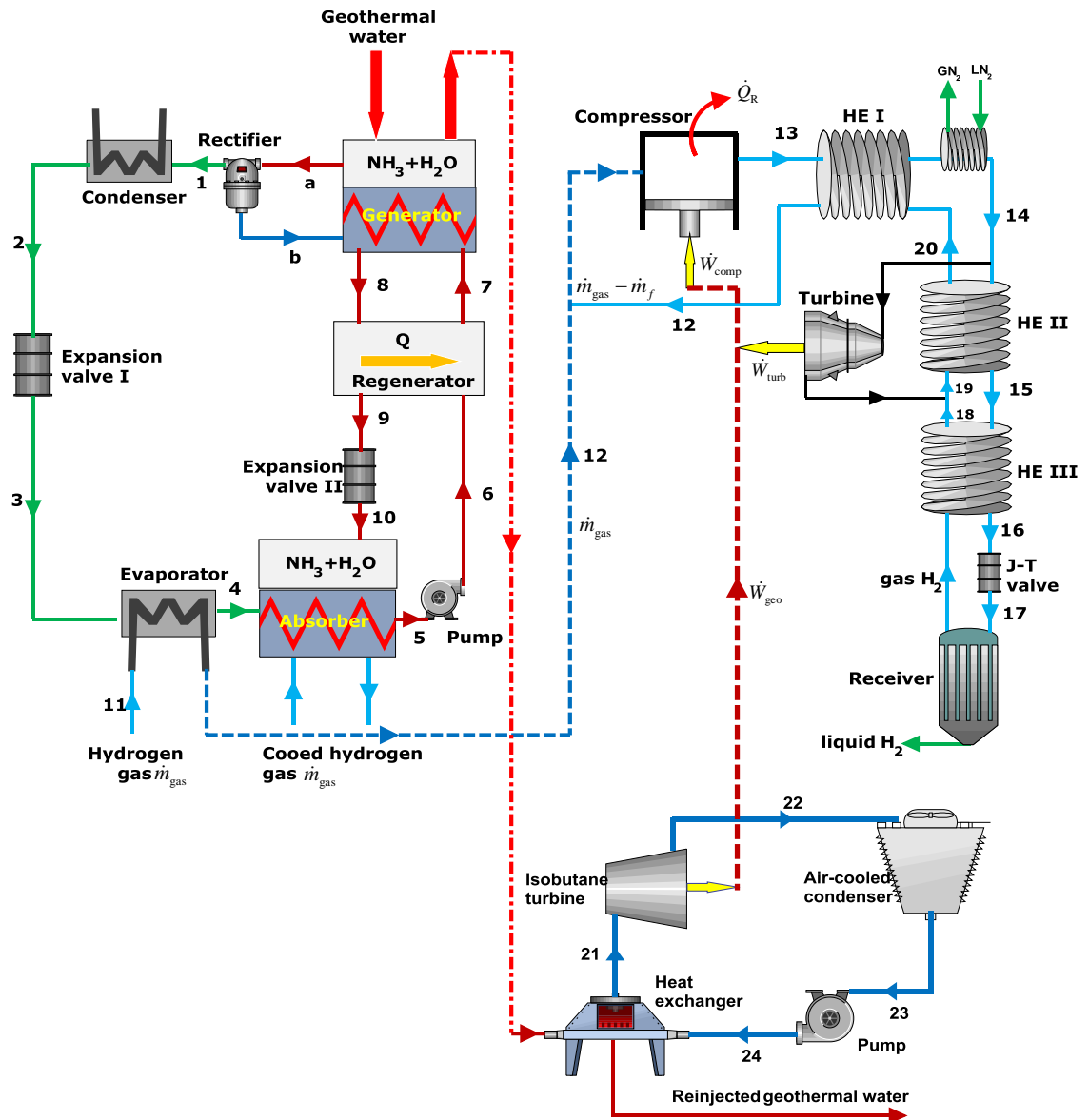


Figure 2.5. In Model 4, hydrogen is cooled in an absorption cycle, power is produced in a binary geothermal power plant, and hydrogen is liquefied in the Claude cycle.

2.7 System description of Model 5

The schematic of Model 5 is given in Fig. 2.6. A flash binary geothermal power plant is used to produce power and this power is used for hydrogen liquefaction in the Claude cycle. Hydrogen gas is supplied from an external source of hydrogen production unit.

Liquefaction work is supplied from geothermal power plant. The most important parameter in a gas liquefaction cycle is compressor work. Second part of this model is Claude liquefaction cycle. The hydrogen gas is first compressed to a higher pressure and then passed through the first heat exchanger. The stream to be liquefied continues through the other heat exchangers and is finally expanded through an expansion valve at state 17 to the receiver (liquid H_2). The cold vapor (hydrogen) from the receiver is returned through the heat exchangers to cool the incoming gas.

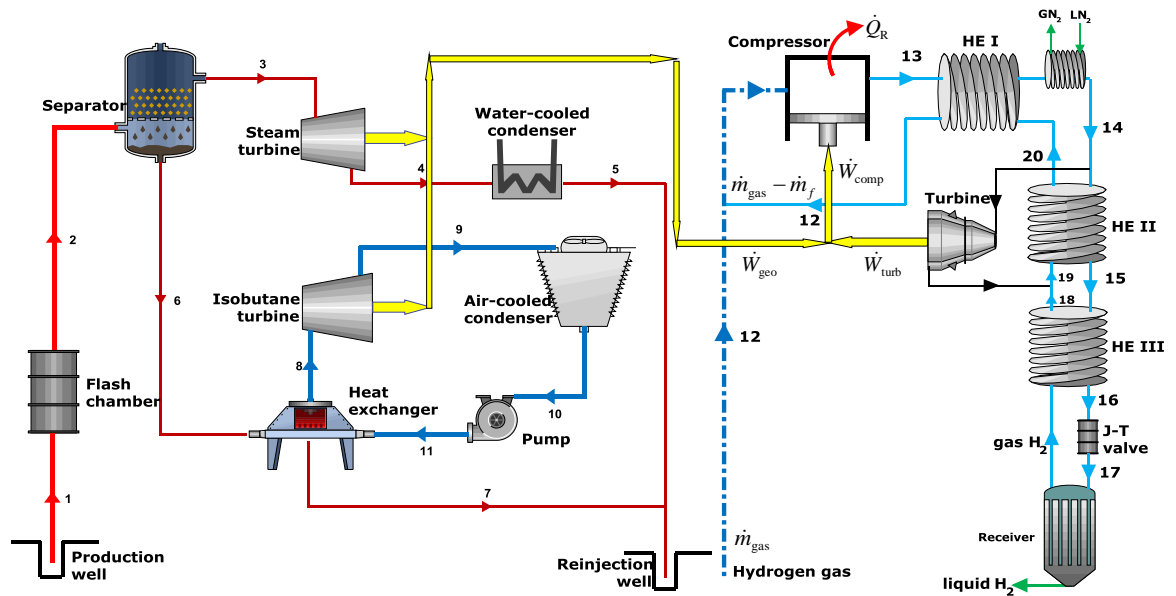


Figure 2.6. In Model 5, electricity is produced in a geothermal power plant and used in the Claude cycle.

2.8 System description of Model 6

The operation of Model 6 is depicted in Fig. 2.7. In this model, hydrogen production and liquefaction by a geothermal source is accomplished. The electrical power for both the electrolysis unit and liquefaction cycle is supplied by the geothermal power plant. The geothermal work is used for electrolysis to produce hydrogen gas and the remaining power is used for the liquefaction of hydrogen gas in the Claude cycle. Main system characteristics of the system are provided with Model 1 and Model 3. In this model, work ratios of each system are determined so that appropriate work is used in production and liquefaction units.

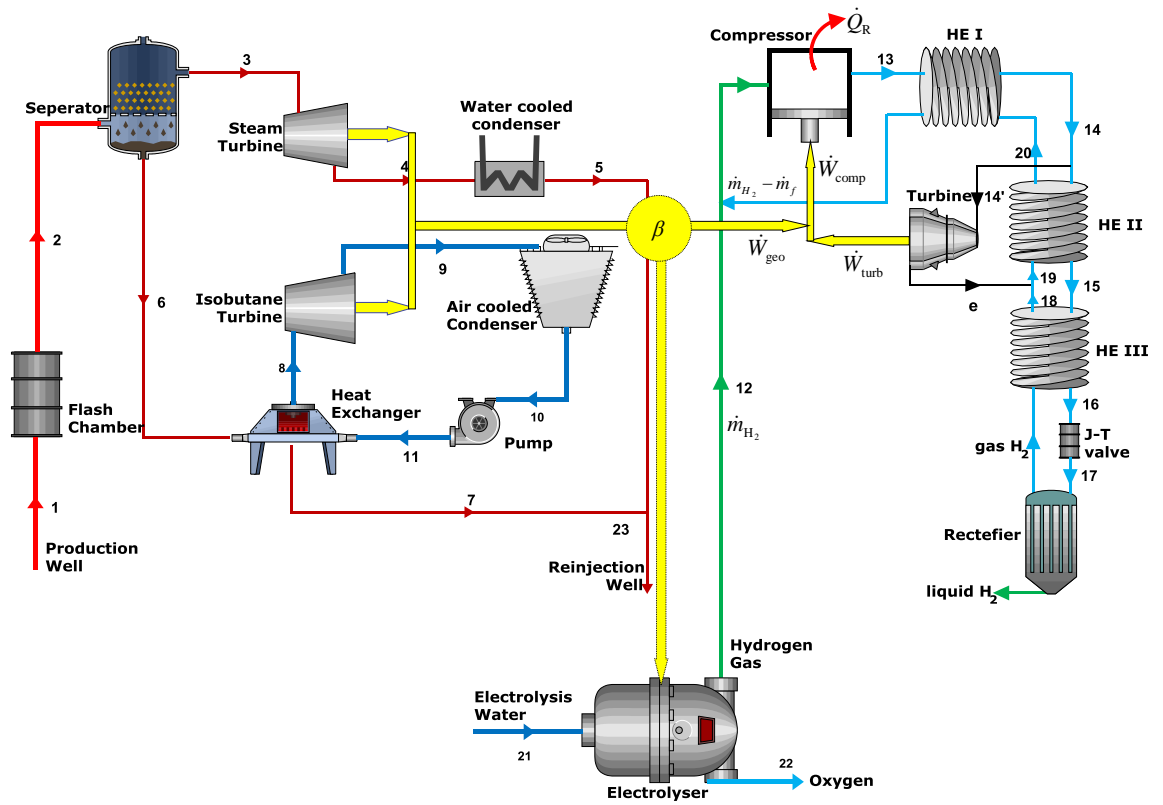


Figure 2.7. In Model 6, part of geothermal power is used for the electrolysis process and the remaining part for liquefaction.

CHAPTER 3

THERMODYNAMIC ANALYSIS

3.1 Energy and Exergy Analyses

The energy of a system consists of internal, kinetic and potential energies. Internal energy consists of thermal, chemical, and nuclear energies. Unless there is a chemical or nuclear reaction, the internal change of a system is due to thermal energy change. In the absence of electric, magnetic, and surface tension effects, among others, the energy balance of a system can be expressed as [45]

$$E_{in} - E_{out} = \Delta E_{system} \quad (3.1)$$

Energy can cross the boundary of a closed system in two distinct forms: heat and work. A control volume can also exchange energy via mass transfer since any time mass is transferred into or out of a system, the energy content of the mass is also transferred with it. So energy balance equation can be expressed as [46]

$$Q - W = \Delta U + \Delta KE + \Delta PE \quad (3.2)$$

where internal, kinetic and potential energy changes are

$$\Delta U = m(u_2 - u_1) \quad (3.3)$$

$$\Delta KE = \frac{1}{2} m(V_2^2 - V_1^2) \quad (3.4)$$

$$\Delta P = mg(z_2 - z_1) \quad (3.5)$$

where the changes in kinetic and potential energies are zero for stationary systems (that is $\Delta KE = \Delta PE = 0$) and the total energy change relation in Eq. (3.2) reduces to $\Delta E = \Delta U$ for such systems.

The first law of thermodynamics deals with quantity of energy and asserts that energy cannot be created or destroyed. The second law of thermodynamics deals with quality of energy. It is considered with the degradation of energy during a process, the entropy generation and lost opportunities to do work and it offers plenty of room for improvement. The second law of thermodynamics has proved to be a very powerful tool in the optimization of complex thermodynamic systems [47].

Control volume involving a steady flow process is considered in this thesis. Mass, energy, entropy and exergy balances for a control volume at steady state with negligible kinetic and potential energy changes can be expressed as [48]

$$\sum \dot{m}_i = \sum \dot{m}_e \quad (3.6)$$

$$\dot{Q} - \dot{W} = \sum \dot{m}_e h_e - \sum \dot{m}_i h_i \quad (3.7)$$

$$\sum \frac{\dot{Q}}{T_s} + \sum \dot{m}_i s_i + \dot{S}_{gen} = \sum \dot{m}_e s_e \quad (3.8)$$

$$\dot{E}x_{heat} - \dot{W} = \sum \dot{m}_e ex_e - \sum \dot{m}_i ex_i + \dot{E}x_{dest} \quad (3.9)$$

where \dot{Q} and \dot{W} are the net heat and work inputs, \dot{m} is the mass flow rate of the fluid stream, h is the enthalpy, ex is the specific flow exergy, $\dot{E}x_{heat}$ is the rate of exergy transfer by heat, $\dot{E}x_{dest}$ is the rate of exergy destruction, and the subscripts i and e stand for inlet and exit states. Also; s is entropy, T_0 is the dead state temperature, and the subscript 0 stands for the restricted dead state.

The specific flow exergy and the rate of total exergy are given by [48]

$$ex = (h - h_0) - T_0(s - s_0) \quad (3.10)$$

$$\dot{E}x = \dot{m}(ex) \quad (3.11)$$

Irreversibilities such as friction, mixing, chemical reactions, heat transfer through a finite temperature difference, unrestrained expansion, and nonquasiequilibrium compression or expansion always generate entropy, and anything that generates entropy destroys exergy. The exergy destroyed is proportional to the entropy generated and is expressed as [48]

$$\dot{E}x_{\text{dest}} = T_0 \dot{S}_{\text{gen}} \quad (3.12)$$

Efficiency is a measure of the effectiveness or performance of a system. Although it may take different forms, depending on the application and purpose, it can generally be defined as the desired output divided by the required input for a system. The definition of energy efficiency is based on the first law of thermodynamics. Energy efficiency is generally defined as [48]

$$\eta_{\text{th}} = \left(\frac{\text{energy in products}}{\text{total energy input}} \right) \quad (3.13)$$

The definition of exergy efficiency is based on the second law of thermodynamics. It is also called the second law efficiency. Exergy efficiency may take different forms depending on the type of the system. Exergy efficiency is generally defined as [48]

$$\eta_{\text{ex}} = \left(\frac{\text{exergy in products}}{\text{total exergy input}} \right) \quad (3.14)$$

3.2 Fuel-Product Approach for Exergy Analysis

Exergy is defined as the work potential. It is the maximum useful work that could be obtained from a system at a given state in a specified environment. An exergy analysis deals with the quality of the energy and its degradation during a process. In an irreversible process, mass and energy are conserved, entropy is generated, and exergy is destroyed due to irreversibilities. No exergy is destroyed in a reversible process [49].

For an exergetic evaluation, the exergy of product ($\dot{E}x_{P,k}$) and the exergy of fuel ($\dot{E}x_{F,k}$) should be defined for each component and the entire system.

The exergy of fuel is the expense of exergy resources to generate the desired output [30]. The exergy destruction, which is the destroyed exergy within the component during the operation, is calculated at the component level as the difference between exergy of fuel and exergy of product [49]:

$$\dot{E}x_{D,k} = \dot{E}x_{F,k} - \dot{E}x_{P,k} \quad (3.15)$$

Here, $\dot{E}x_{D,k}$ is the rate of exergy destruction of any component, $\dot{E}x_{F,k}$ is the rate of fuel exergy into the component, and $\dot{E}x_{P,k}$ is the rate of product exergy from the component. The exergy efficiency is defined as the ratio of the exergy of product and the exergy of fuel that can be expressed for each component as [49]

$$\varepsilon_k = \frac{\dot{E}x_{P,k}}{\dot{E}x_{F,k}} = \frac{\dot{E}x_{F,k} - \dot{E}x_{D,k}}{\dot{E}x_{F,k}} = 1 - \frac{\dot{E}x_{D,k}}{\dot{E}x_{F,k}} \quad (3.16)$$

The exergy efficiency for the overall system is

$$\varepsilon_{overall} = \frac{\dot{E}x_{P,tot}}{\dot{E}x_{F,tot}} = \frac{\dot{E}x_{F,tot} - \dot{E}x_{D,tot}}{\dot{E}x_{F,tot}} = 1 - \frac{\dot{E}x_{D,tot}}{\dot{E}x_{F,tot}} \quad (3.17)$$

The exergy destruction ratio y_k and the relative exergy destruction ratio y_k^* are defined as [49]

$$y_k = \frac{\dot{E}x_{D,k}}{\dot{E}x_{F,tot}} \quad (3.18)$$

$$y_k^* = \frac{\dot{E}x_{D,k}}{\dot{E}x_{D,tot}} \quad (3.19)$$

The definitions of exergy of fuel and exergy of product for each component of the system are given later in the analysis of the models. When defining fuel exergy and product exergy for the electrolysis unit, both chemical and physical exergies are considered.

3.3 Thermodynamic Analysis of Combined Flash-Binary Geothermal Power Plant

A combined flash-binary geothermal power plant (Fig. 3.1) incorporates a binary unit and a flashing unit. The liquid portion of the geothermal mixture serves as the input heat for the binary cycle while the steam portion drives a steam turbine to produce power.

The energy input to the geothermal plant can be taken as the enthalpy difference between the state of the geothermal water at the plant inlet and the enthalpy of liquid water at the environmental state multiplied by the mass flow rate of the geothermal water. This refers to energy of geothermal water at the plant inlet with respect to environmental state (dead state 0) [50].

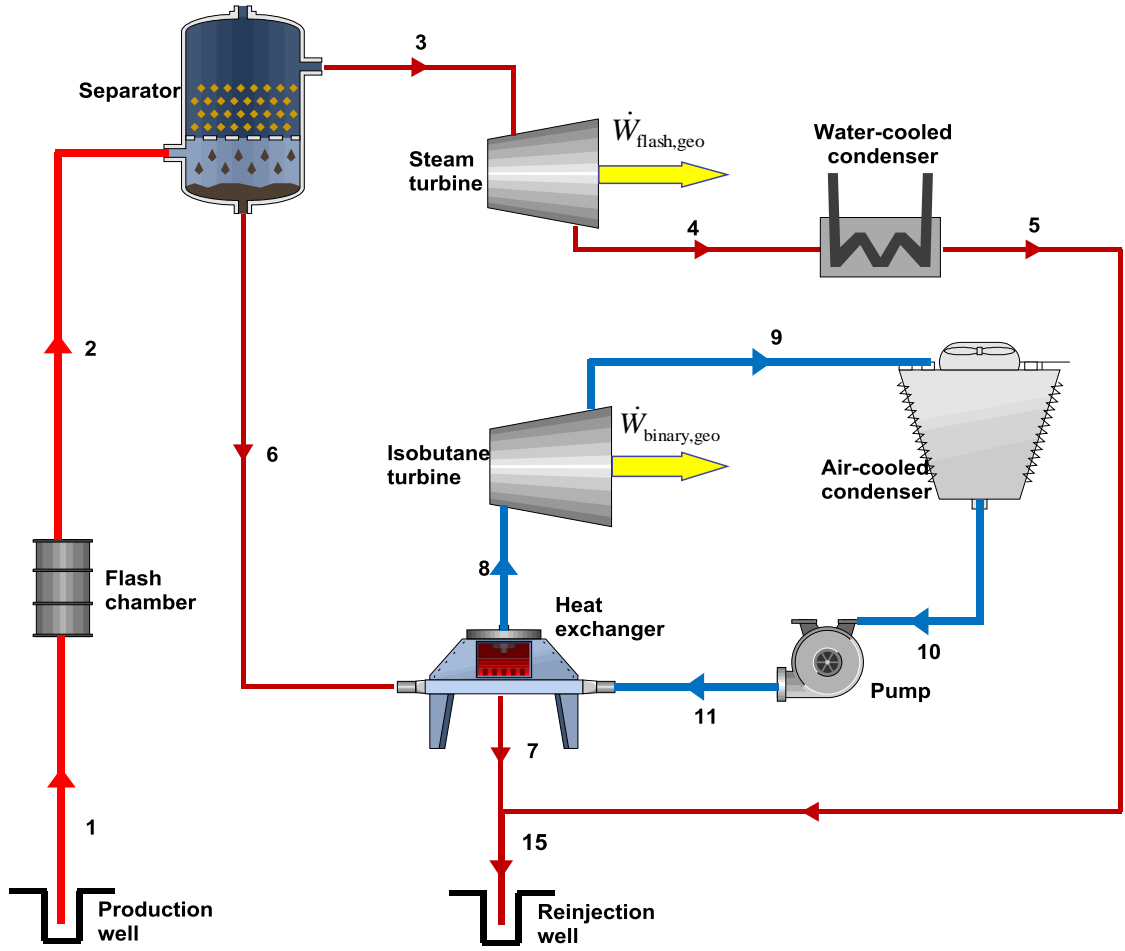


Figure 3.1. Combined flash-binary geothermal power plant.

The energy efficiency of the plant may be defined as the ratio of the power output to the energy input to the plant [51]

$$\eta = \frac{\dot{W}_{\text{net,out}}}{\dot{E}_{\text{in}}} \quad (3.20)$$

Referring to Fig. 3.1, the thermal efficiency of combined flash-binary geothermal power plant can be determined from [51]

$$\eta = \frac{\dot{W}_{\text{turbines}} - \dot{W}_{\text{pump}} - \dot{W}_{\text{fan}}}{\dot{E}_{\text{in}}} = \frac{\dot{m}_3(h_3 - h_4) + \dot{m}_8(h_8 - h_9) - \dot{W}_{\text{pump}} - \dot{W}_{\text{fan}}}{\dot{m}_{\text{geo}}(h_{\text{geo}} - h_0)} \quad (3.21)$$

where \dot{W}_{fan} is the power consumed by the fans in the air-cooled condenser. Note that power is produced from both the steam and binary turbines in the plant.

Using the exergy of geothermal water as the exergy input to the plant and overall system (in the reservoir or at the well head). The exergy efficiency of the combined flash-binary geothermal plant can be expressed as [51]

$$\varepsilon = \frac{\dot{W}_{net,out}}{\dot{m}_{geo}(h_{geo} - h_0 - T_0(s_{geo} - s_0))} \quad (3.22)$$

3.4 Thermodynamic Analysis of Electrolysis Unit

The thermodynamic analysis of electrolysis operation is presented in this section. This analysis is performed to calculate the voltage and flow rate in the electrolysis unit. For the electrolysis unit, the validity range of the temperature range is usually between 25 and 80°C [52]. In the following analysis, all gases involved are assumed to be ideal gases and any side reaction or mixing is neglected. Focusing on electrolysis; a control volume surrounding an isothermal electrolysis process is considered, as shown in Fig. 3.2.

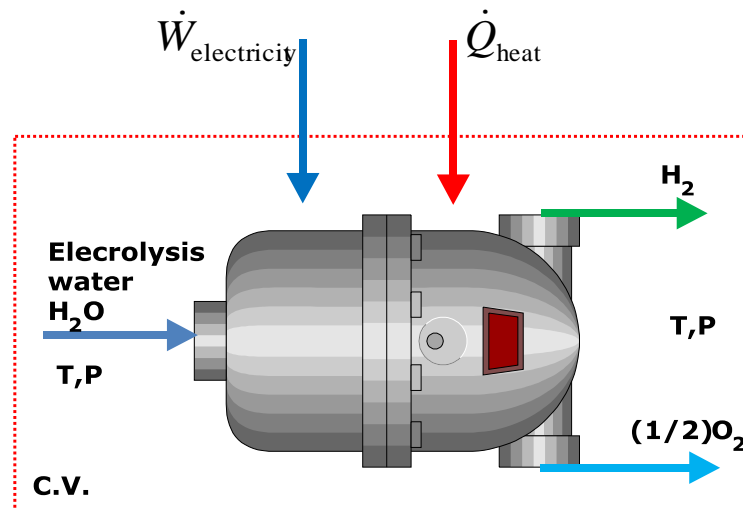


Figure 3.2. Schematic of a water electrolysis process operating at T and P.

For an electrochemical process operating at constant pressure and temperature, the maximum possible useful work (i.e., the reversible work) is equal to the change in Gibbs energy. The electrical work is positive for electrolysis (i.e., work input) and negative (i.e., work output) for fuel cell operations when analyzing chemical reactions. The total energy demand for the electrolysis operation can be calculated as [53]

$$\Delta H = \Delta G + T_{\text{electrolysis}} \Delta S \quad (3.23)$$

where ΔG is the electrical energy demand (change in Gibb's free energy) and $T_{\text{electrolysis}} \Delta S$ is the thermal energy demand (kJ/kmol). The values of G , S , and H for H_2 , O_2 , and H_2O can be obtained from the JANAF table. Two essential voltages, taking into account the energy needed for hydrogen production, can be defined as follows [54]

The enthalpy voltage at T and P :

$$V_{T,P} = \frac{\Delta H_{T,P}}{nF} \quad (3.24)$$

The electrolysis operation voltage at T and P :

$$E_{T,P} = \frac{\Delta G_{T,P}}{nF} \quad (3.25)$$

Here, n is the number of electrons transferred and F is the Faraday constant, which is equal to $96,500 \text{ C mol}^{-1}$. The voltage associated with $\Delta H_{T,P}$ is commonly called the thermo neutral cell voltage, which is the voltage at which a perfectly efficient cell would operate if electricity provided the entire energy requirement. Under these conditions, the cell does not generate any waste heat, nor does it require any heat input; hence it is said to be thermo neutral [55]. Since the enthalpy voltage and the water electrolysis voltage depend on the enthalpy and the Gibbs energy for the formation reaction of water, we can predict the temperature changes by means of thermodynamic relationships [56].

The calculation approach is based on the fact that the enthalpy and Gibbs energy are properties that depend on the initial and final states of the reactants and products of electrolysis. The enthalpies of reactants and products are expressed as a function of temperature as [57]

$$\Delta H^0(T, final) = \Delta H^0(T, initial) + \sum_{species} \int_{T, initial}^{T, final} C_{p, species}^0(T) dT \quad (3.26)$$

where $(T, initial)$ is the initial temperature in K; $(T, final)$ is the final temperature in K; and C_p is the heat capacity of the species in kJ/kmol K. The entropy change is expressed by considering the following relationship of ideal gases [57]

$$\Delta S^0(T, final) = \Delta S^0(T, initial) + \sum_{species} \int_{T, initial}^{T, final} \frac{C_{p, species}^0(T)}{T} dT \quad (3.27)$$

By combining these two equations, Gibbs energy of the formation can be calculated. Neglecting kinetic and potential exergy changes, the exergy of a substance can be determined from [58]

$$ex = ex^{CH} + ex^{PH} \quad (3.28)$$

where ex^{CH} and ex^{PH} are chemical and physical exergies (in kJ/kmol), respectively. The chemical exergy values of various compounds are given in Table 3.1. The physical exergy can be determined from the flow exergy relation as [59]

$$ex^{PH} = h - h_0 - T_0(s - s_0) \quad (3.29)$$

where h , s , and T represent the general thermodynamic properties of enthalpy, entropy and temperature, respectively, and subscript 0 represents the reference environment condition.

Table 3.1. Enthalpy, entropy and Gibbs free energy of formation and standard chemical exergy for electrolysis [60].

Elements	$h_f^0(kJ/kmol)$	$s_f^0(kJ/kmol)$	$g_f^0(kJ/kmol)$	$ex^{ch}(kJ/kmol)$
H ₂ O (l)	285,830	6,992	237,180	900
H ₂ (g)	0	130.57	0	236,100
O ₂ (g)	0	205.3	0	3970

The mass flow rate of H₂ at the outlet can be determined from

$$\dot{m}_{H_2, out} = \frac{J}{2F} M_{H_2} \quad (3.30)$$

where J is the current density, F is the Faraday constant, and M_{H_2} is the molecular weight of H₂. Similarly, the mass flow rate of O₂ at the PEM electrolysis outlet can be calculated as

$$\dot{m}_{O_2, out} = \frac{J}{4F} M_{O_2} \quad (3.31)$$

The energy and exergy of electricity involved in the PEM electrolysis operation can be determined by the following electrochemical model developed in ref. [61] as

$$\dot{W}_{\text{electricity}} = JE_{T,P} \quad (3.32)$$

$$E_{T,P} = \frac{\dot{W}_{\text{electricity}}}{nF} \quad (3.33)$$

where $E_{T,P}$ is the necessary cell voltage for the start up of electrolysis operation, J is the current density, and $\dot{W}_{\text{electricity}}$ is the electrical power consumption in electrolysis. These equations are valid if the current density is not too high.

The total energy demand is the theoretical energy required for H₂O electrolysis without any losses. In actual systems, losses are inevitable and the performance of the system can be evaluated in terms of energy and exergy efficiencies. The energy and exergy efficiencies of the overall system can be defined as the total energy value of the hydrogen produced (heating value of hydrogen times its production rate) divided by the energy (or exergy) input to the system, which is energy (or exergy) value of geothermal water at the plant inlet with respect to the environmental state.

$$\eta_{\text{overall}} = \frac{\text{LHV}_{\text{H}_2} \times \dot{m}_{\text{H}_2, \text{out}}}{\dot{m}_{\text{geo}} (h_{\text{geo}} - h_0)} \quad (3.34)$$

$$\varepsilon_{\text{overall}} = \frac{\dot{E}x_{\text{H}_2}}{\dot{m}_{\text{geo}} (h_{\text{geo}} - h_0 - T_0 (s_{\text{geo}} - s_0))} \quad (3.35)$$

Here, LHV is the lower heating value of H₂, $\dot{m}_{\text{H}_2, \text{out}}$ is the mass flow rate of H₂ at the outlet, $\dot{W}_{\text{net,geo}}$ is the rate of electric energy input by geothermal power plant for the electrolysis operation, respectively, and $\dot{E}x_{\text{H}_2}$ is the exergy rate of H₂ produced in the electrolysis unit.

3.5 Thermodynamic Analysis of Absorption Refrigeration Cycle

Energy analysis of an absorption refrigeration cycle (ARC) refers to the first law of thermodynamics for a control volume. Each component in this cycle is considered a steady state, steady flow process, and energy and exergy balance equations are applied accordingly. The mass flow rate of the refrigerant is not constant due to changing ammonia water composition. Fig. 3.3 shows the operation of water ammonia absorption refrigeration cycle used to cool hydrogen gas in the liquefaction models. In this cycle, ammonia is the refrigerant and water is the absorbent. Ammonia circulates through the condenser, expansion valve, and evaporator as in a vapor compression system.

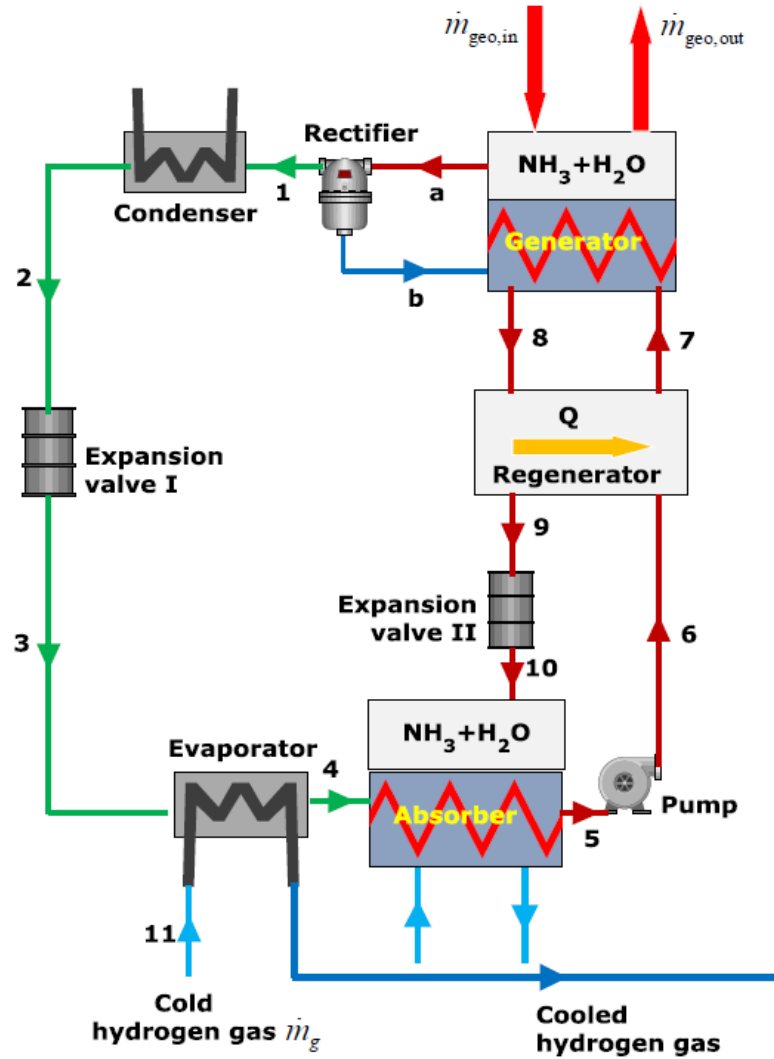


Figure 3.3. Water-ammonia absorption refrigeration cycle used to cool hydrogen gas in liquefaction models.

For the entire ammonia-water absorption refrigeration cycle, the overall energy balance may be expressed as [62]

$$\dot{W}_P + \dot{Q}_L + \dot{Q}_{gen} = \dot{Q}_A + \dot{Q}_H \quad (3.36)$$

The first law performance of a refrigeration cycle can be expressed in terms of the coefficient of performance (COP). The objective of a refrigerator is to remove heat \dot{Q}_L from the refrigerated space. To accomplish this objective, it requires a work input or a heat input in a heat-driven system.

In order to develop a relation for the reversible COP of an absorption refrigeration cycle, a reversible heat engine and a reversible refrigerator are considered. Heat is absorbed from a source at T_s by a reversible heat engine and the waste heat is rejected to an environment at T_0 . Work output from the heat engine is used as the work input for the reversible refrigerator, which keeps a refrigerated space at T_L , while rejecting heat to the environment at T_0 . Using the definition of COP for an absorption refrigeration cycle, thermal efficiency of a reversible heat engine and the COP of a reversible refrigerator, the reversible COP of an absorption refrigeration cycle can be written as [62]

$$\text{COP}_{\text{abs,rev}} = \left(1 - \frac{T_0}{T_s}\right) \left(\frac{T_L}{T_0 - T_L}\right) \quad (3.37)$$

The actual COP of the ARC is

$$\text{COP}_{\text{abs,act}} = \frac{\dot{Q}_{L,ARC}}{\dot{Q}_{\text{gen}} + \dot{W}_P} \cong \frac{\dot{m}_{\text{H}_2} (h_{11} - h_{12})}{\dot{m}_{\text{geo}} (h_{\text{geo,in}} - h_{\text{geo,out}})} \quad (3.38)$$

where \dot{W}_P is the pumping power requirement, and it is neglected.

As given earlier, the change in exergy rate or the rate of exergy loss can be defined in terms of physical terms as follows [62]:

$$\Delta \dot{E}x = \sum \dot{m}_i ex_i - \sum \dot{m}_e ex_e + \dot{Q} \left(1 - \frac{T_0}{T}\right) + \dot{W}_i \quad (3.39)$$

where the first terms are the sum of exergy input and output rates of the flow, respectively. The third term is the heat of exergy (positive if it is heat input; negative if it is heat output). The last term is the work given to the system (e.g., pump work).

The exergy balance equations for the components of the absorption refrigeration cycle will be written with respect to each model configuration in the next chapter. Exergy efficiency can be expressed for the ammonia water absorption refrigeration cycle as the exergy change of hydrogen gas divided by the exergy change of geothermal water

$$\varepsilon_{\text{ARC}} = \frac{\dot{E}x_{12} - \dot{E}x_{11}}{\dot{E}x_{\text{geo,in}} - \dot{E}x_{\text{geo,out}}} \quad (3.40)$$

Note that the exergy change of hydrogen gas is equal to minimum work requirement for the cooling of hydrogen and the exergy decrease of geothermal water represents exergy transferred or expended in the cycle.

3.6 Thermodynamic Analysis of Claude Liquefaction Cycle

In the system considered in this thesis, geothermal water is used as the heat source for an ammonia-water absorption refrigeration cycle which is used to precool the hydrogen gas before it is liquefied in the Claude cycle. The Claude hydrogen liquefaction cycle is shown in Fig. 3.4. The Claude cycle, which uses an isentropic expansion engine in addition to a Joule Thompson valve, is an efficient process for hydrogen liquefaction. The expansion through an expansion valve is a highly irreversible process. In the Claude cycle, energy is removed from the gas stream by allowing it to do some work in a turbine. Compared to an isenthalpic expansion process in a throttling valve, a lower temperature is attained in a turbine exit [63].

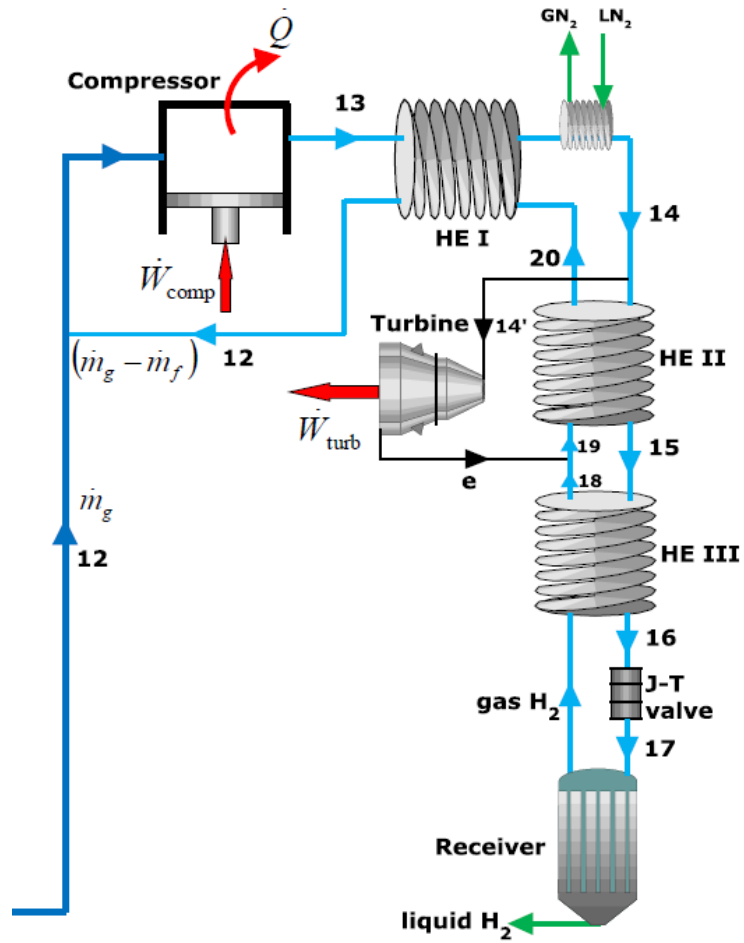


Figure 3.4. Claude liquefaction cycle.

Temperature-entropy ($T-s$) diagram of the Claude cycle is shown in Fig. 3.5 based on state numbers in Fig. 3.4. The compression pressure (pressure at the compressor exit) of Claude liquefaction cycle ranges between 2 and 13 MPa [64]. The parameters of figure of merit (FOM: minimum work over actual work) and specific power consumption are considered as the indicators of performance of a liquefaction cycle.

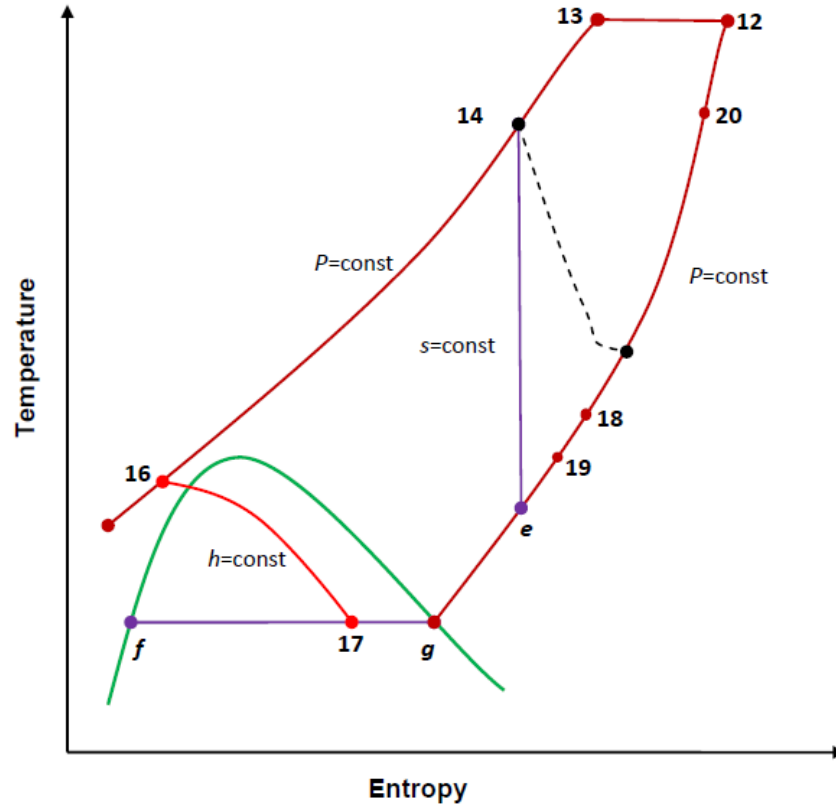


Figure 3.5. Temperature-entropy (T - s) diagram of the Claude liquefaction cycle.

In the Claude cycle, some work is produced in the turbine reducing net work input to the cycle. Feed gas is compressed to 5 MPa pressure and then passed through the first heat exchanger. About 60% of hydrogen gas is then diverted from the mainstream, expanded in the turbine and reunited with the return stream below the second heat exchanger, as shown in Fig. 3.4. The stream to be liquefied continues through the second and third heat exchangers and is finally expanded in an expansion valve. Liquid hydrogen results at the exit of the expansion valve. Neglecting any heat leak into the cycle, an energy balance on the entire Claude cycle gives

$$(\dot{m} - \dot{m}_f)h_{12} + \dot{m}_f h_f + \dot{m}_e h_e - \dot{m}h_{13} - \dot{m}_e h_{14} = 0 \quad (3.41)$$

The fraction of mass flowing through the expander is

$$x = \frac{\dot{m}_e}{\dot{m}} \quad (3.42)$$

Then the fraction of mass that is liquefied becomes

$$y_{\text{liq}} = \frac{\dot{m}_f}{\dot{m}} = \frac{h_{12} - h_{13}}{h_{12} - h_f} + x \frac{h_{14} - h_e}{h_{12} - h_f} \quad (3.43)$$

The power produced in the turbine is given by

$$\dot{W}_{\text{turb}} = \dot{m}_e (h_{14} - h_e) \quad (3.44)$$

The total work input per unit mass of hydrogen gas is determined from

$$w_{\text{in}} = w_{\text{comp}} - w_{\text{turb}} + w_{\text{N}_2} = [T_{12}(s_{12} - s_{13}) - (h_{12} - h_{13})] - x(h_{14} - h_e) + w_{\text{N}_2} \quad (3.45)$$

The total work input for the cycle per unit mass of liquefied hydrogen is

$$W_{\text{liq,act}} = \frac{w_{\text{comp}} + w_{\text{N}_2} - w_{\text{turb}}}{y_{\text{liq}}} \quad (3.46)$$

The total work consumption for liquefaction involves the work consumed by the hydrogen compressor as well as the work requirement for producing liquid nitrogen. In this study, the work input is taken as 7760 kJ/kg for liquid nitrogen based on actual nitrogen liquefier units [65].

The reversible work for the Claude cycle may be expressed by the stream exergy difference between inlet gas state and produced liquid state to be

$$w_{\text{rev,liq}} = h_f - h_{12} - T_0(s_f - s_{12}) \quad (3.47)$$

This relation indicates that the reversible work of liquefaction depends on the hydrogen properties before and after the liquefaction as well as the environment temperature.

The exergy efficiency may be defined as the reversible work input divided by the actual work input, both per unit mass of the liquefaction [66]

$$\varepsilon_{\text{liq}} = \frac{W_{\text{liq,rev}}}{W_{\text{liq,act}}} \quad (3.48)$$

The exergy efficiency of the Claude cycle can also be expressed as the exergy change of the hydrogen from gas state to liquid state divided by the net power input to the cycle (i.e., rotational efficiency)

$$\varepsilon_{\text{liq}} = \frac{\dot{E}x_{\text{H}_2,\text{liq}} - \dot{E}x_{12}}{\dot{W}_{\text{comp}} - \dot{W}_{\text{turb}}} \quad (3.49)$$

where $\dot{E}x_{\text{H}_2,\text{liq}}$ is the exergy rate of liquefied hydrogen at the exit state of the receiver, \dot{W}_{comp} is the net power input to the liquefaction cycle of hydrogen gas, and \dot{W}_{turb} is the power output from to the cryogenic turbine of the liquefaction cycle.

The actual COP of Claude liquefaction cycle is given by

$$\text{COP}_{\text{liq,act}} = \frac{\dot{Q}_{L,\text{liq}}}{\dot{W}_{\text{liq}}} = \frac{\dot{m}_{12}h_{12} - \dot{m}_f h_f}{\dot{W}_{\text{comp}} + \dot{W}_{\text{N}_2} - \dot{W}_{\text{turb}}} \quad (3.50)$$

where $\dot{Q}_{L,\text{liq}}$ is the rate of heat rejection from the hydrogen gas during the liquefaction process and \dot{W}_{liq} is the power input for the liquefaction.

Overall exergy efficiency for a system consisting of absorption system and Claude cycle can be defined by exergy difference of hydrogen gas at the inlet of the absorption system and liquid hydrogen at the exit of the Claude cycle divided by the total exergy input to the overall system that consists of exergy supplied by geothermal water and the net power input

$$\varepsilon_{\text{overall}} = \frac{\dot{E}x_{\text{liq,H}_2} - \dot{E}x_{11}}{\dot{E}x_{\text{geo,in}} - \dot{E}x_{\text{geo,out}} + \dot{W}_{\text{comp}} + \dot{W}_{\text{N}_2} - \dot{W}_{\text{turb}}} \quad (3.51)$$

The purpose of the overall system is to liquefy hydrogen, and this is done by removing heat from the hydrogen. The price we pay for this desired output is the power consumption in the liquefaction cycle and heat input to the absorption cycle. Then, an overall COP for the integrated system can be expressed as

$$\text{COP}_{\text{overall}} = \frac{\dot{Q}_{L,ARC} + \dot{Q}_{L,liq}}{\dot{Q}_{\text{gen}} + \dot{W}_{\text{liq}}} \quad (3.52)$$

Alternatively, an exergy efficiency of the overall system consisting of the absorption cooling cycle and the Claude cycle can be expressed using fuel-product approach as

$$\varepsilon_{\text{overall}} = \frac{\sum_k \dot{E}x_P}{\sum_k \dot{E}x_F} = 1 - \frac{\sum_k \dot{E}x_D}{\sum_k \dot{E}x_F} \quad (3.53)$$

3.7 Thermodynamic Analysis Results of Models

In this section, thermodynamic analysis results of the models are given.

3.7.1 Model 1

The geothermal power plant operates on a liquid dominated resource at 200°C with a mass flow rate of 100 kg/s. In the geothermal plant, liquid is flashed to a lower pressure producing a mixture of steam and liquid. Steam is directed to the turbine while liquid is used as the heat input for the binary cycle. Binary fluid isobutane is vaporized by geothermal water and runs through the turbine to produce power. Power outputs from the steam and isobutane turbines are used for the electrolysis process. The used geothermal water is reinjected back to the ground. The isentropic efficiencies of the turbines and pump are taken to be 85%. It is assumed that 20% of the power output is used for internal demands of binary cycle and 5% of the power output is used for internal uses of the steam cycle.

Most internal uses are due to power requirements of pumps and fans. Application of energy and exergy balances on the Model 1 gives the performance data in Table 3.2. Model 2 is a modified version of Model 1, and we provide thermodynamic analysis and results in detail for Model 2 in the next subsection.

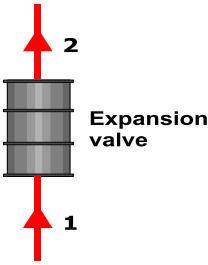
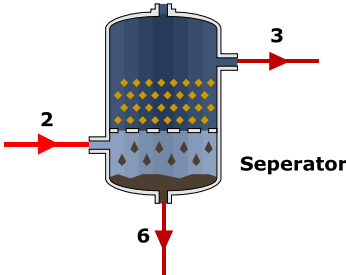
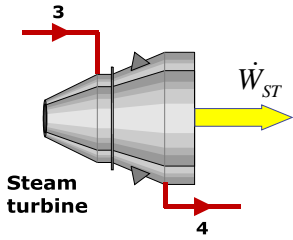
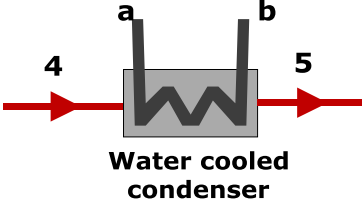
Table 3.2. Thermodynamic analysis results of Model 1.

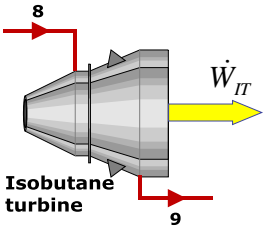
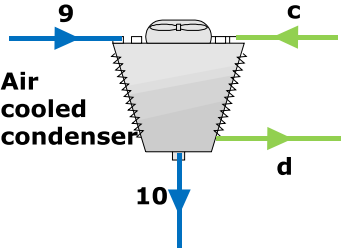
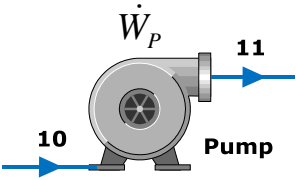
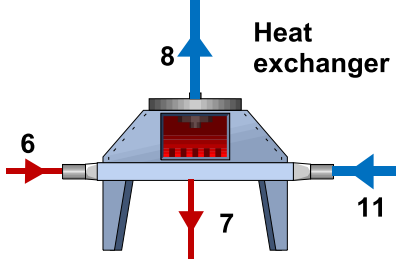
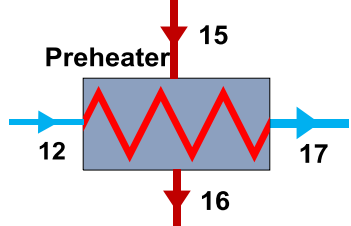
Parameters	Result
Geothermal net power output	7572 kW
Hydrogen production rate	0.0483 kg/s
Unit work input for the electrolysis	156,844 kJ/kg H ₂ (43.5 kWh/kg H ₂)
Energy efficiency of geothermal power plant	10.5%
Exergy efficiency of geothermal power plant	46.7 %
Energy efficiency of electrolysis	76.7 %
Exergy efficiency of electrolysis	74.7 %
Overall system energy efficiency for Model 1	7.8 %
Overall system exergy efficiency for Model 1	44.3% (87.9 % by Fuel-Product approach)

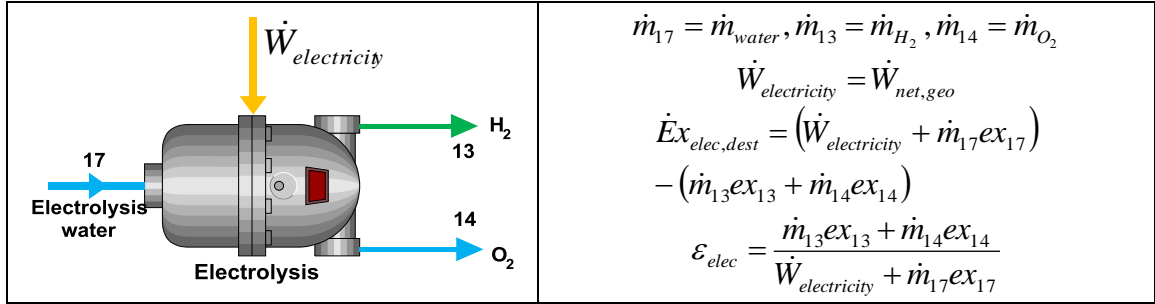
3.7.2 Model 2

Each component in Model 2 is considered a steady state, steady flow process, and apply energy and exergy balance equations are applied accordingly. Table 3.3 gives mass, energy, and exergy balance equations for the system components. The states refer to Fig. 2.3 of Model 2.

Table 3.3. Mass, energy, and exergy relations for the components of Model 2.

Component	Mass, energy and exergy equations
 <p style="text-align: center;">Expansion valve</p>	$\dot{m}_1 = \dot{m}_2 = \dot{m}_{\text{geo}}$ $h_1 = h_2 = h_{\text{geo}@20^\circ\text{C}}$ $ex_{\text{geo}} = h_{\text{geo}} - h_0 - T_0 (s_{\text{geo}} - s_0)$ $\dot{E}x_{\text{dest,EV}} = \dot{m}_{\text{geo}} (ex_1 - ex_2)$ $\varepsilon_{\text{EV}} = \frac{\dot{m}_2 ex_2}{\dot{m}_1 ex_1}$
 <p style="text-align: center;">Separator</p>	$\dot{m}_2 = \dot{m}_{\text{geo}}$ $x_2 = \frac{h_2 - h_3}{h_4 - h_3}$ $\dot{m}_6 = (1 - x_2) \dot{m}_{\text{geo}}$ $\dot{m}_3 = x_2 \dot{m}_1$ $\dot{E}x_{\text{dest,SP}} = \dot{m}_{\text{geo}} ex_2 - (\dot{m}_3 ex_3 + \dot{m}_6 ex_6)$ $\varepsilon_{\text{SP}} = \frac{\dot{m}_3 ex_6 + \dot{m}_6 ex_6}{\dot{m}_2 ex_2}$
 <p style="text-align: center;">Steam turbine</p>	$\dot{m}_4 = \dot{m}_3$ $\dot{W}_{\text{ST,act}} = \dot{m}_3 (h_3 - h_4)$ $\dot{W}_{\text{ST,rev}} = \dot{m}_3 (ex_3 - ex_4)$ $\dot{E}x_{\text{ST,dest}} = \dot{W}_{\text{ST,rev}} - \dot{W}_{\text{ST,act}}$ $\eta_{\text{ST}} = \frac{h_3 - h_4}{h_3 - h_{4s}}, \quad \varepsilon_{\text{ST}} = \frac{\dot{W}_{\text{ST,act}}}{\dot{W}_{\text{ST,rev}}}$
 <p style="text-align: center;">Water cooled condenser</p>	$\dot{m}_5 = \dot{m}_4, \quad \dot{m}_a = \dot{m}_b$ $\dot{m}_4 (h_4 - h_5) = \dot{m}_a (h_b - h_a)$ $\dot{E}x_{\text{WCC,dest}} = \dot{m}_4 (ex_4 - ex_5) - \dot{m}_a (ex_b - ex_a)$ $\varepsilon_{\text{WCC}} = \frac{\dot{m}_a (ex_b - ex_a)}{\dot{m}_4 (ex_4 - ex_5)}$

 <p>Isobutane turbine</p>	$\dot{m}_9 = \dot{m}_8 = \dot{m}_{iso}$ $\dot{W}_{T,act} = \dot{m}_8(h_8 - h_9)$ $\dot{W}_{T,rev} = \dot{m}_8(ex_8 - ex_9)$ $\dot{E}x_{T,dest} = \dot{W}_{T,rev} - \dot{W}_{T,act}$ $\eta_T = \frac{h_8 - h_9}{h_8 - h_{9s}}, \quad \varepsilon_T = \frac{\dot{W}_{ST,act}}{\dot{W}_{ST,rev}}$
 <p>Air cooled condenser</p>	$\dot{m}_{10} = \dot{m}_9 = \dot{m}_{iso}, \quad \dot{m}_c = \dot{m}_d$ $\dot{m}_9(h_9 - h_{10}) = \dot{m}_c(h_d - h_c)$ $\dot{E}x_{ACC,dest} = \dot{m}_9(ex_9 - ex_{10}) - \dot{m}_c(ex_d - ex_c)$ $\varepsilon_{ACC} = \frac{\dot{m}_c(ex_d - ex_c)}{\dot{m}_9(ex_9 - ex_{10})}$
 <p>Pump</p>	$\dot{m}_{11} = \dot{m}_{10} = \dot{m}_{iso}$ $\dot{W}_{P,act} = \dot{m}_{10}(h_{11} - h_{10})$ $\dot{W}_{P,rev} = \dot{m}_{10}(ex_{11} - ex_{10})$ $\dot{E}x_{P,dest} = \dot{W}_{P,act} - \dot{W}_{P,rev}$ $\varepsilon_P = \frac{\dot{W}_{P,rev}}{\dot{W}_{P,act}}$
 <p>Heat exchanger</p>	$\dot{m}_7 = \dot{m}_6, \quad \dot{m}_{11} = \dot{m}_8$ $\dot{m}_6(h_6 - h_7) = \dot{m}_8(h_8 - h_{11})$ $\dot{E}x_{HE,dest} = \dot{m}_6(ex_6 - ex_7) - \dot{m}_8(ex_8 - ex_{11})$ $\varepsilon_{HE} = \frac{\dot{m}_8(ex_8 - ex_{11})}{\dot{m}_6(ex_6 - ex_7)}$
 <p>Preheater</p>	$\dot{m}_{12} = \dot{m}_{17} = \dot{m}_{water}, \quad \dot{m}_{16} = \dot{m}_{15} = \dot{m}_{geo}$ $\dot{m}_{12}(h_{17} - h_{12}) = \dot{m}_{15}(h_{15} - h_{16})$ $\dot{E}x_{PH,dest} = \dot{m}_{15}(ex_{15} - ex_{16}) - \dot{m}_{12}(ex_{17} - ex_{12})$ $\varepsilon_{PH} = \frac{\dot{m}_{12}(ex_{17} - ex_{12})}{\dot{m}_{15}(ex_{15} - ex_{16})}$



Application of energy and exergy balances on the components of combined flash-binary geothermal power plant and electrolysis unit gives the data in Table 3.4. The state numbers in Table 3.4 refer to Fig. 2.3. State 0, 0' and 0'' are the restricted dead states for geothermal water, binary working fluid, and air, respectively. The dead state is taken as 25°C and 100 kPa. For geothermal fluid, thermodynamic properties of water are used. The energy and exergy data in Table 3.4 is calculated using mass, energy and exergy balances based on the system operation and input data which include mass flow rate, temperature, and pressure values.

Table 3.4. System data, thermodynamic properties, and exergies with respect to state points in Fig. 2.3.

State	Fluid	Mass flow rate \dot{m} (kg/s)	Temperature T (°C)	Pressure P (kPa)	Enthalpy h (kJ/kg)	Entropy s (kJ/kg·K)	Specific exergy ex (kJ/kg)	Exergy rate $\dot{E}x$ (kW)
0	Geothermal	100	25	100	104.8	0.3672	0	0
0'	Isobutane	100	25	100	598.9	2.513	0	0
0''	Air	2793	25	100	298.6	5.695	0	0
1	Geothermal	100	200	1555	852.3	2.331	162.3	16,227
2	Geothermal	100	158.8	600	852.3	2.352	155.9	15,591
3	Geothermal	8.720	15.8	600	2756	6.759	746.4	6509
4	Geothermal	91.28	45.8	10	2233	7.049	137.0	1194
5	Geothermal	8.720	45.8	10	191.8	0.6492	2.851	24.86
6	Geothermal	91.28	158.8	600	670.4	1.931	99.50	9082
7	Geothermal	91.28	76.1	600	318.6	1.029	16.51	1507
8	Isobutane	60.79	148.8	2100	802.7	2.689	151.5	9209
9	Isobutane	60.79	100.4	400	732.5	2.722	71.27	4332
10	Isobutane	60.79	29.6	400	270.8	1.245	50.03	3041
11	Isobutane	60.79	30.7	2100	274.5	1.246	53.15	3231
12	Water	0.445	25	100	104.8	0.3669	0	0
13	Hydrogen	0.0498	70	100	688.6	64.83	117,113	5837

14	Oxygen	0.395	70	100	44.06	6.412	124.06	1606
15	Geothermal	100	74	36	307.6	0.9971	14.92	1492
16	Geothermal	100	73	36	306.6	0.9943	14.65	1465
17	Water	1	70	100	293.0	0.9549	12.95	12.95

Figure 3.6 shows exergy flows and losses in the system. The rate of exergy output by hydrogen is 7444 kW when the rate of exergy input by geothermal is 16,227 kW. The exergy flow diagram shows that 54.1% of the exergy rate entering the plant is lost. Most exergy losses occur in heat exchangers accounting for 51.7% of total exergy losses. This is mainly due to large temperature differences between the fluid streams. Electrolysis process accounts for 19.7% of the exergy losses and these losses are due to irreversible chemical reaction. Irreversible expansion of steam and isobutane is responsible for 1359 kW of exergy destruction rate. The exergy losses given in Figure 3.6 for individual components help us identify the most wasteful components in the system. An improvement of the system should start with the components with the greatest exergy losses. Reducing exergy losses is possible by reducing irreversibilities such as minimizing friction and heat transfer across a finite temperature difference, and avoiding irreversible chemical reactions.

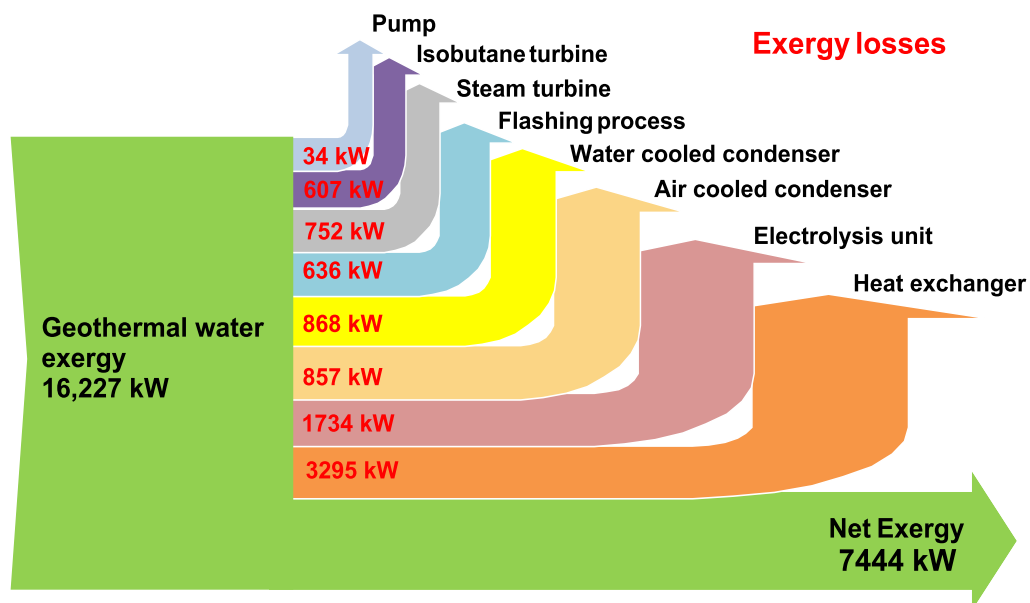


Figure 3.6. Exergy flow diagram of Model 2.

A liquid geothermal water resource at 200°C with a flow rate of 100 kg/s is used as the energy source. Under realistic operating conditions, 7572 kW power can be produced in the flash-binary geothermal power plant. The produced power is used for the electrolysis process. The electrolysis water can be preheated to 70°C by the geothermal water leaving the power plant and hydrogen can be produced at a rate of 0.050 kg/s. The actual specific work input for the electrolysis of hydrogen is calculated to be 151,964 kJ/kg H₂ or 42.2 kWh/kg H₂ at an electrolysis water temperature of 70°C. A higher electrolysis temperature increases hydrogen production rate and decreases electricity consumption. At an electrolysis temperature of 70°C, hydrogen can be produced at a rate of 0.050 kg/s while consuming 42.2 kWh of electricity per kg of hydrogen produced. At 25°C, the values are 0.0483 kg/s and 43.5 kWh, respectively. When electrolysis water temperature is increased from 25°C to 70°C, the work consumption decreases by about 3%.

The energy and exergy efficiencies of the flash-binary geothermal power plant are 10.4% and 46.6%, respectively. The corresponding efficiencies for the electrolysis system are 79.1% and 77.1.6%, respectively, and those for the overall system are 8.0% and 45.8%, respectively. A summary of thermodynamic analysis results are given in Table 3.5 for Model 2.

Table 3.5. Thermodynamic analysis results for Model 2.

Parameters	Results
Geothermal power net work output	7572 kW
Unit amount of hydrogen production	0.050 kg/s
Unit work input for electrolysis	151,964 kJ/kg H ₂ (42.2 kWh/kg H ₂)
Energy efficiency of geothermal power plant	10.4 %
Exergy efficiency of geothermal power plant	46.6 %
Energy efficiency of electrolysis unit	79.1 %
Exergy efficiency of electrolysis unit	77.1 %
Overall system energy efficiency	8.0 %
Overall system exergy efficiency	45.8 % (88.6 % by Fuel-Product approach)

The results of exergy analysis for system components are given in Table 3.6. The exergetic factor for all components was in the range between 0.1% and 0.7%. The highest value is for the electrolysis, which is the most destructive part mainly due to its high chemical disorder and short lifetime.

Table 3.6. Exergy analysis results for Model 2.

Component	$\dot{E}x_F$ (kW)	$\dot{E}x_P$ (kW)	$\dot{E}x_D$ (kW)	y^* (%)	y (%)	ε (%)
Steam turbine	5314	4562	752.0	10.60	1.25	85.81
Isobutane turbine	4877	3238	607.0	8.61	1.01	87.57
Pump	223.5	190.2	33.36	0.52	0.05	85.07
Heat exchanger	7575	5978	1597	22.50	2.66	78.91
Air cooler	1291	433.8	857.2	12.10	1.43	33.62
Water cooler	1170	300.8	868.3	12.21	1.45	25.71
Separator	15,591	15,591	0	0	0	100.0
Flash chamber	16,227	15,591	636.0	9.01	1.06	96.11
Preheater	27	12.95	13.13	0.22	0.022	48.00
Electrolyses	7572	5838	1734	22.50	2.90	77.00
Total system	59,868	51,736	7098	100.0	11.83	45.80

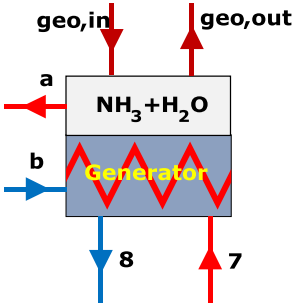
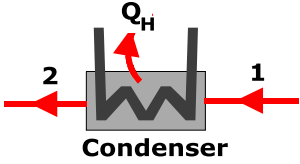
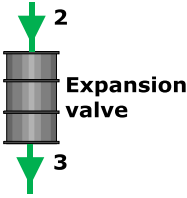
3.7.3 Model 3

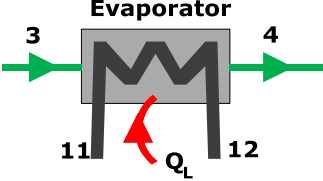
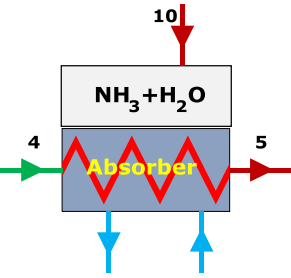
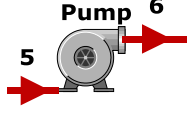
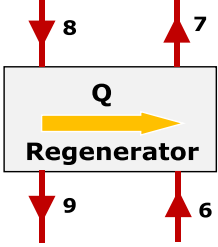
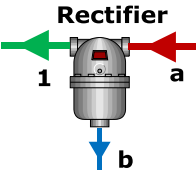
Again, the geothermal water resource is considered at 200°C with 100 kg/s flow rate. In the first part of this model, geothermal water is used as the heat source for the water ammonia absorption refrigeration system which is used to precool the hydrogen gas before it is liquefied. Thermophysical properties of the working fluids (geothermal water, ammonia-water, air, and hydrogen) are obtained from EES software with built-in thermodynamic property functions. The heat supplied by the geothermal water in the

generator of the absorption system is calculated to be 39,080 kW. In this operation, the geothermal water leaves the generator at 180°C. The system can cool hydrogen gas from 25°C to -26.9°C at a rate of 29.53 kg/s. Heat is removed from hydrogen at a rate of 21,733 kW.

The mass flow rate of the refrigerant is not constant due to changing ammonia-water composition. Table 3.7 gives mass, energy, and exergy balance equations for the system components. The states refer to Fig. 2.4.

Table 3.7. Mass, energy, and exergy relations for the components of the ammonia-water absorption refrigeration cycle.

System component	Mass, energy and exergy equations
	$\dot{Q}_{\text{gen}} = \dot{m}_{\text{geo}}(h_{\text{geo,in}} - h_{\text{geo,out}}), \quad \dot{m}_7 = \dot{m}_a$ $\dot{m}_7 h_7 + \dot{m}_b h_b + \dot{Q}_{\text{gen}} = \dot{m}_a h_a + \dot{m}_8 h_8$ $\dot{E}x_{\text{gen,dest}} = \dot{m}_{\text{geo}} ex_{\text{geo,in}} + \dot{m}_7 ex_7 + \dot{m}_b ex_b - \dot{m}_{\text{geo}} ex_{\text{geo,out}} - \dot{m}_a ex_a - \dot{m}_8 ex_8$ $\varepsilon_{\text{gen}} = \frac{\dot{m}_{\text{geo}} ex_{\text{geo,in}} + \dot{m}_7 ex_7 + \dot{m}_b ex_b}{\dot{m}_a ex_a + \dot{m}_8 ex_8 + \dot{m}_{\text{geo}} ex_{\text{geo,out}}}$
	$\dot{m}_1 = \dot{m}_2$ $\dot{m}_1 h_1 = \dot{Q}_H + \dot{m}_2 h_2$ $\dot{E}x_{\text{dest,cond}} = T_0 \left[\dot{m}_1 (s_2 - s_1) + \frac{\dot{Q}_H}{T_H} \right] \quad (T_H = T_0)$ $\varepsilon_{\text{cond}} = \frac{\dot{Q}_H (1 - T_0 / T_H)}{\dot{m}_1 (ex_1 - ex_2)}$
	$\dot{m}_3 = \dot{m}_2$ $h_3 = h_2$ $\dot{E}x_{\text{dest,EV}} = \dot{m}_2 (ex_2 - ex_3)$ $\varepsilon_{\text{EV}} = \frac{\dot{m}_3 ex_3}{\dot{m}_2 ex_2}$

	$\dot{m}_4 = \dot{m}_3$ $\dot{m}_3 h_3 = \dot{m}_4 h_4 + \dot{Q}_L$ $\dot{E}x_{\text{dest, evap}} = T_0 \left[\dot{m}_3 (s_4 - s_3) - \frac{\dot{Q}_L}{T_L} \right]$ $\varepsilon_{\text{evap}} = \frac{\dot{Q}_L (T_0 - T_L) / T_L}{\dot{m}_3 (ex_4 - ex_3)}$
	$\dot{m}_4 + \dot{m}_{10} = \dot{m}_5$ $\dot{m}_4 h_4 + \dot{m}_{10} h_{10} = \dot{m}_5 h_5 + \dot{Q}_A$ $\dot{E}x_{\text{dest, abs}} = \dot{m}_4 ex_4 + \dot{m}_{10} ex_{10} - \dot{m}_5 ex_5 - \dot{Q}_A \left(1 - \frac{T_0}{T_A} \right) (T_A = T_0)$ $\varepsilon_{\text{abs}} = \frac{\dot{m}_5 ex_5}{\dot{m}_4 ex_4 + \dot{m}_{10} ex_{10}}$
	$\dot{m}_6 = \dot{m}_5$ $\dot{W}_{P, \text{act}} = \dot{m}_6 h_6 - \dot{m}_5 h_5 \quad \text{and} \quad \dot{W}_{P, \text{rev}} = \dot{m}_6 ex_6 - \dot{m}_5 ex_5$ $\dot{E}x_{\text{dest, P}} = \dot{W}_{P, \text{act}} - \dot{W}_{P, \text{rev}}, \quad \varepsilon_P = \frac{\dot{W}_{P, \text{rev}}}{\dot{W}_{P, \text{act}}}$
	$\dot{m}_7 = \dot{m}_6 \quad \dot{m}_9 = \dot{m}_8$ $\dot{m}_6 h_6 + \dot{m}_8 h_8 = \dot{m}_7 h_7 + \dot{m}_9 h_9$ $\dot{E}x_{\text{dest, R}} = \dot{m}_6 (ex_6 - ex_7) - \dot{m}_8 (ex_8 - ex_9)$ $\varepsilon_R = \frac{\dot{m}_8 (ex_8 - ex_9)}{\dot{m}_6 (ex_6 - ex_7)}$
	$\dot{m}_a = \dot{m}_1 + \dot{m}_b$ $\dot{m}_a x_a = \dot{m}_1 x_1 + \dot{m}_b x_b$ $\dot{E}x_{\text{dest, rect}} = \dot{m}_a ex_a - \dot{m}_1 ex_1 - \dot{m}_b ex_b$ $\varepsilon_{\text{rect}} = \frac{\dot{m}_1 ex_1 + \dot{m}_b ex_b}{\dot{m}_a ex_a}$

In Table 3.7, \dot{Q} is the heat load; x is the mass fraction of ammonia and \dot{m}_1 is the mass flow rate of the ammonia used as the refrigerant. State 5 is taken as a saturated liquid at the temperature of the cooling water. The compression process is almost isothermal in the pump. The process is isenthalpic in the expansion valve. Using the operating data of the system and the formulations in Table 3.7, various performance parameters are obtained and listed in Table 3.8.

Table 3.8. System data, thermodynamic properties, mass flow rates, and exergy data of the system with respect to the state points of the ammonia-water absorption refrigeration cycle in Fig. 2.4.

State	Fluid	Temperature T (°C)	Pressure P (kPa)	Enthalpy h (kJ/kg)	Entropy s (kJ/kg·°C)	Specific exergy ex (kJ/kg)	Mass flow rate \dot{m} (kg/s)	Exergy rate $\dot{E}x$ (kW)
0	Geothermal	25	101.3	104.8	0.3672	0	100	-
0'	NH ₃ -H ₂ O	25	101.3	29.43	0.7321	0	89.19	-
geo,in	Geothermal water	200	-	851.6	2.329	162	100	16,202
geo,out	Geothermal water	180	-	460.8	1.417	42.97	100	4297
a	NH ₃ -H ₂ O	130.8	1501.3	661.3	2.368	144.2	89.19	12,863
b	Weak solution	130.8	1501.3	401.1	1.648	98.77	71.41	7053
1	Pure ammonia	130.8	1501.3	1706	5.263	326.7	17.78	5810
2	Pure ammonia	25	1501.3	10.76	0.3568	93.17	17.78	1657
3	Pure ammonia	-29.3	101.3	10.76	0.463	61.51	17.78	1094
4	Pure ammonia	-29.3	101.3	1233	5.168	-118.6	17.78	-2108
5	NH ₃ -H ₂ O	25	101.3	29.43	0.7321	0	89.19	0
6	NH ₃ -H ₂ O	57.6	1501.3	31.67	0.7045	10.45	89.19	932.2
7	NH ₃ -H ₂ O	100	1501.3	223.1	1.249	39.61	89.19	3533
8	Weak solution	130.8	1501.3	401.1	1.648	98.77	71.41	7053
9	Weak solution	77.5	1501.3	161.9	1.013	48.74	71.41	3480

10	Weak solution	46.9	101.3	161.9	1.041	40.47	71.41	2890
11	Hydrogen	25	101.3	3929	53.37	0	29.53	0
12	Hydrogen	-26.9	101.3	3194	50.65	72.42	29.53	2138

The COP of the ammonia-water absorption cycle is determined to be 0.556, and the exergy efficiency is calculated to be 67.0% using the fuel-product approach. Also, the rotational exergy efficiency is calculated to be 18.0%.

Figure 3.7 shows an exergy flow diagram depicting the exergy destructions throughout the cycle. The total exergy input is 41,615 kW while the total exergy product is 32,114 kW, indicating a cycle exergy efficiency of 67.0%. The most destructive components (condenser, generator, and evaporator) involve highly irreversible processes such as mixture heat absorption and high gradient heat transfer.

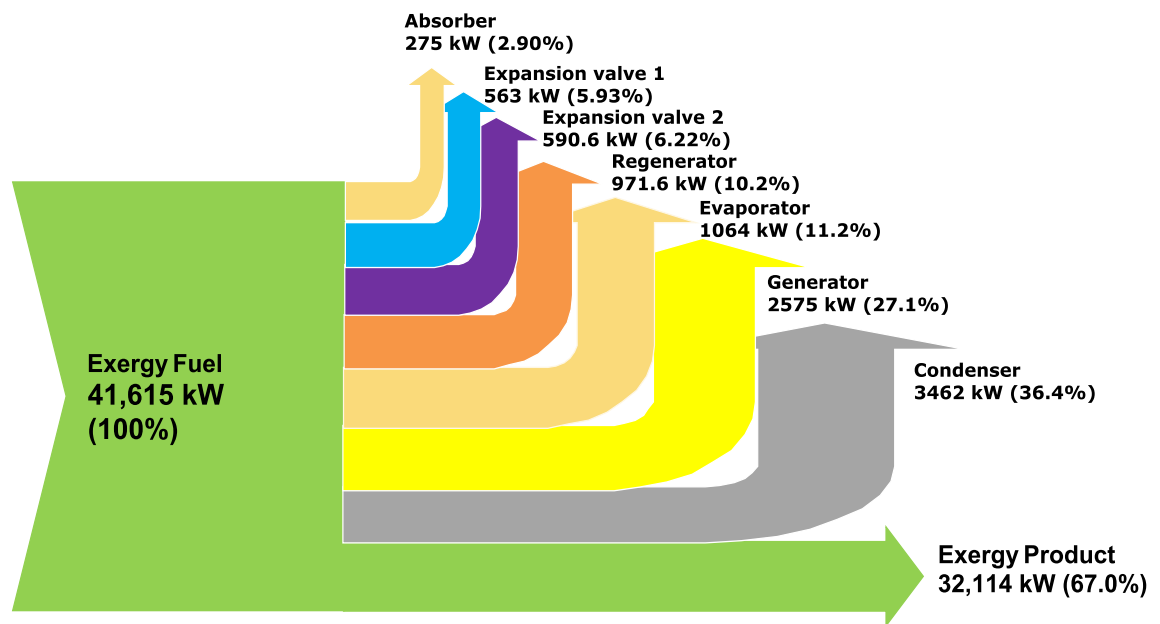


Figure 3.7. Exergy flow diagram depicting the exergy destructions in the components of absorption refrigeration cycle.

For the operations of the Claude cycle, the following assumptions are used: Compressor isothermal efficiency = 70%, Turbine isentropic efficiency = 80%, Heat exchanger effectiveness = 95%, Compressor exit pressure = 5 MPa. Hydrogen gas enters the

Claude cycle at -26.9°C and 100 kPa, and is liquefied to -253°C . The parameter of figure of merit (FOM) is considered as an indicator of performance of a liquefaction cycle. In Fig. 3.8, the effect of compression pressure on the liquefaction work and FOM value defined as the reversible work input of liquefaction divided by the actual work input are investigated.

As the pressure is increased, the FOM first increases, reaches a maximum, and then decreases. It turns out that the FOM reaches its maximum value at a pressure of 5 MPa. This point also represents the optimum point for minimum work consumption. This optimum pressure is used in this study.

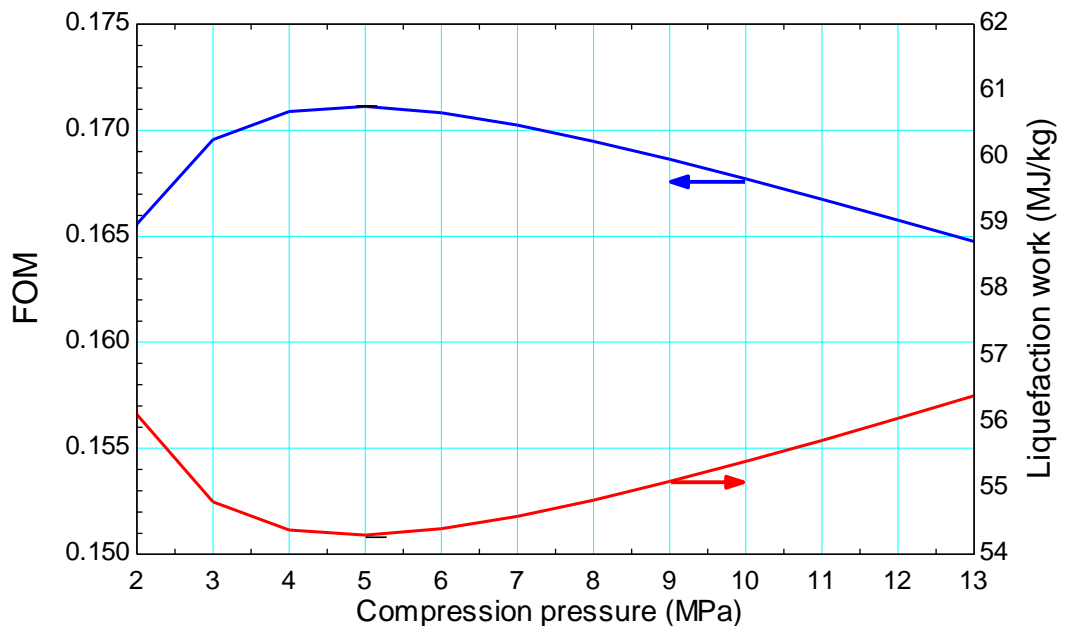
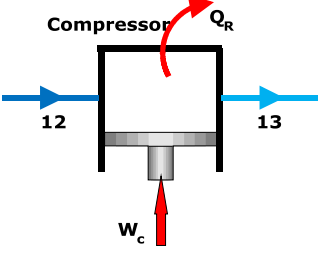
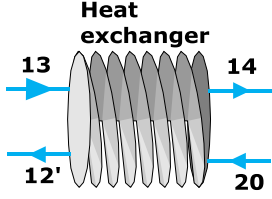
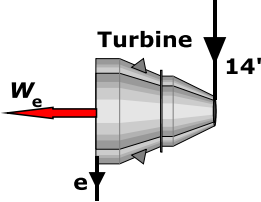
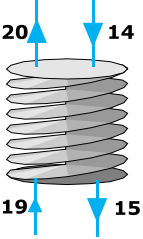


Figure 3.8. Optimum compression pressure of Claude liquefaction cycle.

In Table 3.9, mass, energy and exergy relations for the Claude liquefaction cycle are given. The states refer to Fig. 2.4. Using the operating data of the system and the formulations in Table 3.9, various performance parameters are obtained and listed in Table 3.10.

Table 3.9. Mass, energy and exergy relations for the components of the Claude liquefaction cycle.

Component	Mass, energy and exergy equations
	$\dot{m}_{12} = \dot{m}_{13}$ $\dot{W}_{comp,act} = \frac{\dot{m}_{12} RT_0 \ln(P_{13}/P_{12})}{\eta_{comp}}$ $\dot{W}_{comp,rev} = \dot{m}_{12} (ex_{13} - ex_{12})$ $\dot{E}x_{comp,dest} = \dot{W}_{comp,act} - \dot{W}_{comp,rev}$ $\varepsilon_{comp} = \frac{\dot{W}_{comp,rev}}{\dot{W}_{comp,act}}, \quad \eta_{comp} = \frac{h_{13s} - h_{12}}{h_{13} - h_{12}}$
	$\dot{m}_{13} = \dot{m}_{14} \quad \dot{m}_{12'} = \dot{m}_{20} = \dot{m} - \dot{m}_f$ $\dot{m}_{13} (h_{13} - h_{14}) = \dot{m}_{20} (h_{12'} - h_{20})$ $\dot{E}x_{HX1,dest} = \dot{m}_{13} (ex_{13} - ex_{14}) - \dot{m}_{20} (ex_{12'} - ex_{20})$ $\varepsilon_{HX1} = \frac{\dot{m}_{20} (ex_{12'} - ex_{20})}{\dot{m}_{13} (ex_{13} - ex_{14})}$
	$\dot{m}_{14'} = \dot{m}_e$ $\dot{W}_{turb,act} = \dot{m}_e (h_{14'} - h_e), \quad \eta_{turb} = \frac{h_{14'} - h_e}{h_{14'} - h_{es}}$ $\dot{W}_{turb,rev} = \dot{m}_e (ex_{14'} - ex_e), \quad \varepsilon_{turb} = \frac{\dot{W}_{turb,act}}{\dot{W}_{turb,rev}}$ $\dot{E}x_{turb,dest} = \dot{W}_{turb,rev} - \dot{W}_{turb,act}$
	$\dot{m}_{14} = \dot{m}_{15}, \quad \dot{m}_{14} = \dot{m} - \dot{m}_e, \quad \dot{m}_{19} = \dot{m}_{20}$ $\dot{m}_{14} (h_{14} - h_{15}) = \dot{m}_{19} (h_{20} - h_{12'})$ $\dot{E}x_{HX2,dest} = \dot{m}_{14} (ex_{14} - ex_{15}) - \dot{m}_{19} (ex_{20} - ex_{19})$ $\varepsilon_{HX2} = \frac{\dot{m}_{19} (ex_{20} - ex_{19})}{\dot{m}_{14} (ex_{14} - ex_{15})}$

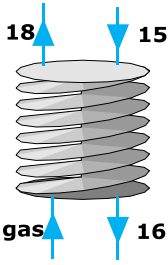
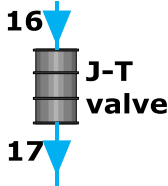
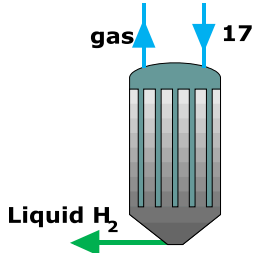
	$\dot{m}_{15} = \dot{m}_{16} \quad \dot{m}_{18} = \dot{m}_{\text{gas}} \quad \dot{m}_{\text{gas}} = \dot{m} - \dot{m}_e - \dot{m}_f$ $\dot{m}_{15}(h_{15} - h_{14}) = \dot{m}_{\text{gas}}(h_{18} - h_{\text{gas}})$ $\dot{E}x_{HX3,\text{dest}} = \dot{m}_{15}(ex_{15} - ex_{16}) - \dot{m}_{\text{gas}}(ex_{18} - ex_{\text{gas}})$ $\varepsilon_{HX3} = \frac{\dot{m}_{\text{gas}}(ex_{18} - ex_{\text{gas}})}{\dot{m}_{15}(ex_{15} - ex_{16})}$
	$\dot{m}_{16} = \dot{m}_{17}$ $h_{16} = h_{17}$ $\dot{E}x_{JT,\text{dest}} = \dot{m}_{16}(ex_{16} - ex_{17})$ $\varepsilon_{JT} = \frac{\dot{m}_{17}ex_{17}}{\dot{m}_{16}ex_{16}}$
	$\dot{m}_7 = \dot{m} - \dot{m}_e \quad \dot{m}_{\text{gas}} = \dot{m} - \dot{m}_e - \dot{m}_f$ $\dot{m}_{13}h_{13} = (\dot{m} - \dot{m}_f)h_{12} + \dot{m}_e(h_{14} - h_e) + \dot{m}_f h_f$ $\dot{m}_f h_f = \dot{m}_{\text{gas}} h_{\text{gas}} + \dot{m}_{17} h_{17}$ $\dot{E}x_{Liq,\text{dest}} = \dot{m}_{17}ex_{17} - \dot{m}_{\text{gas}}ex_{\text{gas}} - \dot{m}_f ex_f$ $\varepsilon_{Liq} = \frac{\dot{m}_{\text{gas}}ex_{\text{gas}} + \dot{m}_f ex_f}{\dot{m}_{17}ex_{17}}$

Table 3.10. System data, thermodynamic properties, mass flow rates, and exergy data of the system with respect to the state points of the Claude liquefaction cycle.

State	Fluid (Hydrogen)	Temperature T (°C)	Pressure P (kPa)	Enthalpy h (kJ/kg)	Entropy s (kJ/kg·°C)	Specific exergy ex (kJ/kg)	Mass flow rate \dot{m} (kg/s)	Exergy rate $\dot{E}x$ (kW)
0	Gas	25	101.3	3929	53.37	0	29.53	0
12	Gas	-26.9	101.3	3194	50.65	72.35	29.53	2138
13	Gas	-26.9	5000	3207	34.5	4901	29.53	144,717
14	Gas	-113	5000	2015	28.55	5481	11.81	64,739
14'	Gas	-113	5000	2015	28.55	5481	17.72	97,124
15	Gas	-213.66	5000	684.1	15.27	8107	11.81	95,755
16	Gas	-225.84	5000	450.4	10.84	9194	11.81	108,598
17	Liquid	-252.59	101.3	450.4	22.11	5835	11.81	68,923

18	Gas	-208	101.3	926	34.56	2602	23.5	15,050
19	Gas	-198.46	101.3	1027	36	2271	23.5	53,378
20	Gas	-137.3	101.3	1696	26.39	5806	23.5	136,462
<i>e</i>	Gas	-210	101.3	906	34.25	2675	17.72	47,390
<i>g</i>	Gas	-252.59	101.3	448.7	22.03	5858	5.784	33,751
<i>f</i>	Liquid	-252.59	101.3	0.001913	0.00009282	11974	6.028	72,175

The minimum work requirement in the Claude liquefaction cycle is calculated to be 9272 kJ/kg H₂ (or 2.57 kWh/kg H₂) for an inlet temperature of -26.9°C and a pressure of 100 kPa. The power input for a hydrogen mass flow rate of 29.53 kg/s is determined to be 273,812 kW. For the actual operation of the cycle, out of 29.53 kg/s hydrogen entering the system, only 6.028 kg/s can be liquefied. This corresponds to $f_{\text{liquid}} = 0.2041$. The actual work consumption in the liquefaction cycle is calculated as 54,301 kJ/kg H₂ (or 15.08 kWh/kg H₂) for a gas inlet temperature of -26.9°C. These values correspond to a Figure of Merit (FOM) value of 17.0%. If an inlet gas temperature of 25°C is used, the work consumption becomes 72,785 kJ/kg H₂ (or 20.22 kWh/kg H₂). Therefore, precooling of hydrogen gas in the absorption refrigeration cycle decreases the work consumption in liquefaction by 25.4%.

The COP of the Claude liquefaction cycle is calculated to be 0.012. The Claude cycle exergy efficiency is calculated to be 17.0% by taking the ratio of the minimum and actual work inputs. According to the fuel-product approach, the exergy efficiency of the cycle is 67.3%. Using the rotational exergy efficiency, the liquefaction cycle is 54.3%. The rotational efficiency is defined as the work input of compressor and inlet exergy of hydrogen gas at state 12 divided by the turbine work output and liquid hydrogen exergy. Fig. 3.9 gives exergy destructions for the cycle components. The most destructive components are heat exchangers 1 and 2 and the J-T valve, representing 26.3%, 25.2%, and 19.2% of the total exergy destruction in the cycle, respectively. An investigation of the exergy flow diagram for the Claude cycle given in Fig. 3.9 shows that 32.7% of the exergy entering the system is destroyed. The remaining 67.3% is converted to exergy product. Heat exchangers have largest irreversibilities due to high temperature difference between the fluids exchanging heat.

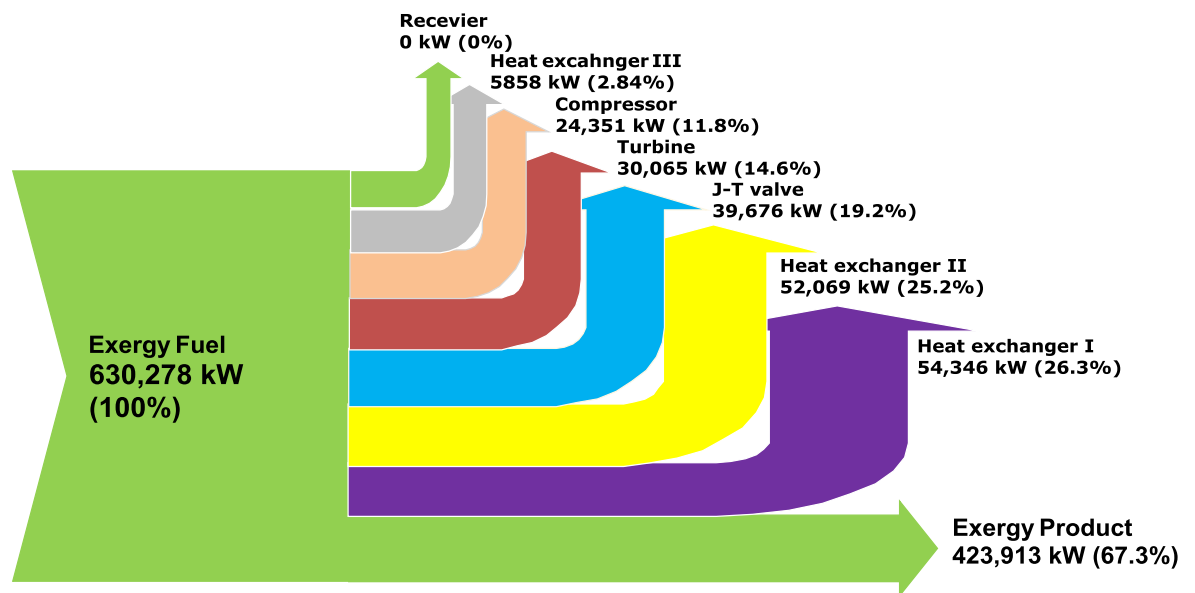


Figure 3.9. Exergy flow diagram depicting the exergy destructions in the Claude liquefaction cycle.

The exergy destruction results for individual components help us identify the most wasteful components in the system. An improvement of the system should start with the components with greatest exergy destructions.

Reducing exergy destructions is possible by reducing irreversibilities such as minimizing friction and heat transfer across a finite temperature difference. The exergy analysis is particularly valuable for geothermal systems since their work potentials are low due to low resource temperatures. For geothermal powered cooling systems, the system COP is related to the first law of thermodynamics while exergy efficiency is related to the second law. A measure of improvement potential of the system is possible with exergy analysis by means of increasing exergy efficiency and decreasing exergy destruction.

The overall system exergy input, output, and destructions shown in Fig. 3.10 are based on the fuel-product approach. The net exergy output of the overall system is calculated to be 456,027 kW while the total input exergy is 671,893 kW. The exergy flow diagram given in Fig. 3.10 shows that 32.1% of the exergy entering the plant is destroyed, and the remaining 67.9% is converted into exergy output.

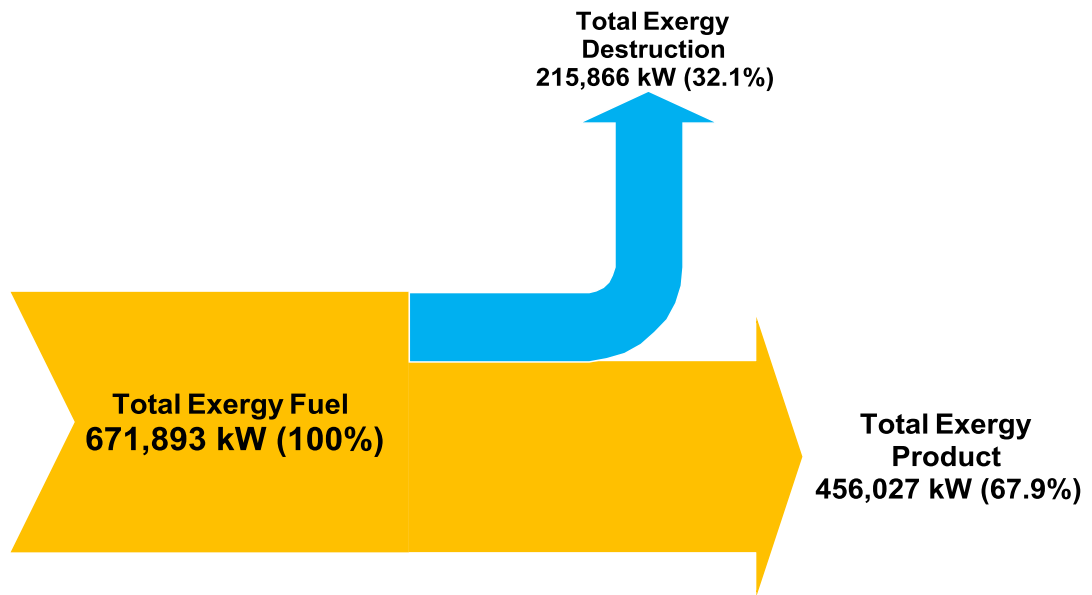


Figure 3.10. Exergy flow diagram of the overall system based on fuel-product approach.

In Fig. 3.11, we show the integrated system in a box and illustrate various exergy input and output streams and terms. This diagram does not consider internal irreversibilities of each system component. Main system exergy inputs are due to geothermal water, compressor work, and hydrogen gas (zero exergy). The main exergy outputs of the system are turbine work, geothermal water, and liquefied hydrogen. The ratio of total exergy output to exergy input is less than one for an irreversible process, and the magnitude of the deviation from the unity is a measure of the degree of irreversibility for the process. For a fully reversible process, the ratio is one. This definition of exergy efficiency is also called rotational efficiency. Based on Fig. 3.11, the rotational exergy efficiency of overall system is calculated to be 22.5%. Also, the overall COP of the integrated system is determined to be 0.162.

Thermodynamic analysis results of Model 3 are summarized in Table 3.11.

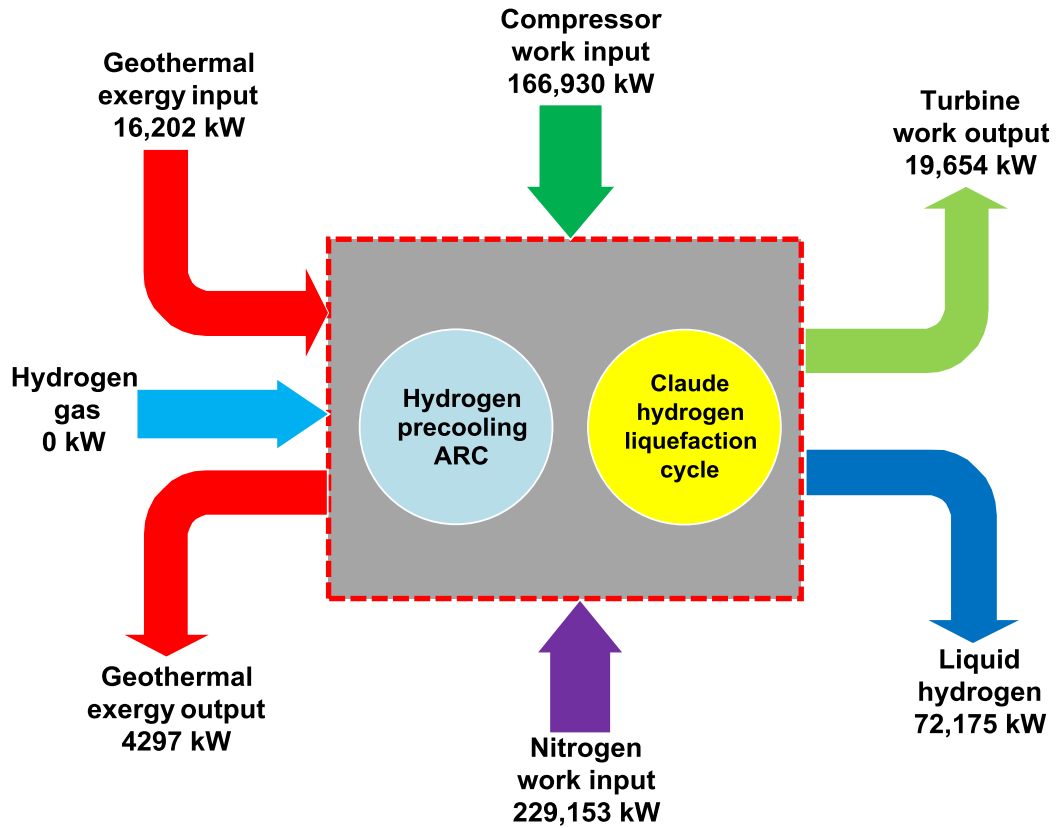


Figure 3.11. Various exergy input and output parameters in Model 3.

Table 3.11. Thermodynamic analysis results of Model 3.

Parameter	Result
Cooling load of absorption cycle (\dot{Q}_L)	21,733 kW
Hydrogen gas cooling temperature and its flow rate	-26.9°C and 29.53 kg/s
COP of ammonia-water absorption cycle COP	0.556
Exergy efficiency of ammonia-water absorption cycle	67.0 %
Minimum work consumption in the liquefaction cycle	9272 kJ/kg H ₂ (2.57 kWh/kg H ₂)
Liquefaction rate of cycle \dot{m}_f	6.028 kg/s
Liquefaction fraction of cycle (f_{liquid})	0.2041
Actual work consumption in the liquefaction cycle	36,799 kJ/kg H ₂ (10.22 kWh/kg H ₂)

COP of Claude liquefaction cycle	0.012
Claude cycle exergy efficiency	17.1 %
Exergy efficiency of Claude cycle (Fuel- Product approach)	67.3 %
Rotational exergy efficiency of Claude liquefaction cycle (FOM)	25.1 %
Overall COP of Model 3	0.162
Overall exergy efficiency of Model 3	22.5 % (67.9 % by Fuel- Product approach)

3.7.4 Model 4

In this model, hydrogen is cooled in an absorption refrigeration cycle. High temperature geothermal water leaving the absorption cooling cycle is used to produce electricity in a power plant. Geothermal electricity is used to liquefy precooled hydrogen gas in the Claude liquefaction cycle. Under realistic operating conditions, 1022 kW power can be produced in the geothermal power plant.

The produced power is used for the Claude liquefaction cycle to liquefy the hydrogen. Thermodynamic analysis results of Model 4 are given in Table 3.12.

Table 3.12. Thermodynamic analysis results of Model 4.

Parameter	Result
Cooling load of absorption cycle, \dot{Q}_L	21,733 kW
Hydrogen gas cooling temperature and its flow rate	-26.9°C and 29.53 kg/s
Minimum work consumption in the liquefaction cycle	9272 kJ/kg H ₂ (2.57 kWh/kg H ₂)
Liquefaction rate of hydrogen, \dot{m}_f	6.028 kg/s
Liquefaction fraction, f_{liquid}	0.2041

Actual work consumption in the liquefaction cycle	36,226 kJ/kg H ₂ (10.06 kWh/kg H ₂).
Energy efficiency of geothermal power plant	5.7 %
Exergy efficiency of geothermal power plant	32.56 %
Geothermal plant net power output	1022 kW
Rotational exergy efficiency of liquefaction cycle (FOM)	25.5 %
Overall COP of Model 4	0.556
Overall exergy efficiency of Model 4	27.36 % (67.0 % by Fuel-Product approach)

3.7.5 Model 5

In this model, hydrogen liquefaction by a Claude liquefaction cycle using power from a geothermal power plant is considered. The model is simulated in computer environment and thermodynamic analysis is performed. The results of Model 5 are given in Table 3.13.

Table 3.13. Thermodynamic analysis results of Model 5.

Parameter	Result
Geothermal plant power output	7572 kW
Ideal work consumption of liquefaction cycle	11,097 kJ/kg H ₂ (3.08 kWh/kg H ₂)
Actual work consumption of liquefaction cycle	54,292 kJ/kg H ₂ (15.08 kWh/kg H ₂)
Unit liquefaction rate of hydrogen, \dot{m}_f	0.1714 kg/s
Energy efficiency of geothermal power plant	10.4 %
Exergy efficiency of geothermal power plant	46.6 %
Exergy efficiency of liquefaction cycle	20.4%
COP of the liquefaction cycle	0.153

Overall energy efficiency of Model 5	13.9 %
Overall exergy efficiency of Model 5	19.2 % (84.1 % by Fuel-Product approach)

3.7.6 Model 6

In this model, the electrical power of electrolysis and liquefaction processes is supplied from the geothermal power plant. Part of geothermal power is used for electrolysis to produce hydrogen gas and the remaining part is used for liquefaction of hydrogen gas. In this system, the first flash pressure is taken 600 kPa at state 2. The pressures at the inlet and exit of binary turbines are 2100 and 400 kPa, respectively. The pressure at the steam turbine exit is 10 kPa. Isentropic efficiencies of all turbines and pumps are assumed to be 85%. Electrolysis operation pressure and temperature are assumed to be 1 atm and 25°C, respectively. Liquefaction cycle compressor pressure is taken as 4000 kPa. The cryogenic turbine gas fraction (x) is assumed to be 0.6.

A parameter " β " is defined as the ratio of the work used in liquefaction cycle to the work used in electrolysis unit:

$$\beta = \frac{\dot{W}_{liquid,H_2}}{\dot{W}_{electrolysis,H_2}} \quad (3.54)$$

Thermodynamic analysis results of the Model 6 are summarized in Table 3.14.

Table 3.14. Thermodynamic analysis results of Model 6.

Parameter	Result
Geothermal power output	7572 kW
Unit work input of electrolysis	156,844 kJ/kg H ₂ (43.5 kWh/kg H ₂)
Unit work consumption in liquefaction cycle	54,292 kJ/kg H ₂

	(15.08 kWh/kg H ₂)
Work ratio (β)	0.346
Hydrogen production rate	0.029 kg/s
Hydrogen liquefaction rate	0.005 kg/s
Overall energy efficiency of Model 6	5.63 %
Overall exergy efficiency of Model 6	28.8 % (87.3 % by Fuel-Product approach)

CHAPTER 4

THERMOECONOMIC ANALYSIS

4.1 Introduction

Since exergy measures the true thermodynamic values of the work, heat, and other interactions between the system and its surroundings as well as the effect of irreversibilities within the system, exergy is a rational basis for applying costs. This aspect of thermoeconomics is called exergy costing.

There are typically four steps in the methodology of an exergoeconomic analysis. The first step is calculation of mass, energy and exergy balances of the analyzed system. The second step is performing a conventional exergy analysis including definition of fuel exergy and product exergy for each stream and the entire system. The third step is calculation of levelized cost rate for each component based on its purchased equipment cost (PEC). For calculating the levelized cost, the total revenue requirement (TRR) method is applied with appropriate economic assumptions. The fourth step is application of the exergy costing method to combine the cost and exergy values, and the calculation of useful exergoeconomic variables [67].

The working capacity of the models is taken as 95% with an annual operating hours of 8322 hours. The capacity factor is taken as 90% for absorption cooling and liquefaction cycle [68].

Within the concept of the assumed economic conditions, the capital recovery factor (CRF) is calculated to be 0.205. This value is used in the analysis of basic economic analysis of the models. Constant escalation levelization factor (CELF) is calculated to be 1.335. Aspen Plus software is used for some economic assumptions and data as well as EES program for the analysis [68, 69].

4.2 Economic Analysis

The economic analysis takes into account the cost of the each component, operating and maintenance costs and the cost of fuel consumption. Component costs have to be expressed as functions of thermodynamic variables. For an economic analysis, the levelized values of capital investment, fuel costs, and operating and maintenance costs (OMC) for the entire economic life of the analyzed plant are typically calculated. Here, total revenue requirement (TRR) method is applied. Table 4.1 summarizes the main assumptions and parameters used in the economic analysis. The economic life for all components and for the overall system is assumed to be 20 years except for the water electrolysis unit. The electrolysis unit life time is assumed to be 40,000 h, and therefore the electrolysis unit should be replaced every 5 years since 40,000 h with 85% of capacity factor cover nearly 5 years. The future value of the purchased equipment cost of the electrolysis unit is predicted using the nominal escalation rate (e.g. 5.0%), and discounted to the present value using the average interest rate of return (e.g. 15%) [68].

Table 4.1. Aspen Plus assumptions for the economic analysis of system [68].

Parameter	Value
IF (ROR Interest Factor)	1.5
Nominal escalation rate (%)	5
Construction period (yr) (1 January 2014 - 1 January 2015)	1
Start of commercial operation	January 2016
Economic life time for the plant (yr)	20
Tax related plant life time (yr)	15
Average annual capacity factor (%)	85
Average labour cost (\$/yr)	482,130
Fixed O&M cost (\$/yr)	161,075
Unit cost of isobutane (\$/GJ)	15.6

Salvage Value (Percent of Initial Capital Cost, %)	20
Depreciation Method	Straight Line
Tax Rate (%)	40
AF (ROR Annuity Factor, %)	5
ROR (Desired Rate of Return/Interest Rate, %)	15
Working Capital Percentage (%)	5

The purchased equipment costs (PEC) of all components are calculated based on the Aspen Plus economic analysis library and updated to the values for January 1, 2014 [68]. The capital recovery factor (CRF) depends on the interest rate as well as estimated equipment life time. CRF is determined using [70]

$$\text{CRF} = \frac{i(1+i)^N}{(1+i)^N - 1} \quad (4.1)$$

where i is the interest rate and N is the total operating period of the system in years.

The term \dot{Z}_k is the total cost rate (\$/h) associated with capital investment and the maintenance costs for the k th equipment item

$$\dot{Z}_k = \dot{Z}_k^{\text{CI}} + \dot{Z}_k^{\text{OM}} \quad (4.2)$$

The annual levelized capital investment and operating and maintenance costs for the k th component can be calculated as

$$\dot{Z}_k^{\text{CI}} = \frac{\text{CRF}}{\tau} C_k (1 + r_n)^2 \quad (4.3)$$

$$\dot{Z}_k^{\text{OM}} = \left(\text{CRF} \frac{C_{\text{L,OM}}}{\tau} \right) \sum_k C_k \quad (4.4)$$

where C_k is the purchased equipment cost of k -th component in US dollar, τ is the annual plant operation hours at full load, $C_{L,OM}$ is the overall levelized operating and maintenance cost of system, and r_n is the nominal escalation rate of investment. The levelized operating and maintenance cost of $C_{L,OM}$ are calculated and the values are distributed to each component, also proportionally to the purchased equipment cost. Finally, the values are converted considering the capacity factor of the entire plant operation by total cost rate of each component (\dot{Z}_k).

4.3 Specific Exergy Costing (SPECOC) Method

Cost accounting is concerned primarily with (a) determining the actual cost of products or services, (b) providing a rational basis for pricing goods or services, (c) providing a means for allocating and controlling expenditures, and (d) providing information on which operating decisions may be based and evaluated [71]. This frequently calls for the use of cost balances. In a conventional economic analysis, a cost balance is usually formulated for the overall system (subscript tot) operating at steady state

$$\dot{C}_{P,TOT} = \dot{C}_{F,TOT} + \dot{Z}_{TOT}^{CI} + \dot{Z}_{TOT}^{OMC} \quad (4.5)$$

The cost balance expresses that the cost rate associated with the product of the system (C_P) equals the total rate of expenditures made to generate the product, namely the fuel cost rate (C_F) and the cost rates associated with capital investment (\dot{Z}_k^{CI}) and operating and maintenance cost (\dot{Z}_k^{OMC}). When referring to a single stream associated with a fuel or product, the expression fuel stream or product stream is used.

There are different thermoeconomic approaches in the literature. Among them specific exergy costing method (SPECOC) [72] is used throughout this study. This method is based on specific exergies and costs per exergy unit, exergy efficiencies, and the auxiliary costing equations for components of thermal systems. The method consists of the following three steps: (i) identification of exergy streams, (ii) definition of fuel and product for each component of thermal system and (iii) allocation of cost equations.

In exergy costing, a cost is associated with each exergy stream. Exergy transfers by the entering and exiting streams of matter and by power and heat transfer rates may be written respectively as

$$\dot{C}_i = c_i \dot{E}x_i = c_i (\dot{m}_i ex_i) \quad (4.6)$$

$$\dot{C}_e = c_e \dot{E}x_e = c_e (\dot{m}_e ex_e) \quad (4.7)$$

$$\dot{C}_w = c_w \dot{W} \quad (4.8)$$

$$\dot{C}_q = c_q \dot{E}x_q \quad (4.9)$$

Accordingly, for a component receiving heat transfer and generating power, we may write [73]

$$\sum_e (c_e \dot{E}x_e)_k + c_{w,k} \dot{W}_k = c_{q,k} \dot{E}x_{q,k} + \sum_i (c_i \dot{E}x_i)_k + \dot{Z}_k \quad (4.10)$$

where c_i , c_e , c_w and c_q denote average costs per unit of exergy in dollars per gigajoule (\$/GJ). A cost balance applied to the k_{th} system component shows that the sum of cost rates associated with all exiting exergy streams equals the sum of cost rates of all entering exergy streams plus the appropriate charges due to capital investment (\dot{Z}_k^{CI}) and operating and maintenance expenses (\dot{Z}_k^{OMC}). The sum of last two terms is denoted by \dot{Z}_k . This equation simply states that the total cost of the exiting exergy streams equals the total expenditure to obtain them: the cost of the entering exergy streams plus the capital and other costs. Note that when a component receives power (as in a compressor or a pump) the second term on the left hand side would move with its positive sign to the right side of this expression.

To calculate the specific cost of each stream, a cost balance for each component should be stated as shown in Eq. (4.11), and it can be re-stated as Eq. (4.12) based on the concept of fuel exergy and product exergy for the component. Eq. (4.11) implies that the cost of the exergy of fuel and the cost of capital investment for each component are charged to the exergy of product of the same component.

$$\sum_1^m \dot{C}_i + \dot{Z}_k = \sum_1^n \dot{C}_e \quad (4.11)$$

$$\dot{C}_F + \dot{Z}_k = \dot{C}_P \quad (4.12)$$

Here, the subscripts F and P represent fuel and product, respectively and \dot{Z}_k is the component cost rate.

In general, if the number of streams that exit the component is larger than 1, the appropriate auxiliary equations are required to complete the calculation for the auxiliary equations. The F-rule is applied on the fuel exergy side and the P-rule is applied on the product exergy side [74]. In addition to the F-rule and P-rule, boundary conditions of incoming streams must be used as auxiliary equations. For example, the cost of the supplied fuel, water, air, and of other raw materials must be specified. The specific cost of incoming stream of air and water can be regarded as zero with no significant error.

When the cost rate equations and auxiliary equations are solved mathematically, the parameters for the exergoeconomic analysis can be calculated [75]. The cost of exergy destruction is

$$\dot{C}_{D,k} = c_{F,k} \dot{E}x_{D,k} \quad (4.13)$$

where $c_{F,k}$ is a specific cost of the fuel exergy for the k -th component and is calculated from

$$c_{F,k} = \frac{\dot{C}_{F,k}}{\dot{E}x_{F,k}} \quad (4.14)$$

The specific cost of the product exergy $c_{P,k}$ for the k -th component can be calculated as

$$c_{P,k} = \frac{\dot{C}_{P,k}}{\dot{E}x_{P,k}} \quad (4.15)$$

The exergoeconomic factor f_k , which indicates how much the capital investment contributes to the total cost, is calculated by

$$f_k = \frac{\dot{Z}_k}{\dot{Z}_k + \dot{C}_{D,k}} \quad (4.16)$$

In components showing a high value of exergoeconomic factor, the capital investment has a dominant effect on the total cost for the component. Therefore, reducing investment cost at the expense of thermodynamic efficiency can be considered for reducing the cost of the product for the overall system. A relatively low value of exergoeconomic factor implies that the efficiency of the k -th component could be improved by increasing the capital investment cost to reduce the exergy destruction, and the consequent exergy destruction cost of the component.

Another important variable for the exergoeconomic evaluation is the relative cost difference r_k , which is defined as

$$r_k = \frac{c_{P,k} - c_{F,k}}{c_{F,k}} = \frac{\dot{C}_{D,k} + \dot{Z}_k}{c_{F,k} \dot{E}x_{P,k}} \quad (4.17)$$

4.3.1 Model 1

Thermoeconomic analysis of Model 1 is performed and cost model of each component is given in Table 4.2. Exergetic cost of hydrogen production incorporates each component's cost and each state's exergetic cost rates. Table 4.2 gives the cost rates associated with capital investment and operating and maintenance costs for the components of the system. The rates of capital investment cost and the operating and maintenance costs of the geothermal hydrogen production system are found to be 246.3 \$/h and 85.58 \$/h, respectively.

Table 4.2. Purchased equipment cost and cost rates of each system component [68].

Component	C_k (10^3 \$)	\dot{Z}_k^{CI} (\$/h)	\dot{Z}_k^{OMC} (\$/h)	\dot{Z}_k (\$/h)
Flash chamber	20.500	0.5289	0.1838	0.6349
Separator	65.200	1.682	0.5846	2.019
Steam turbine	942.600	24.32	8.451	29.19
Water cooled condenser	242.900	6.266	2.178	7.522
Heat exchanger	465.600	8.993	3.125	10.8
Isobutane turbine	973.400	25.11	8.727	30.15
Air cooled condenser	229.900	5.931	2.061	7.12
Pump	153.400	3.957	1.375	4.751
Electrolysis unit	6,531.300	168.5	58.56	202.3
Other system components	37.765	0.9743	0.3386	1.17
Total purchased equipment cost	9,662.565	246.3	85.58	331.8
Total operating and maintenance cost	1,595.939 (\$/yr)	-	-	-

The cost balance of geothermal hydrogen production system for the components, operating in steady state, is given in Fig. 4.1. Each term of Fig. 4.1 has dimension of cost per unit of time (\dot{C} , \$/s), in a similar form used for mass, energy, and exergy balances in steady state conditions. The average unit cost c (\$/kJ) is defined by above equations.

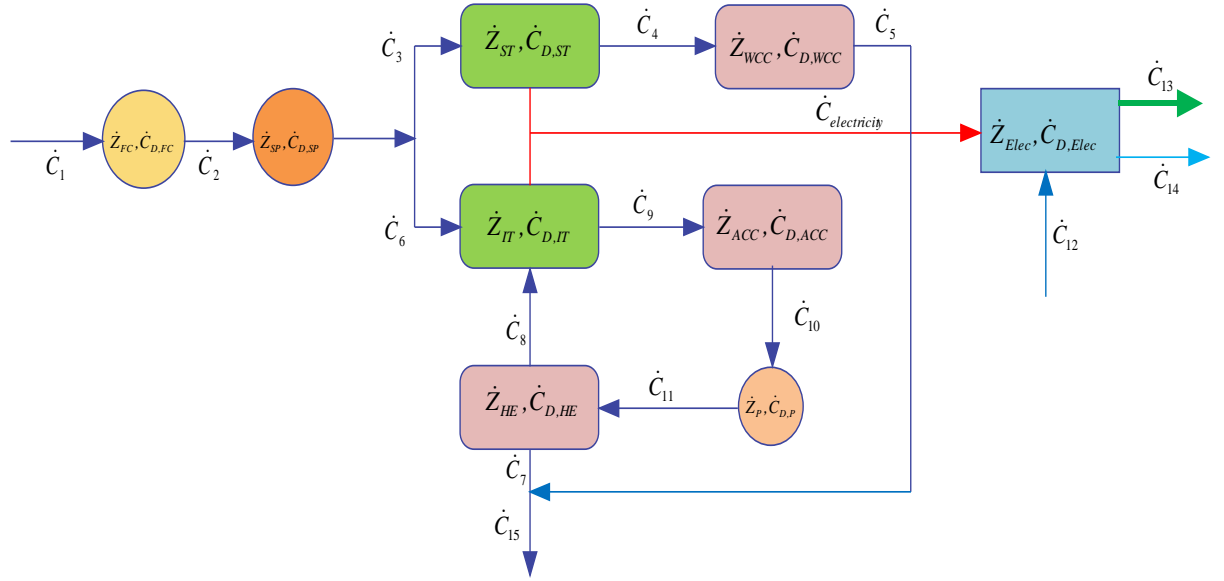


Figure 4.1. Exergy costing configuration of Model 1.

When the number of streams that exit the component is larger than 1, the appropriate auxiliary equations are required. The cost of the supplied fuel, water, air, and of other raw materials must be specified. The specific cost of incoming stream of air and water can be regarded as zero with no significant error. Then, c_8 , c_{10} , and c_{12} are taken to be zero in this study. All cost balance equations and auxiliary equations applied to the system are summarized in Table 4.3. These equations form a linear system of equations, which can be solved to obtain the cost flow rates and the unit exergetic costs associated with each stream of the plant. When the cost rate equations and auxiliary equations are solved mathematically, the parameters for the exergoeconomic analysis can be calculated.

Table 4.3. Cost balance equations and auxiliary equations for the exergy costing of the system.

Component	Exergetic cost rate balance equation	Auxiliary Equations
Expansion valve	$\dot{C}_1 + \dot{Z}_{EV} = \dot{C}_2$	c_1 (known) c_2 (variable)
Separator	$\dot{C}_2 + \dot{Z}_{SEP} = \dot{C}_3 + \dot{C}_6$	$c_3 = c_6$

Steam turbine	$\dot{C}_3 + \dot{Z}_{ST} = \dot{C}_{W_{ST}} + \dot{C}_4$	$c_4 = c_3$ $c_{electricity}$ (variable)
Water cooled condenser	$(\dot{C}_b - \dot{C}_a) + \dot{Z}_{WCC} = \dot{C}_4 - \dot{C}_5$	$c_5 = c_4$ $c_a = 0$ c_b (variable)
Heat exchanger	$(\dot{C}_6 - \dot{C}_7) + \dot{Z}_{HE} = \dot{C}_8 - \dot{C}_{11}$	$c_7 = c_6$ c_8 (variable)
Isobutane turbine	$\dot{C}_8 + \dot{Z}_{IT} = \dot{C}_{W_{IT}} + \dot{C}_9$	$c_9 = c_8$ $c_{electricity}$ (variable)
Air cooled condenser	$(\dot{C}_d - \dot{C}_c) + \dot{Z}_{ACC} = \dot{C}_9 - \dot{C}_{10}$	$c_{10} = c_9$ $c_c = 0$ c_d (variable)
Pump	$\dot{C}_{10} + \dot{Z}_P + \dot{C}_{W_{Pump}} = +\dot{C}_{11}$	c_{10} (known) c_{11} (variable)
Electrolysis	$\dot{C}_{12} + \dot{Z}_{Electrolysis} + \dot{C}_{Electricity} = \dot{C}_{13} + \dot{C}_{14}$	$c_{12} = 0$ $c_{14} = 0$ c_{13} (variable)

The results of exergetic and exergoeconomic analysis at system states are given in Table 4.4. The calculated data in Table 4.4 are obtained using input economic data of Tables 4.2 and 4.3. The average exergetic cost of geothermal water as a fuel input in the overall system is calculated to be 1.373 \$/GJ. The corresponding exergetic cost rate is 80.21 \$/h.

Table 4.4. Exergetic and exergoeconomic analyses results of the system states of Model

1.

State	$\dot{E}x$ (kW)	c (\$/GJ)	\dot{C} (\$/h)
1	16227	1.373	80.21
2	15591	1.437	80.65
3	6509	1.462	34.26
4	1194	1.462	6.286

5	24.86	1.462	0.1309
6	9082	1.462	47.8
7	1507	1.462	7.93
8	9209	2.587	85.76
9	4332	2.587	40.35
10	3041	2.587	28.32
11	3231	3.01	35.01
12	0	0	0
13	5653	12.57	255.8
14	47.53	0	0
15	1492	1.501	8.061
\dot{W}_{Pump}	223.5	3.60	3.354
\dot{W}_{ST}	4562	2.897	49.06
\dot{W}_{IT}	4270	4.296	66.04
Electricity	7572	3.60	113.6
Hydrogen	5653	9.899	201.5

The levelized values of the carrying charges, capital cost of investment, operating and maintenance cost, and the isobutane cost are calculated to be 419.6 \$/h, 247.4 \$/h, 48.65 \$/h and 170.8 \$/h, respectively. The high values of the levelized costs are due to high purchased equipment cost of the electrolysis unit.

Total purchase equipment cost of the system components is calculated to be 9,662,565 \$ and levelized OMC is 1,595,939 \$/year based on 20 years life time of plant. Also, when all economic parameters are contributed, the total net capital investment cost of the system is calculated to be 44,149,581 \$. The exergetic cost of geothermal electricity is 0.01299 \$/kWh (3.60 \$/GJ) and that of hydrogen is 1.190 \$/kg (9.899 \$/GJ).

With the exergy costing method, cost loss can be calculated depending on the irreversibility of the system components. The system component exergy loss is inversely proportional with the “Fuel” flow cost. Exergy loss of the electrolysis unit in

Model 1 is calculated to be 409.6 kW. The electrolysis unit exergetic cost of Fuel is 3.60 \$/GJ which is the same value of electricity unit exergetic cost. Thus, rate of exergetic cost loss of the electrolysis unit is 16.4 \$/h. In exergoeconomic analysis, cost performance of a system subcomponent is varied depending on operating and maintenance cost and system exergy destruction cost. This cost is defined as the expression of exergy performance factors (f_k) and it is beneficial in the optimization process. Exergoeconomic factor is calculated as 0.92 for the electrolysis unit. Thermo-economic analysis results are summarized in Table 4.5 for Model 1.

Table 4.5. Thermo-economic analysis results of Model 1.

Parameter	Result
Total cost of investment	44,149.581 \$
Total purchase equipment cost	9,662.565 \$
Operation and maintenance cost	1,595.939 \$/yr
Exergetic fuel cost	295.9 \$/h
Exergetic product cost	2708 \$/h
Exergetic destruction cost	35.81 \$/h
Exergetic unit cost of electricity	0.01299 \$/kWh
Exergetic cost of hydrogen production	1.190 \$/kg

4.3.2 Model 2

Thermo-economic analysis methodology for Model 2 is the same as Model 1. Therefore, we provide the results of Model 2 in Table 4.6. The unit exergetic cost of electricity produced in the geothermal power plant is 0.01105 \$/kWh (3.07 \$/GJ) and that of the produced hydrogen is 1.149 \$/kg H₂ (9.555 \$/GJ). At an electrolysis temperature of 25°C, the unit exergetic cost of hydrogen is 1.190 \$/kg H₂ and at an electrolysis temperature of 70°C the unit exergetic cost of hydrogen is 1.490 \$/kg H₂, respectively. The corresponding values at 70°C are about 3.44% lower than those at 25°C.

Table 4.6. Thermoeconomic analysis results of Model 2.

Parameter	Result
Total cost of investment	45,015,379 \$
Total purchase equipment cost	9,874,200 \$
Operation and maintenance cost	1,595,939 \$/yr
Exergetic fuel cost	295.9 \$/h
Exergetic product cost	2607 \$/h
Exergetic destruction cost	34.87 \$/h
Exergetic unit cost of electricity	0.01105 \$/kWh
Exergetic cost of hydrogen production	1.149 \$/kg H ₂

4.3.3 Model 3

In Model 3, the exergetic cost rates of the geothermal water at the inlet and exit of generator are obtained as 80.21 \$/h and 21.24 \$/h, respectively. The average exergetic cost of geothermal water as a fuel input in the integrated system is 1.373 \$/GJ. The exergetic unit cost the liquefied hydrogen is calculated to be 12.94 \$/GJ or 1.555 \$/kg H₂. Exergetic cost of cooled hydrogen is 1.190 \$/kg at state 11. The exergetic cost of hydrogen gas cooled to -26.9 °C is 1.083 \$/GJ at state 12. The unit exergetic cost of hydrogen at -253.6°C is calculated to be 1.555 \$/kg. In Model 1, exergetic unit cost of the produced hydrogen was found to be 9.899 \$/GJ. The cost of hydrogen gas entering the system is 1.190 \$/kg (or 9.899 \$/GJ) at 25°C and 100 kPa. Exergetic cost of hydrogen gas decreases with the precooling in the absorption cycle. As a result, exergetic cost value is calculated to be 1.083 \$/kg H₂ (or 9.0 \$/GJ) at -29.6°C. The exergetic cost of liquefied hydrogen is calculated to be 1.555 \$/kg (or 12.94 \$/GJ) at -253.6 °C. Thermoeconomic analysis results for Model 3 are given in Table 4.7.

Table 4.7. Thermoeconomic analysis results of Model 3.

Parameter	Result
Total cost of investment	48,658,120 \$
Total purchase equipment cost	14,410,000 \$
Operation and maintenance cost	3,191,878 \$/yr
Exergetic fuel cost	2849 \$/h
Exergetic product cost	12756 \$/h
Exergetic destruction cost	1347 \$/h
Exergetic unit cost of cooled hydrogen	1.083 \$/kg H ₂
Exergetic cost of hydrogen liquefaction	1.555 \$/kg H ₂

4.3.4 Model 4

Exergetic cost of hydrogen is determined as 9.899 \$/GJ under the atmospheric conditions. In the absorption refrigeration cycle, exergetic unit cost of hydrogen gas cooled at -26.9°C is calculated to be 9.016 \$/GJ. The unit exergetic cost of electricity produced in the geothermal power plant is 9.90 \$/GJ. In Model 4, exergetic unit cost of liquefied hydrogen is calculated to be 10.56 \$/GJ. Thermoeconomic results of Model 4 are given in Table 4.8.

Table 4.8. Thermoeconomic analysis results of Model 4.

Parameter	Result
Total cost of investment	51,995,294 \$
Total purchase equipment cost	16,090,000 \$
Operation and maintenance cost	4,787,817 \$/yr
Exergetic fuel cost	2849 \$/h
Exergetic product cost	21755 \$/h

Exergetic destruction cost	742.6 \$/h
Exergetic unit cost of electricity	0.0340 \$/kWh
Exergetic unit cost of cooled hydrogen	1.084 \$/kg H ₂
Exergetic cost of hydrogen liquefaction	1.296 \$/kg H ₂

4.3.5 Model 5

The unit exergetic cost of electricity produced in the geothermal power plant is calculated to be 3.360 \$/GJ. The unit exergetic cost of hydrogen gas entering the liquefaction cycle is 14.4 \$/GJ at 25°C and 100 kPa. Hydrogen gas is leaving the liquefaction cycle in the liquid form with an exergetic cost of 14.4 \$/GJ (or 1.731 \$/kg) at -252.9 °C and 100 kPa. Therefore, the unit exergetic cost of hydrogen is increased by 10.22% when compared to the value in Model 3. The exergetic cost of hydrogen gas entering the system is increased by 31.3% before hydrogen leaves the system in liquid form. Thermoeconomics analysis results of Model 5 are given in Table 4.9.

Table 4.9. Thermoeconomic analysis results of Model 5.

Parameter	Result
Total cost of investment	42,358,129 \$
Total purchase equipment cost	11,370,000 \$
Operation and maintenance cost	2,766,390 \$/yr
Exergetic fuel cost	369.4 \$/h
Exergetic product cost	179.8 \$/h
Exergetic destruction cost	58.76 \$/h
Exergetic unit cost of electricity	0.01296 \$/kWh
Exergetic unit cost of cooled hydrogen	1.084 \$/kg H ₂
Exergetic cost of hydrogen liquefaction	1.733 \$/kg H ₂

4.3.6 Model 6

In Model 6, the unit exergetic cost of hydrogen produced in electrolysis unit is calculated as 11.83 \$/GJ and that of liquefied hydrogen is 16.93 \$/kg. Here, the unit exergetic cost differences between production and liquefaction of hydrogen is 40%. Thermo-economic results of Model 6 are summarized in Table 4.10.

Table 4.10. Thermo-economic analysis results of Model 6.

Parameter	Result
Total cost of investment	61,392.397 \$
Total purchase equipment cost	17,900,000 \$
Operation and maintenance cost	2,962,878 \$/yr
Exergetic fuel cost	290 \$/h
Exergetic product cost	3042 \$/h
Exergetic destruction cost	34.34 \$/h
Exergetic unit cost of electricity	0.01294 \$/kWh
Exergetic unit cost of hydrogen production	1.423 \$/kg H ₂
Exergetic cost of hydrogen liquefaction	2.360 \$/kg H ₂

4.4 Thermo-economic Results of Models

The higher cost of liquefied hydrogen compared to produced hydrogen is due to the cost of external hydrogen supplied to the system. Model 1 and 2 are hydrogen production models that use geothermal electricity.

While the exergetic production cost of hydrogen is 1.190 \$/kg in Model 1, as a result of water preheating process before electrolysis, the cost is decreased to 1.149 \$/kg in Model 2. That is, the unit exergetic cost of hydrogen is decreased by 3.44% due to preheating electrolysis water. The unit exergetic production cost of hydrogen in model 6

is 1.423 \$/kg. This cost is 16.3% higher compared to Model 1. That is due to the fact that part of electricity produced in geothermal power plant is used for liquefaction.

When we look at the unit exergetic liquefaction cost of precooling process, geothermal heat is used for hydrogen precooling and liquefaction work is supplied by an outside power source. This leads to an extra cost. As a result, the unit exergetic liquefaction cost is 1.555 \$/kg in Model 3. In Model 4, high temperature geothermal water leaving the absorption cooling cycle is used to produce electricity in a geothermal power plant. This electricity is used to liquefy precooled hydrogen gas in the Claude liquefaction cycle. In this system, the unit exergetic cost of the liquefied hydrogen is 1.296 \$/kg. That is, the unit exergetic cost of liquefied hydrogen is observed to decrease by 16% in Model 4. In Model 5, all geothermal electricity is used to liquefy hydrogen gas. In Model 5, the unit exergetic cost of liquefied hydrogen is calculated to be 1.733 \$/kg H₂. Hydrogen liquefaction cost is higher than production cost in this case. The reason is that in the liquefaction cycle hydrogen liquefaction work is 40% lower than the hydrogen production work in electrolysis unit. In thermoeconomic analyses, each inlet and exit flow in the system has a cost value. In Model 5, cost assignment for the hydrogen entering to the system is taken from Model 1. As a result, the unit exergetic cost of hydrogen liquefaction in this model is calculated to be 1.733 \$/kg H₂.

CHAPTER 5

THERMOECONOMIC OPTIMIZATION

5.1 Introduction

Thermoeconomic optimization procedure is applied using genetic algorithm method to the models of this study. The objective is to minimize the unit costs of the products (electricity, hydrogen production and liquefaction) of the composed system. The optimization approach is developed based on the cost optimal exergy efficiency that is obtained for a component isolated from the remaining of the system components. Objectives to be optimized given certain constraints and with variables are developed for each component of the system. Using genetic algorithm method of optimization, the variables, relative cost differences, and exergy efficiencies with the corresponding optimal values are obtained.

Optimization is performed based on thermoeconomic analysis. Not only the effect of the component itself but also the effects of all system components of a system should be taken into account. Main cost analyses are performed by Aspen Plus program and optimization calculations are coded in EES program. Thermodynamic boundary conditions can be taken into account with the optimization toolbar of EES program.

Genetic algorithm is an optimization method based on natural genetics of the universe. Genetic algorithm was developed by Hollanday [77] in an attempt to simulate growth and decay of living organisms in a natural environment. This is a search method used in computing to find exact or appropriate values to optimization and search problems. The genetic algorithm differs from more traditional optimization methods because it includes a search from a population of solutions and not from a single point. The term appropriate denotes the ability of the genetic algorithm for finding the global optimum point, for any optimization problem. A set of points inside the optimization space is generated by random selection of points. Then, this set of points is transformed into a new one. Moreover, this new set will contain more points that are closer to the global optimum solution. The transformation procedure is based only on the information of

how optimal each point is in the set, consists of very simple string manipulations, and is repeated several times. This simplicity in application and the fact that the only information necessary is a measure of how optimal each point is in the optimization space, make genetic algorithms attractive as optimizers. The fundamental advantages of these genetic algorithms which are the constraints of any type can be easily applied and genetic algorithms usually find more than one near-optimal point in the optimization space, thus permitting the use of the most applicable solution for the optimization problem at hand. The fundamental steps for the application of a genetic algorithm for an optimization problem are expressed in Fig. 5.1 [78].

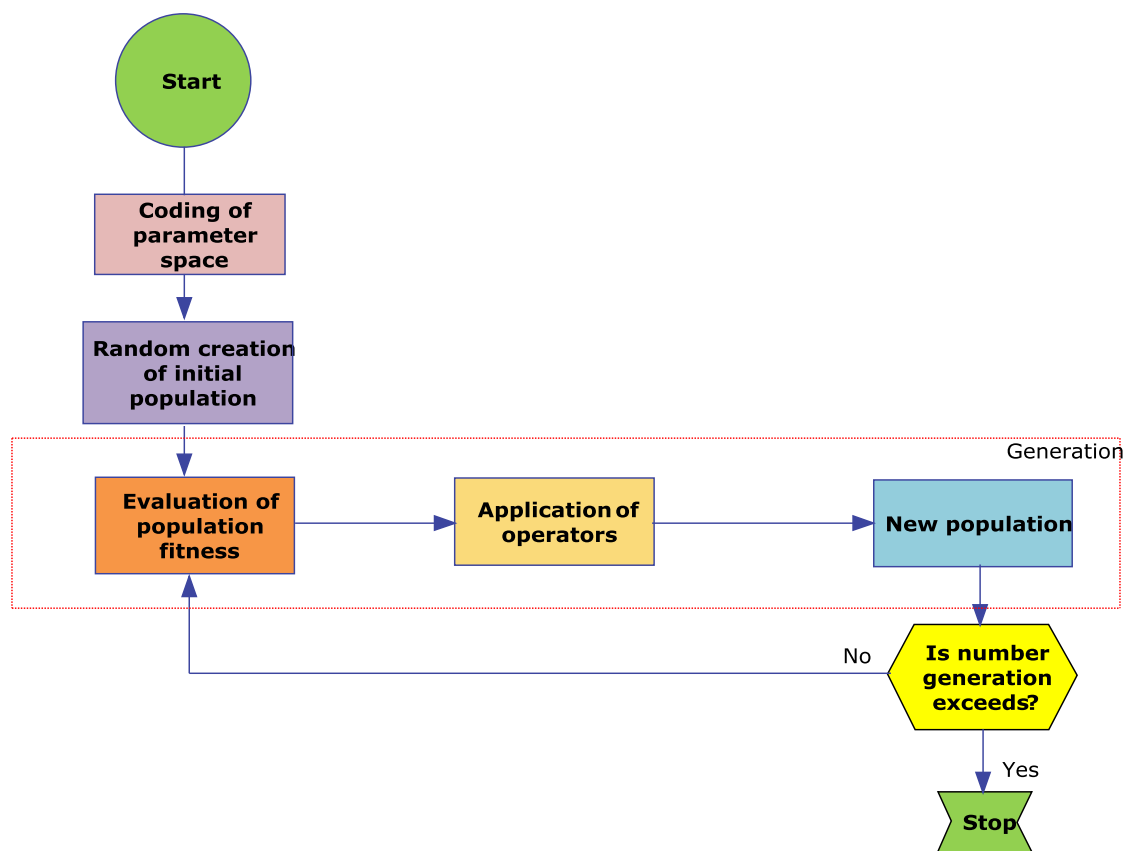


Figure 5.1. Working principle of the genetic algorithm optimization technique.

The objective of the application is aimed at minimizing its overall products' unit costs (electricity and hydrogen production and liquefaction). The genetic algorithm plugged in EES program is derived from the public domain PIKAIA optimization subroutine which is based on the genetic algorithm written in FORTRAN 77. The main properties

of program are supplied in ref. [79]. The parameters of genetic algorithm in the optimization criteria are given in Table 5.1.

Table 5.1. Genetic algorithm optimization parameters [69].

Parameter	Value
Number of individuals in the population	50
Number of generations	80
Maximum mutation rate	0.25
Initial mutation rate	0.005
Minimum mutation rate	0.0005
Crossover probability	0.90

The first three parameters in Table 5.1 are the most responsible ones to identify the optimum solution and can be specified by the EES user. Other parameters and functions of the genetic algorithm that have been set to the default values suggested in the PIKAIA subroutine and are not variable within the EES. The PIKAIA subroutine incorporates stochastic sampling mechanism based on the roulette wheel algorithm (or on the particle swarm), reproduction plan based on the full generational replacement, one-point crossover operator and one point mutation operator which allows the mutation rate to vary dynamically in the course of the evolutionary run. The optimization algorithm stops when the given number of generations is reached [69]. The number of generations is selected to be 80 as values higher than this does not result in an improvement of the optimal solution.

The definition of the objective functions of the thermoeconomic optimization problem requires two conflicting objectives. The first one is to increase in exergy efficiency and the other is to decrease in products' cost. The first objective is defined by thermodynamic requirements and the second by economic constraints.

Therefore, objective function should be defined in such a way that the optimization satisfies both requirements. The optimization problem should be formulated as an

optimal values (minimization or maximization) problem. The thermoeconomic analysis gives a clear picture about the costs related to the exergy destructions. The maximization of exergy efficiency means minimization of exergy destruction costs. Thus, the objective function becomes a minimization problem. The objective functions for this problem are defined as to minimize the total cost rate of operation $\dot{C}_{P,overall}$ and maximize an exergy efficiency which can be modeled as

$$\varepsilon_{overall} = \frac{\dot{E}x_{P,total}}{\dot{E}x_{F,total}} \quad (5.1)$$

The objective function expresses the optimization criterion as a function of the dependent and independent variables. In a thermal system case study, for example, the objective function obtained by

$$\text{Minimize } \dot{C}_{P,overall} = \dot{C}_{F,overall} + \dot{Z}_{k,overall} \quad (5.2)$$

The choice of decision variables for the system is selected to the optimization.

The minimization of the product cost for a single component is illustrated in Figure 5.2. This figure shows the effects of fuel cost and capital cost on the average cost per exergy unit of product c_p as function of the exergy efficiency ε , and the sum of exergy destruction and exergy loss $(\dot{E}_D + \dot{E}_L)$. The abscissa is linear with respect to $(\dot{E}_D + \dot{E}_L)$ and nonlinear with respect to the ε . The total cost is the sum of capital and fuel costs. For design point indicated by A, the figure shows the parts of capital cost and fuel cost that depend on $(\dot{E}_D + \dot{E}_L)$. The average cost per exergy unit of fuel c_F is taken as constant.

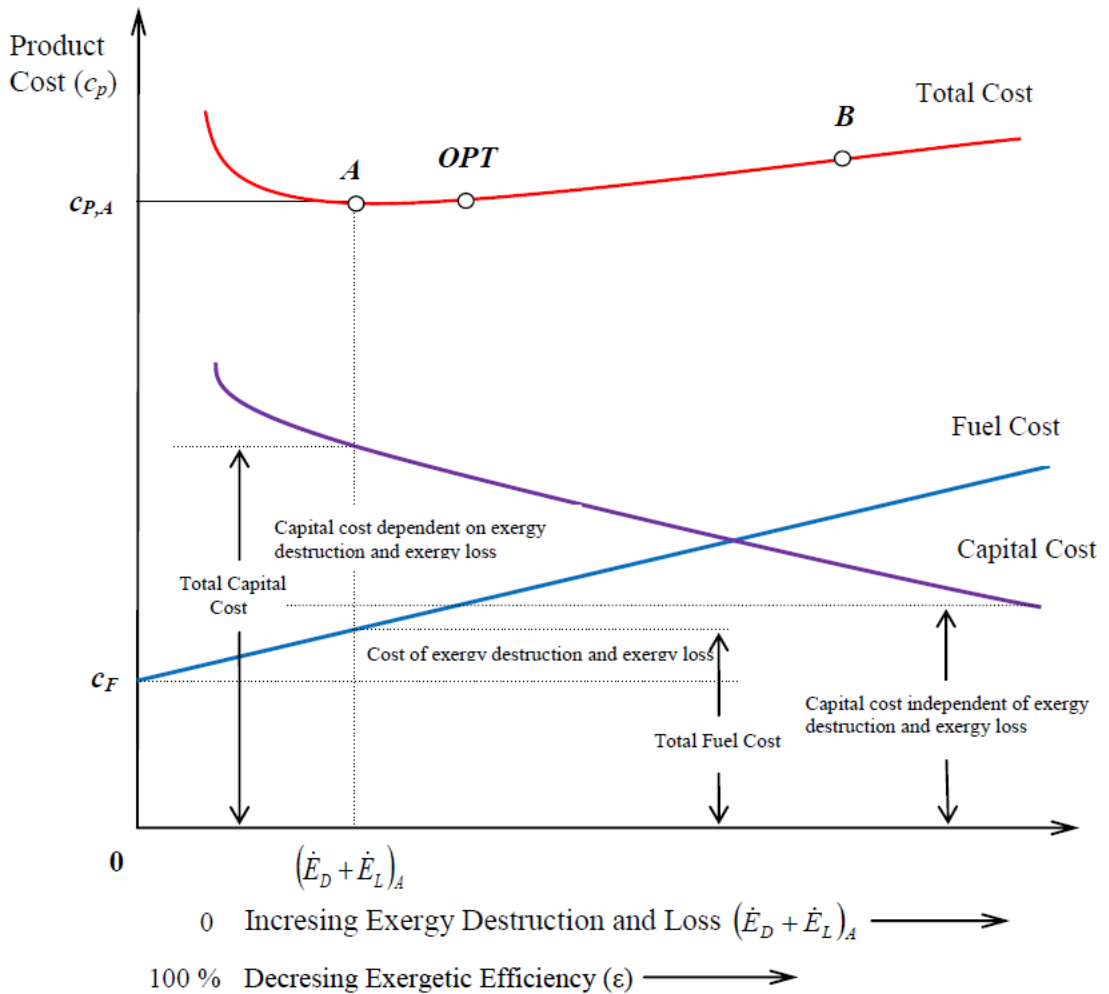


Figure 5.2. Schematic of the contributions of fuel cost and capital cost to the total product cost, as a function of the exergy efficiency and the sum of exergy destruction and exergy loss [80].

In Figure 5.2, point A is characterized by capital costs that are too high, whereas the fuel cost at point B is also too high. The optimal design point is denoted by OPT. The total cost curve is usually flat around the optimal point. Therefore, several points around the optimal point may be regarded as nearly optimal. For simplicity, only capital investment and fuel costs have been considered in Figure 5.2. However, practically, the same curves would be obtained qualitatively if we would include the contribution of the fixed OMC costs together with the investment costs and the variable OMC costs and fuel costs.

5.2 Thermo-economic Optimization of Model 1

Thermo-economic optimization procedure is applied by genetic algorithm method to an integrated system consisting of an alkaline water electrolysis unit for hydrogen production and a combined flash-binary geothermal power plant for providing power input for the electrolyzer. The initial sample size of population of parent individuals, the scaling factor and the maximum number of offspring generations are taken as 50, 0.25, and 80, respectively. Boundary conditions of the thermodynamic variables considered for this model are: $100 \leq P_2 \leq 1000$ kPa, $5 \leq \Delta T_{pp} \leq 30$ °C, $0.70 \leq \eta_{turbines} \leq 0.90$, $130 \leq T_8 \leq 190$ °C, $0.70 \leq \eta_p \leq 0.90$, $1000 \leq P_{11} \leq 3000$ kPa. The decision variables are generated randomly within the admissible range mentioned above. Base conditions (assumptions) and boundary conditions are as used in Chapter 3 for Model 1.

The decision variables for the optimum case are given in Table 5.2. For comparison purposes, the values for the base case are also presented in Table 5.2. The optimum geothermal water flash pressure is 460.8 kPa, the binary heat exchanger pressure is 1767 kPa, the pinch point temperature of the heat exchanger is 5.0, the pump isentropic efficiency is 89.39%, the steam turbine isentropic efficiency is 89.87%, the isobutane turbine isentropic efficiency is 90%, and the binary heat exchanger temperature is 138.8°C. The unit production rate of hydrogen is increased from 0.04827 kg/s in the base case to 0.0514 kg/s in the optimum case. The production rates of hydrogen increased by 6.09% as a result of thermo-economic optimization. The energy and exergy efficiencies are increased from 7.764% and 35.13% in the base case to 8.267% and 37.41% in the optimum case.

Table 5.2. The base case and optimal case conditions of Model 1.

Decision variable	Base case	Optimum case
Flash pressure, P_2 (kPa)	600	460.8
Binary heat exchanger pressure, P_{11} (kPa)	2100	1767
Binary heat exchanger temperature, T_8 (°C)	148.8	138.8
Pinch point temperature, ΔT_{pp} (°C)	5.0	5.0
Pump isentropic efficiency (%)	85	89.39

Steam turbine isentropic efficiency (%)	85	89.87
Isobutane turbine isentropic efficiency (%)	85	90
Geothermal electricity production, (kW)	7572	8063
Electrolysis energy demand, (kWh/kg)	43.57	43.57
Electrolysis unit hydrogen production, (kg/s)	0.04827	0.0514
Energy efficiency, η (%)	7.764	8.267
Exergy efficiency, ε (%)	35.13	37.41

The exergy cost rate of the geothermal water is calculated to be 80.21 \$/h. The average exergetic cost of geothermal water as a fuel input in the integrated system is 1.373 \$/GJ. The unit exergetic production costs of electricity and hydrogen are calculated to be 3.398 \$/GJ and 9.313 \$/GJ, respectively in the optimum case. The optimization results of exergetic and exergoeconomic analyses at system states are given in Table 5.3. The calculated data in Table 5.3 are obtained using input thermodynamic and economic data of Tables 5.1 and exergetic cost relations of thermoeconomic analysis methodology in Chapter 4.

Table 5.3. Thermoeconomic optimization results of the exergetic and exergoeconomic analysis results for Model 1.

State	$\dot{E}x$ (kW)	c (\$/GJ)	\dot{C} (\$/h)
1	16227	1.373	80.21
2	15245	1.467	80.53
3	7537	1.486	40.32
4	1454	1.486	7.775
5	30.34	1.486	0.1623
6	7709	1.486	41.24
7	1305	1.486	6.981
8	7896	2.538	72.14
9	3861	2.538	35.27
10	2806	2.538	25.64
11	2947	2.826	29.99

12	0	0	0
13	6020	9.313	201.8
14	50.61	0	0
15	1297	1.530	7.144
\dot{W}_P	157.7	3.398	1.920
\dot{W}_{IT}	3700	3.892	51.84
\dot{W}_{ST}	5504	2.361	46.78
Hydrogen production	6020	9.313	201.8

The comparative results of the base and the optimum case are given in Table 5.4. In the optimized system, the exergetic cost of hydrogen production is decreased from 1.19 \$/kg to 1.119 \$/kg, a reduction of 6.2%.

Table 5.4. Comparative results of the optimum case and the base case data of Model 1.

Parameter	Base case	Optimum case	% Variation
Fuel exergy (kW)	59,862	58,716	-1.950
Product exergy (kW)	52,617	51,610	-1.913
Exergy destruction (kW)	7245	7105	-1.932
Fuel cost (\$/h)	295.9	290.2	-1.926
Product cost (\$/h)	2708	2492	-8.013
Exergy destruction cost (\$/h)	35.81	35.12	-1.926
Exergetic unit cost of electricity (\$/kWh)	0.01299	0.01223	-5.850
Exergetic cost of hydrogen production (\$/kg)	1.190	1.119	-6.202

5.3 Thermoeconomic Optimization of Model 2

In this model, the boundary conditions of the thermodynamic variables are the same as Model 1. We use the same procedure as Model 1 to perform thermoeconomic optimization of Model 2. Base conditions (assumptions) and boundary conditions are

taken from Chapter 3 for Model 2. The decision variables for the base case and optimum case are given in Table 5.5.

Table 5.5. The base case and optimal case conditions of Model 2.

Decision variable	Base case	Optimum case
Flash pressure, P_2 (kPa)	600	482.1
Binary heat exchanger pressure, P_{11} (kPa)	2100	2052
Binary heat exchanger temperature, T_8 (°C)	148.8	140.5
Pinch point temperature, ΔT_{pp} (°C)	5.0	5.172
Pump isentropic efficiency (%)	85	89
Steam turbine isentropic efficiency (%)	85	90
Isobutane turbine isentropic efficiency (%)	85	87.9
Geothermal electricity production, (kW)	7572	7992
Electrolysis energy demand, (kWh/kg)	43.57	41.07
Hydrogen production rate, (kg/s)	0.04827	0.05278
Energy efficiency, η (%)	7.764	8.489
Exergy efficiency, ε (%)	35.13	38.44

The exergy cost rate of the geothermal water is calculated to be 80.21 \$/h. The average exergetic cost of geothermal water as a fuel input to the system is 1.373 \$/GJ. The unit exergetic production costs of electricity and hydrogen are calculated to be 3.397 \$/GJ and 11.44 \$/GJ, respectively, in the optimum case. The unit production cost of hydrogen has decreased by 5.61% as a result of thermoeconomic optimization. The comparative results of the base and the optimum case are given in Table. 5.6. There are significant variations between base case and optimum case values. By using optimum operating conditions, the unit production rate of hydrogen is increased to 0.05278 kg/s from a base case value of 0.04827 kg/s. Also, the energy and exergy efficiencies of the system are increased from 7.764% and 35.13% in the base case to 8.489% and 38.44% in the optimum case.

Table 5.6. Comparative results of the optimum case and the base case of Model 2.

Parameter	Base case	Optimum case	% Variation
Fuel exergy (kW)	59,873	58,559	-2.194
Product exergy (kW)	52,819	51,886	-1.766
Exergy destruction (kW)	7,055	6,673	-5.414
Fuel cost (\$/h)	295.9	289.4	-2.196
Product cost (\$/h)	2607	2412	-7.479
Exergy destruction cost (\$/h)	34.87	32.96	-5.420
Exergetic unit cost of electricity (\$/kWh)	0.01105	0.01066	-3.658
Exergetic cost of hydrogen production (\$/kg)	1.149	1.088	-5.308

5.4 Thermoeconomic Optimization of Model 3

In Model 3, thermodynamic assumptions for absorption refrigeration cycle are as follows:

Low pressure of the cycle $P_5=100$ kPa

Generator pressure range (high pressure) $500 \leq P_{\text{generator}} \leq 2000$ kPa

Mass concentration of ammonia $0 \leq x (\text{NH}_3/\text{kg solution}) \leq 1$

Absorber and condenser pressure and temperature are 100 kPa and 25°C.

In this model, design variables and base assumptions of the thermoeconomic optimization of absorption refrigeration cycle are as follows:

$$25 \leq T_{\text{condenser}} \leq 40^\circ\text{C}$$

$$25 \leq T_{\text{evaporator}} \leq 40^\circ\text{C}$$

$$25 \leq T_{\text{absorber}} \leq 40^\circ\text{C}$$

Specific heat of condenser and absorber cooling water $c_p = 4.183$ kJ/kg·K

Specific heat of evaporator and generator heating water $c_p = 4.183$ kJ/kg·K

The cooling water inlet temperature of condenser and absorber $T_k = T_x = 25^\circ\text{C}$

Evaporator inlet temperature of hydrogen gas $T_{11}=25^\circ\text{C}$

The temperature range of geothermal water leaving the generator $100 \leq T_{\text{geo,out}} \leq 180^\circ\text{C}$

Thermodynamic limit and assumptions for the liquefaction cycle are as follows:

$$1000 \leq P_{\text{comp}} \leq 5000 \text{ kPa}$$

$$0.70 \leq \eta_{\text{comp}} \leq 0.90$$

$$0.70 \leq \eta_{\text{p}} \leq 0.90$$

$$0.5 \leq x \leq 0.8.$$

Based on these values, the thermodynamic decision variables for the base case and optimum case for Model 3 are given in Table 5.7.

Table 5.7. The base case and optimal working conditions obtained by the genetic algorithm optimization of the system [69].

Decision variable	Base case	Optimum case
High pressure, P_6 (kPa)	1500	973.6
Ammonia mass concentration, x (kg NH_3 /kg solution)	0.38	0.4556
Geothermal water exit temperature, $T_{\text{geo,out}}$ ($^\circ\text{C}$)	110	100
Condenser temperature, T_2 ($^\circ\text{C}$)	25	25
Evaporator temperature, T_4 ($^\circ\text{C}$)	-30	-30
Absorber temperature, T_5 ($^\circ\text{C}$)	25	25
Solution mass, m (kg/s)	89	100
Compressor isentropic efficiency of liquefaction cycle, (%)	70	86
Cooling load, (kW)	39,080	30,942
Cooled hydrogen mass, m_{12} (kg/s)	29.53	39.05
Compressor pressure of liquefaction cycle, P_{11} (kPa)	4000	3200
Gas concentration of liquefaction cycle, x	0.6	0.7665
Liquefied hydrogen mass, (kg/s)	6.028	8.56
Maximum cooling temperature, T_{12} ($^\circ\text{C}$)	-26.9	-30
Overall exergy efficiency, ε (%)	67.9	69.44

The exergy cost rate of the geothermal water is calculated to be 80.08 \$/h. The average exergetic cost of geothermal water as a fuel input in the integrated system is calculated to be 1.373 \$/GJ. The unit exergetic cost of liquefied hydrogen produced in Model 3 is calculated to be 4.905 \$/GJ (1.349 \$/kg H₂) in the optimum case. As a result of optimization, the unit liquefaction cost of hydrogen is decreased by 13.24%. The comparative results of the base case and the optimum case are given in Table. 5.8 for Model 3.

Table 5.8. Comparative results of the optimum case and the base case for Model 3.

Parameter	Base case	Optimum case	% Variation
Fuel exergy (kW)	576398	1062000	+45.7
Product exergy (kW)	303783	565613	+46.3
Exergy destruction rate (kW)	272615	496496	+45.1
Fuel cost rate (\$/h)	2849	5250	+45.7
Product cost rate (\$/h)	12756	18755	+31.9
Exergy destruction cost rate (\$/h)	1347	2454	+45.1
Exergetic unit cost of liquefied hydrogen (\$/kg)	1.555	1.349	-13.24

5.5 Thermoeconomic Optimization of Model 4

In this model, geothermal temperature range at the exit of generator is taken $100 \leq T_{\text{geo,out}} \leq 180^\circ\text{C}$ for system optimization. Thermodynamic limits and assumptions for the liquefaction system are as follows:

$$1000 \leq P_{\text{comp}} \leq 5000 \text{ kPa}$$

$$0.70 \leq \eta_{\text{comp}} \leq 0.90$$

$$0.70 \leq \eta_{\text{p}} \leq 0.90$$

$$0.5 \leq x \leq 0.8$$

Isentropic efficiencies of the turbines and pump are 85%.

Thermodynamic boundary conditions for the optimization are selected as follows:

$$0.70 \leq \eta_{\text{pump}} \leq 0.90$$

$$0.70 \leq \eta_{\text{turbine}} \leq 0.90$$

$$1000 \leq P_{24} \leq 3000 \text{ kPa}$$

$$5 \leq \Delta T_{\text{pp}} \leq 30^\circ\text{C}$$

The decision variables for the base case and optimum case are given in Table 5.9 for Model 4.

Table 5.9. The base case assumptions and optimal working conditions.

Decision variable	Base case	Optimum case
High pressure, P_6 (kPa)	1500	973.6
Ammonia mass concentration, x (kg NH ₃ /kg solution)	0.38	0.4556
Geothermal water exit temperature, $T_{\text{geo,out}}$ (°C)	110	100
Condenser temperature, T_2 (°C)	25	25
Evaporator temperature, T_4 (°C)	-30	-30
Absorber temperature, T_5 (°C)	25	25
Solution mass, m (kg/s)	89	100
Isentropic efficiency of liquefaction compressor (%)	70	86
Cooling load, (kW)	39,080	10,833
Cooled hydrogen mass, \dot{m}_{12} (kg/s)	29.53	13.67
Compressor pressure of liquefaction cycle, P_{11} (kPa)	4000	3200
Gas fraction of liquefaction cycle, x	0.6	0.7665
Liquefied hydrogen mass, (kg/s)	6.028	8.56
Maximum liquefaction temperature, T_{12} (°C)	-26.9	-30
Binary heat exchanger pressure, P_{24} (kPa)	3000	2100
Pinch point temperature, ΔT_{pp} (°C)	5	5.18
Pump isentropic efficiency (%)	85	88
Isobutane turbine isentropic efficiency (%)	85	89
Geothermal electricity, (kW)	1112	1509
Overall system exergy efficiency, ε (%)	76.1	78.30

The unit exergetic cost of liquefied hydrogen is calculated to be 1.296 \$/kg H₂. After optimization, this value is 1.114 \$/kg H₂. As a result, the unit liquefaction cost of hydrogen is decreased by 12.21%. The comparative results of the base case and the optimum case are given in Table. 5.10 for Model 4.

Table 5.10. Comparative results of the optimum case and the base case of Model 4.

Parameter	Base case	Optimum case	% Variation
Fuel exergy (kW)	576343	812421	+29.05
Product exergy (kW)	426097	606402	+29.73
Exergy destruction rate (kW)	150246	206019	+27.07
Fuel cost rate (\$/h)	2849	4016	+29.05
Product cost rate (\$/h)	21755	23430	+7.148
Exergy destruction cost rate (\$/h)	742.6	1018	+27.05
Exergetic unit cost of hydrogen liquefaction (\$/kg)	1.269	1.114	-12.21

5.6 Thermo-economic Optimization of Model 5

In this model, we use the range of variables as given in Model 1 and Model 3. As a result of the calculations made using these assumptions, the unit exergetic cost of electricity produced in the geothermal power plant is calculated to be 0.0149 \$/GJ and the unit exergetic cost of liquefied hydrogen is 0.04039 \$/kg H₂. The overall system exergy efficiency is calculated to be 87.46 %. The net power output from the geothermal plant is calculated to be 7572 kW and liquefied hydrogen rate is 0.2153 kg/s. In this system, the unit exergetic cost of hydrogen is taken from Model 1 to be 11.79 \$/GJ. Base case values and optimum results obtained from the optimization analysis are given in Table 5.11.

Table 5.11. The base case values and optimal working conditions based on optimization of Model 5.

Decision variable	Base case	Optimum case
Flash pressure P_2 (kPa)	600	553.9
Binary heat exchanger pressure, P_{11} (kPa)	2100	1814
Binary heat exchanger temperature, T_8 (°C)	148.8	155.7
Pinch point temperature, ΔT_{pp} (°C)	5	5.17
Pump isentropic efficiency (%)	85	79.4
Binary turbine isentropic efficiency (%)	85	77.04
Isobutane turbine isentropic efficiency (%)	85	90
Compressor isentropic efficiency of liquefaction cycle (%)	70	70.93
Geothermal electricity production , (kW)	7572	7322
Liquefaction cycle inlet mass of hydrogen, (kg/s)	1	1
Compressor pressure of liquefaction cycle, P_{11} (kPa)	4000	4000
Gas fraction of liquefaction cycle, x	0.6	0.7665
Liquefied hydrogen mass, (kg/s)	0.1714	0.2324
Overall system exergy efficiency, ε (%)	84.09	85.96

The exergy cost rate of the geothermal water is calculated to be 80.08 \$/h and the exergetic cost of geothermal water as a fuel input to the integrated system is 1.373 \$/GJ. The exergetic costs of electricity and liquefied hydrogen in Model 5 are calculated to be 3.397 \$/GJ and 11.44 \$/GJ, respectively in the optimum case. The comparative results of the base case and the optimum case are given in Table. 5.10 for Model 5.

Table 5.12. Comparative results of the optimum case and the base case of Model 5.

Parameter	Base case	Optimum case	% Variation
Fuel exergy (kW)	74735	67933	-9.101
Product exergy (kW)	62846	58397	-7.079

Exergy destruction (kW)	11889	9536	-19.79
Fuel cost rate (\$/h)	369.4	335.8	-9.095
Product cost rate (\$/h)	179.8	100.9	-56.117
Exergy destruction cost rate (\$/h)	58.76	47.14	-19.77
Unit exergetic electricity cost (\$/kWh)	0.01296	0.01222	-5.709
Unit exergetic hydrogen liquefaction cost (\$/kg)	1.733	1.335	-22.96

5.7 Thermoeconomic Optimization of Model 6

In this model, thermodynamic range of variables are given in Model 1 and Model 3. Base case and optimum case decision variables obtained by genetic algorithm are given in Table 5.13.

Table 5.13. The base case assumptions and optimal working conditions obtained by the optimization of Model 6.

Decision variable	Base case	Optimum case
Flash pressure, P_2 (kPa)	600	479.4
Binary heat exchanger pressure, P_{11} (kPa)	2100	1880
Binary heat exchanger temperature, T_8 (°C)	148.8	140.3
Pinch point temperature, ΔT_{pp} (°C)	5	5.17
Pump isentropic efficiency (%)	85	86.01
Steam turbine isentropic efficiency (%)	85	89.26
Isobutane isentropic efficiency (%)	85	90
Compressor isentropic efficiency of liquefaction cycle (%)	70	82.40
Geothermal electricity, (kW)	7572	8026
Hydrogen production of electrolysis, (kg/s)	0.03482	0.04125
Compressor pressure of liquefaction	4000	5000

cycle, P_{11} (kPa)		
Gas fraction of liquefaction cycle, x	0.6	0.7677
Liquefied hydrogen mass, (kg/s)	0.005942	0.009805
Overall system exergy efficiency, ε (%)	88.16	88.33

The exergy cost rate of the geothermal water is the same as before, 80.21 \$/h. The average exergetic cost of geothermal water as a fuel input to the system is 1.373 \$/GJ. The exergetic costs of electricity and liquefied hydrogen in Model 6 are calculated to be 0.01243 \$/kWh and 1.993 \$/kg H₂, respectively in the optimum case. The unit liquefaction cost of hydrogen is decreased by 15.55% as a result of thermoeconomic optimization. The comparative results of the base case and the optimum case are given in Table 5.11 for Model 6.

Table 5.14. Comparative results of the optimum case and the base case of Model 6.

Parameter	Base case	Optimum case	% Variation
Fuel exergy (kW)	58671	58065	-1.032
Product exergy (kW)	51723	51288	-0.841
Exergy destruction (kW)	6948	6776	-2.475
Fuel cost rate (\$/h)	290	287	-1.034
Product cost rate (\$/h)	3042	1514	-50.23
Exergy destruction cost rate (\$/h)	34.34	33.49	-2.475
Unit exergetic cost of electricity (\$/kWh)	0.01294	0.01243	-3.941
Unit exergetic cost of production hydrogen (\$/kg)	1.423	1.296	-8.924
Unit exergetic cost of liquefaction hydrogen (\$/kg)	2.360	1.993	-15.55

5.8 Thermo-economic Optimization Results

A summary of thermo-economic optimization results of the models are given in Table 5.15. It is seen that unit exergetic costs of the system decrease in reference to base case results. For example, the unit exergetic cost of hydrogen is decreased by 5.97% in Model 1 and 5.31% in Model 2 as a result of thermo-economic optimization. In Model 6, the exergetic cost of liquefied hydrogen is observed to decrease by 9.80%. For Model 6, the first cost value refers to hydrogen production and second cost value refers to total cost value including hydrogen production and liquefaction. In liquefaction models, the unit exergetic cost value of liquefied hydrogen decreases by 25.9% for Model 3, 14.04% for Model 4, 22.96% for Model 5, and 15.55% for Model 6.

Table 5.15. Summary of thermo-economic optimization results of the models.

Models	Base case (\$/kg H ₂)	Optimized case (\$/kg H ₂)	Variation in unit cost of hydrogen (%)
Model 1	1.190	1.119	-5.97
Model 2	1.149	1.088	-5.31
Model 3	1.555	1.349	-25.9
Model 4	1.296	1.114	-14.04
Model 5	1.733	1.335	-22.96
Model 6	1.423/2.360	1.296/1.993	-9.80/-15.55

CHAPTER 6

GENERAL RESULTS AND CONCLUSIONS

6.1 Parametric Studies

In Figures 6.1-6.8, we present thermoeconomic optimization results with respect to geothermal water temperature. In Figs. 6-1 and 6.2, effect of geothermal water temperature on energy and exergy efficiencies of Model 1 and Model 2 is presented. Energy efficiency increases almost linearly while exergy efficiency first increases, reaches a maximum, and then decreases. Exergy efficiency decreases at a point logarithmically, because system must be optimized again flash pressure and reorganized according to the new geothermal water temperature of the models. The other thermodynamic parameters must be reevaluated at that point.

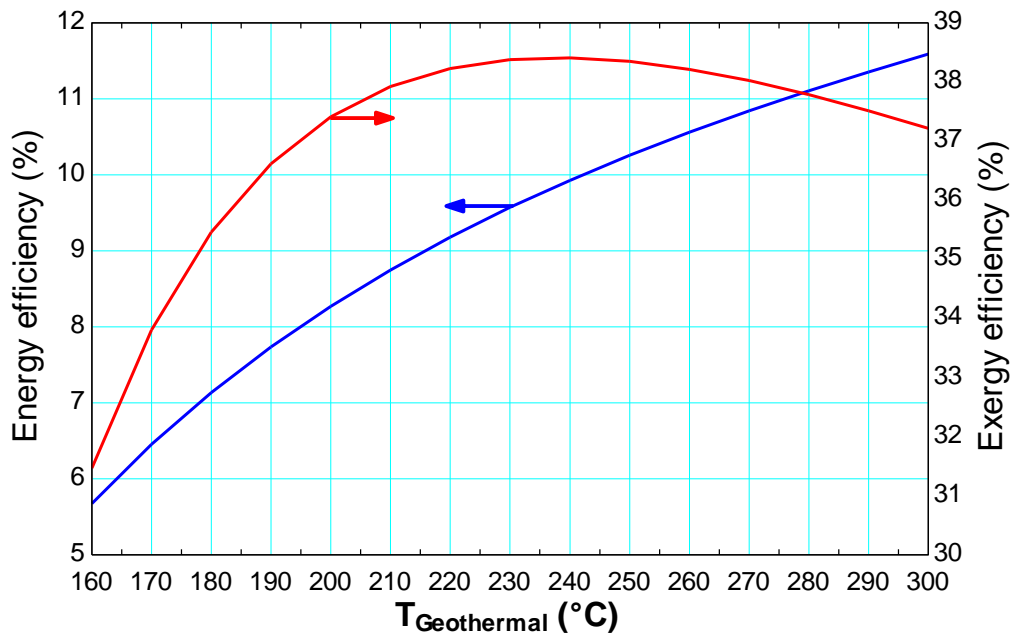


Figure 6.1. Variation of energy and exergy efficiencies with geothermal water temperature in Model 1.

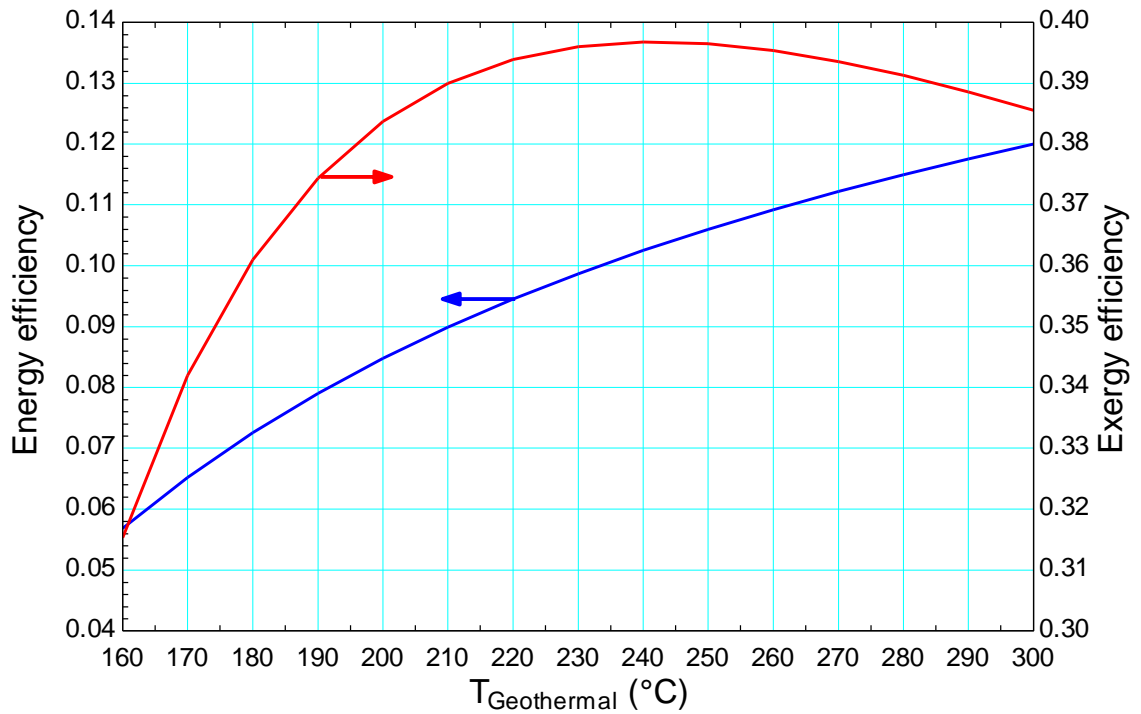


Figure 6.2. Variation of energy and exergy efficiencies with geothermal water temperature in Model 2.

Fig. 6.3 shows the temperature of the cooled hydrogen gas in the liquefaction models as a function of geothermal water temperature. As the geothermal water temperature increases, hydrogen gas can be cooled to lower temperatures. As the geothermal temperature increases from 160°C to 300°C, hydrogen gas temperature decreases from -22.6°C to -33.4°C. At a geothermal temperature of 200°C, hydrogen can be cooled to -26.9°C at a rate of 29.53 kg/s while it can be cooled to the same temperature at a rate of 31.23 kg/s at a geothermal temperature of 250°C.

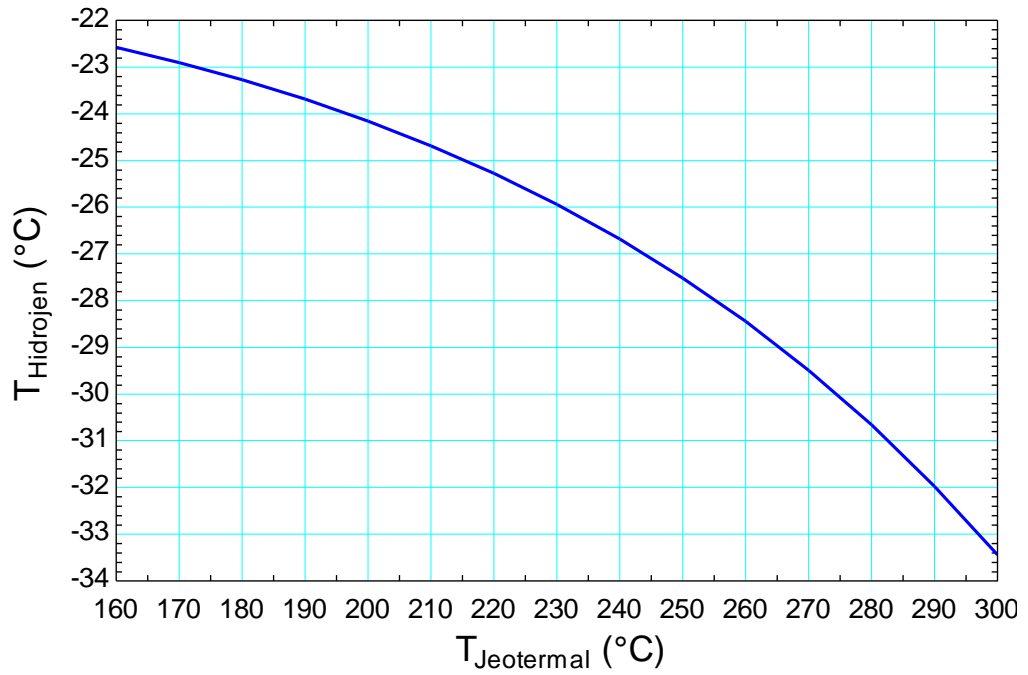


Figure 6.3. Variation of the precooling temperature of hydrogen with geothermal water temperature.

Fig. 6.4 shows variations of liquefied hydrogen mass fraction and liquefaction work as a function of cooled hydrogen gas temperature in liquefaction models. For lower values of hydrogen cooling temperatures, greater fractions of hydrogen gas can be liquefied and the liquefaction work requirement is reduced. Hydrogen should be cooled to minimum possible temperatures in the absorption cooling cycle. Thermophysical properties of ammonia and the pressure ranges applicable in the system are limiting factors in obtaining the lowest hydrogen temperatures in the cycle.

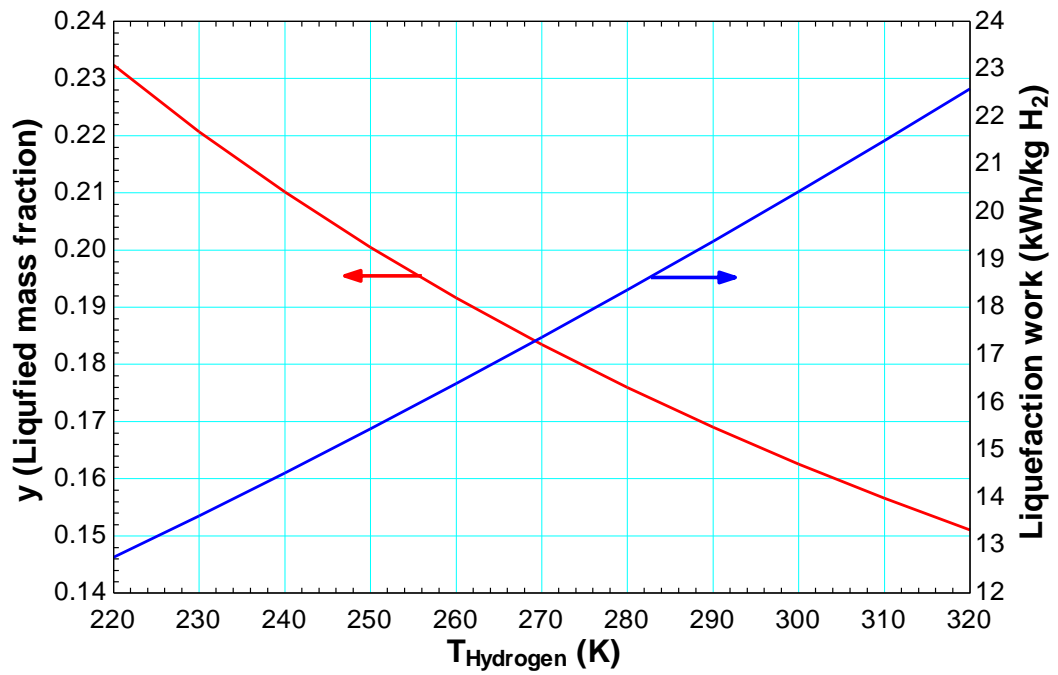


Figure 6.4. Variations of liquefaction mass fraction and liquefaction work as a function of cooled hydrogen gas temperature.

Figs. 6.5 and 6.6 show variations of exergy efficiency and COP of the overall system as a function of geothermal water temperature for Model 3 and Model 4. Both parameters increase as the geothermal temperature increases. In Model 3, at a geothermal temperature of 200°C, the COP is 0.4081 and the exergy efficiency is 76.1% while at 250°C, the corresponding values are 0.4168 and 82.5%, respectively.

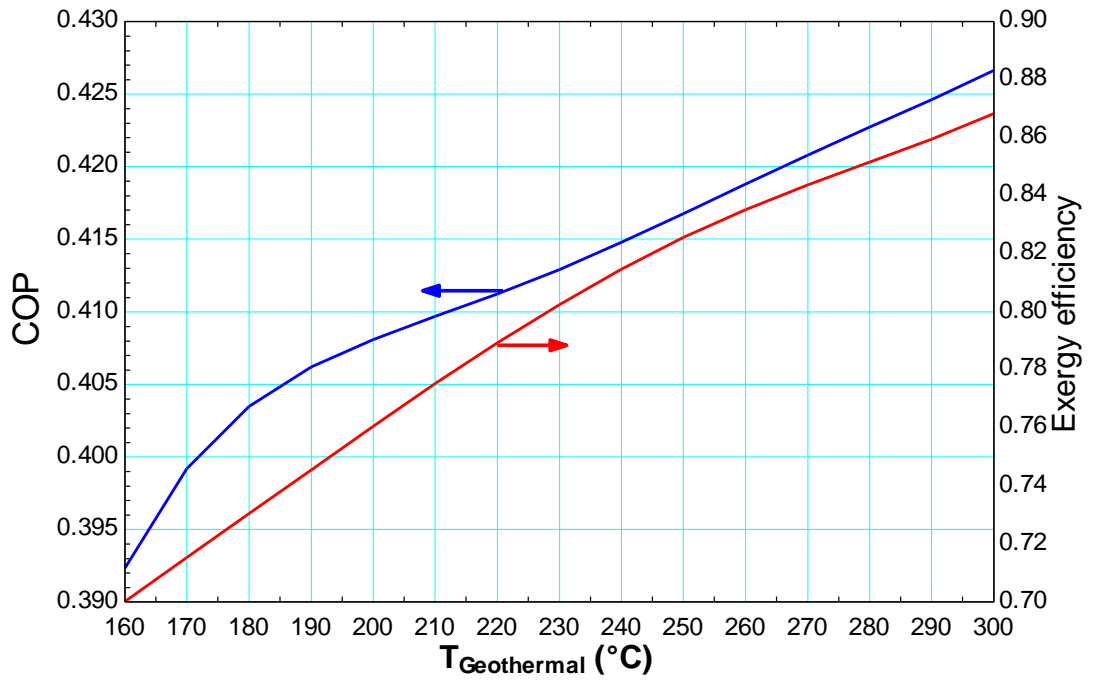


Figure 6.5. Variations of overall exergy efficiency and overall COP as a function of geothermal water temperature in Model 3.

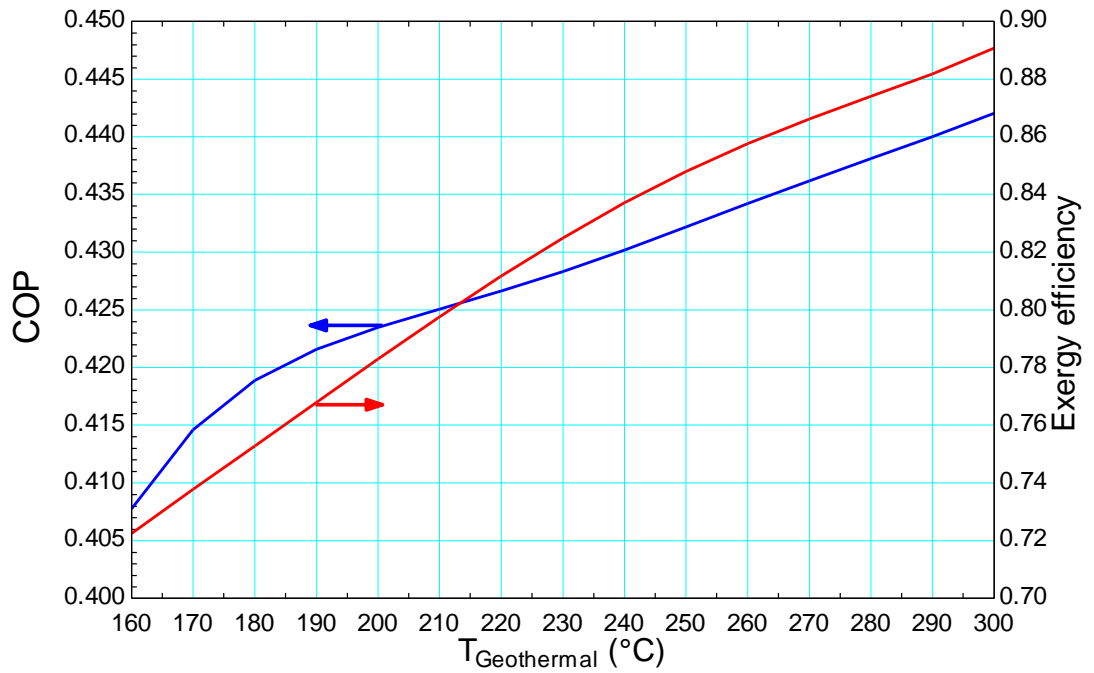


Figure 6.6. Variations of overall exergy efficiency and overall COP as a function of geothermal water temperature in Model 4.

Effect of geothermal temperature on energy and exergy efficiencies of Model 5 and Model 6 is given in Figs. 6.7 and 6.8. Energy efficiency increases with geothermal temperature but exergy efficiency first increases, reaches a maximum, and decreases.

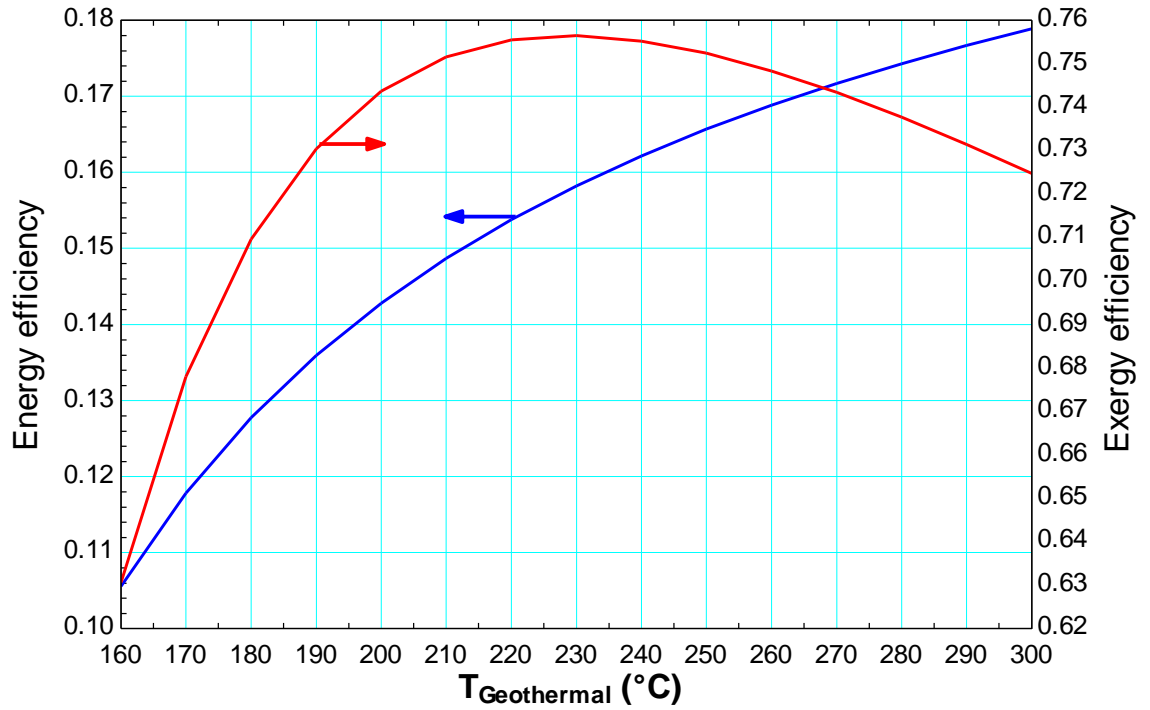


Figure 6.7. Variation of energy and exergy efficiencies with geothermal water temperature in Model 5.

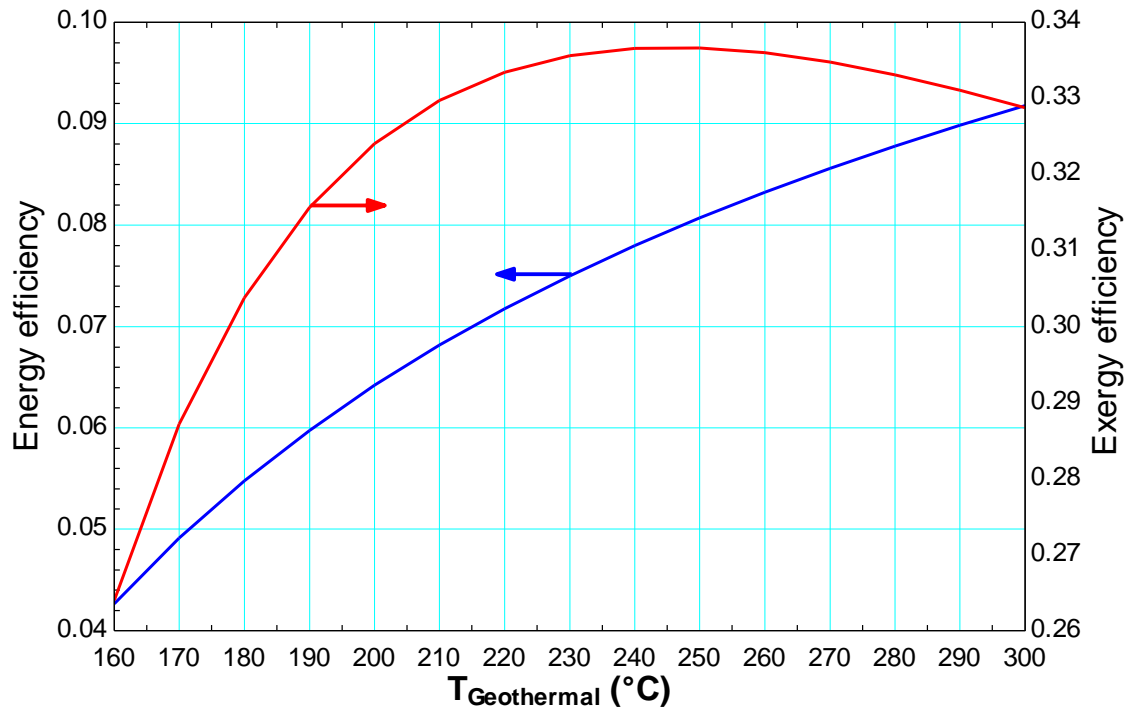


Figure 6.8. Variation of energy and exergy efficiencies with geothermal water temperature in Model 6.

We investigate the effect of geothermal water temperature on the exergetic costs of hydrogen production and liquefaction, and electricity, as shown in Figs. 6.9 through 6.14. As the geothermal water temperature increases exergetic costs of both electricity and hydrogen decrease. This trend can be explained due to the fact that both energy and the exergy efficiencies of geothermal power plant are higher at higher geothermal water temperatures. In another words, geothermal plant produces more power at higher resource temperatures for an available flow rate. This translates into a greater hydrogen production rate. According to the results of Model 1, Model 2, and Model 6, the unit exergetic cost of the hydrogen production is decreased by about 35% when geothermal water at 240°C is used instead of that at 200°C. Liquefaction cost also decreases with increasing geothermal temperatures. This is due to higher COP and exergy efficiency values in absorption cooling and liquefaction cycles at higher geothermal temperatures.

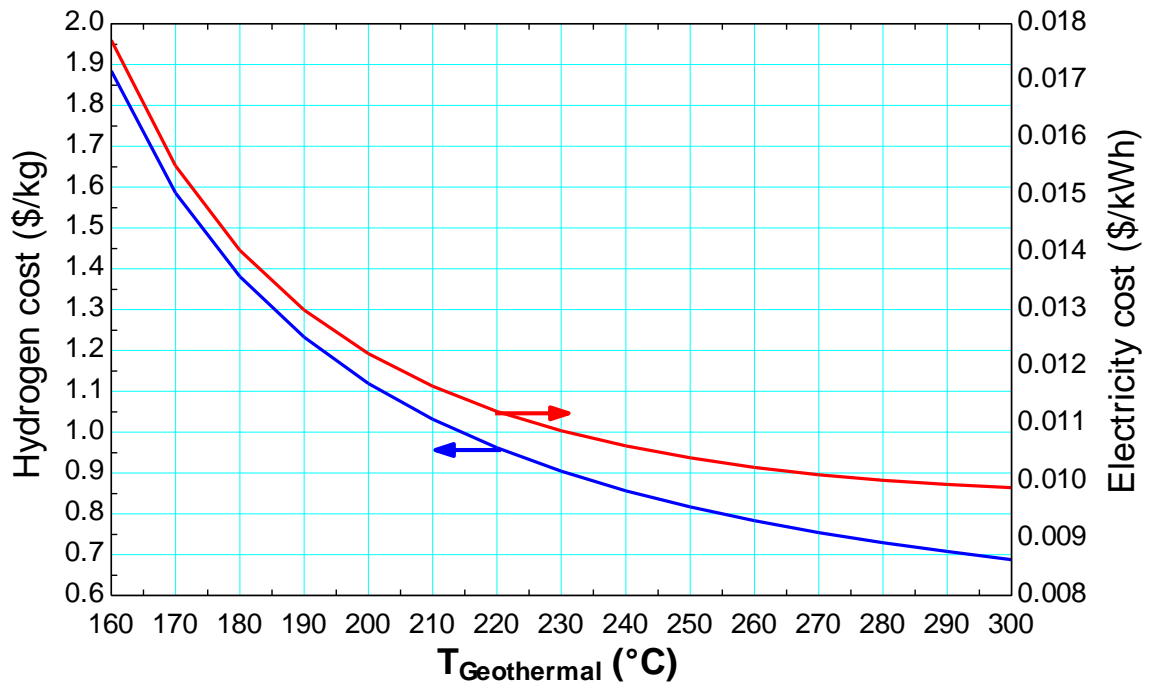


Figure 6.9. Variation of unit exergetic cost of hydrogen and electricity with respect to geothermal water temperature in Model 1.

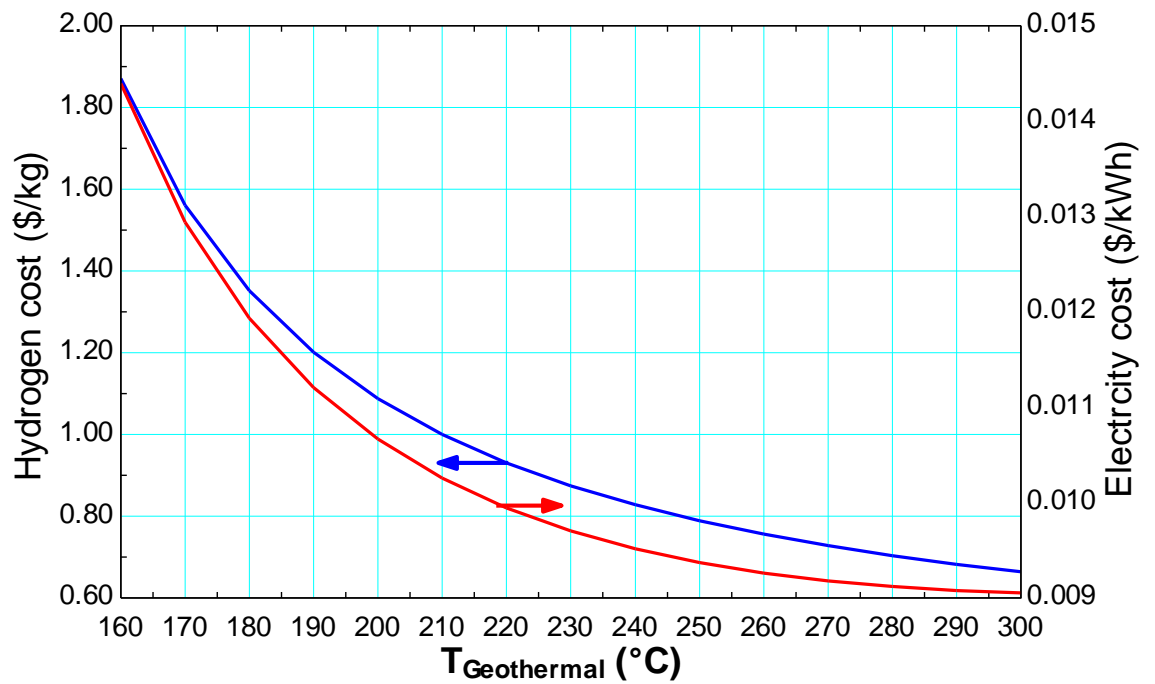


Figure 6.10. Variation of unit exergetic cost of hydrogen and electricity with respect to geothermal water temperature in Model 2.

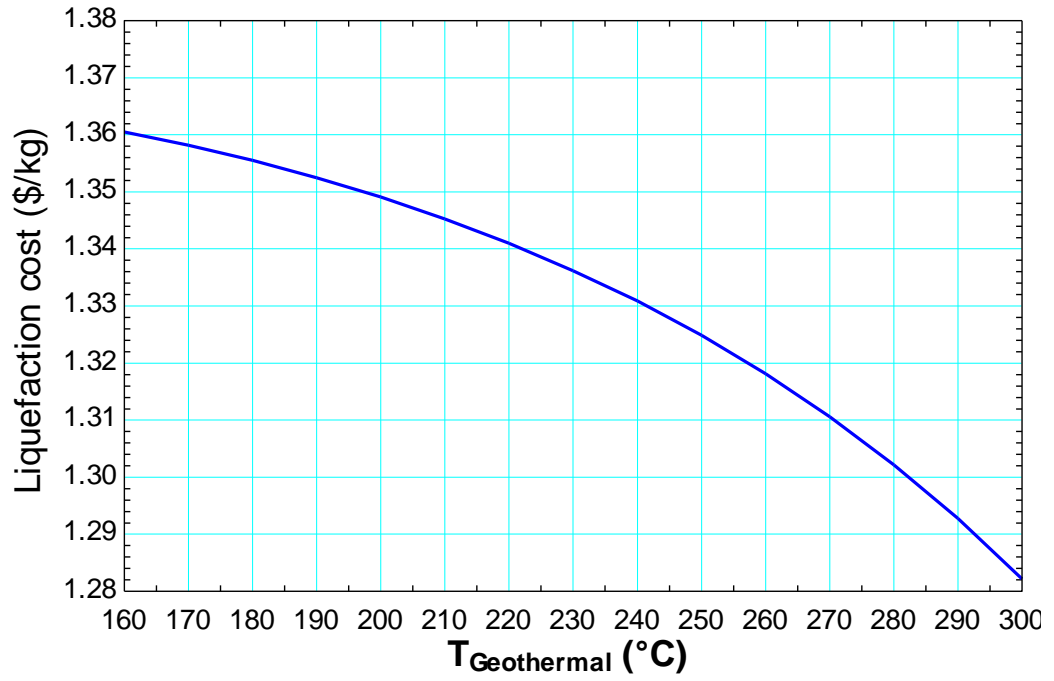


Figure 6.11. Variation of unit exergetic cost of hydrogen liquefaction with respect to geothermal water temperature in Model 3.

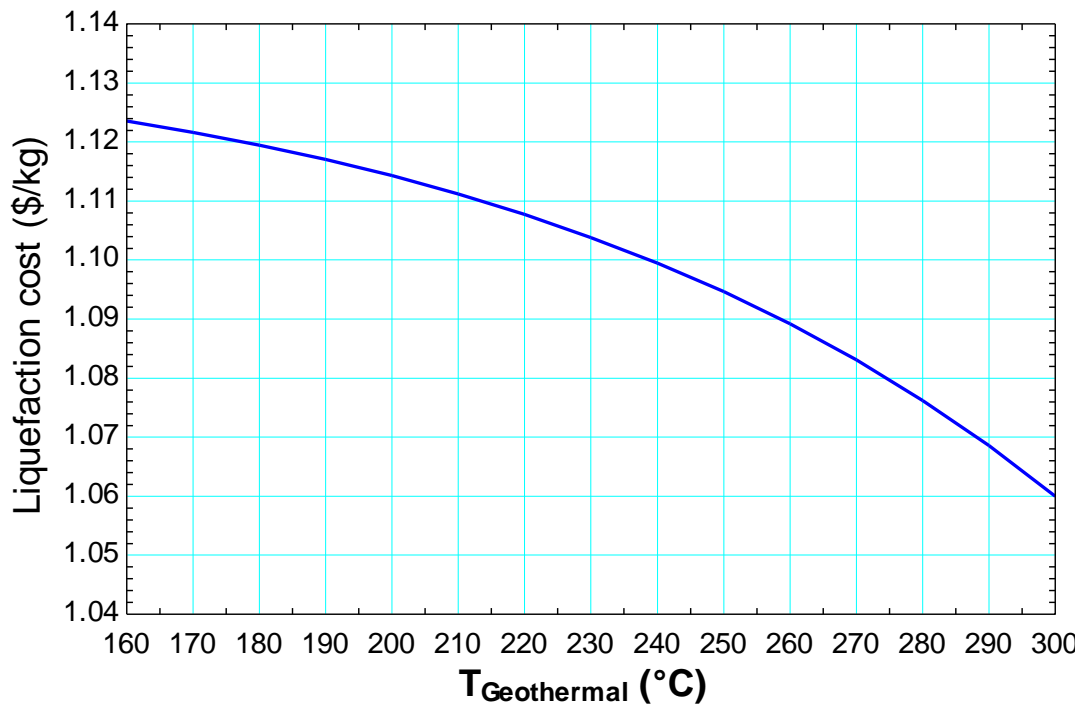


Figure 6.12. Variation of unit exergetic cost of hydrogen liquefaction with respect to geothermal water temperature in Model 4.

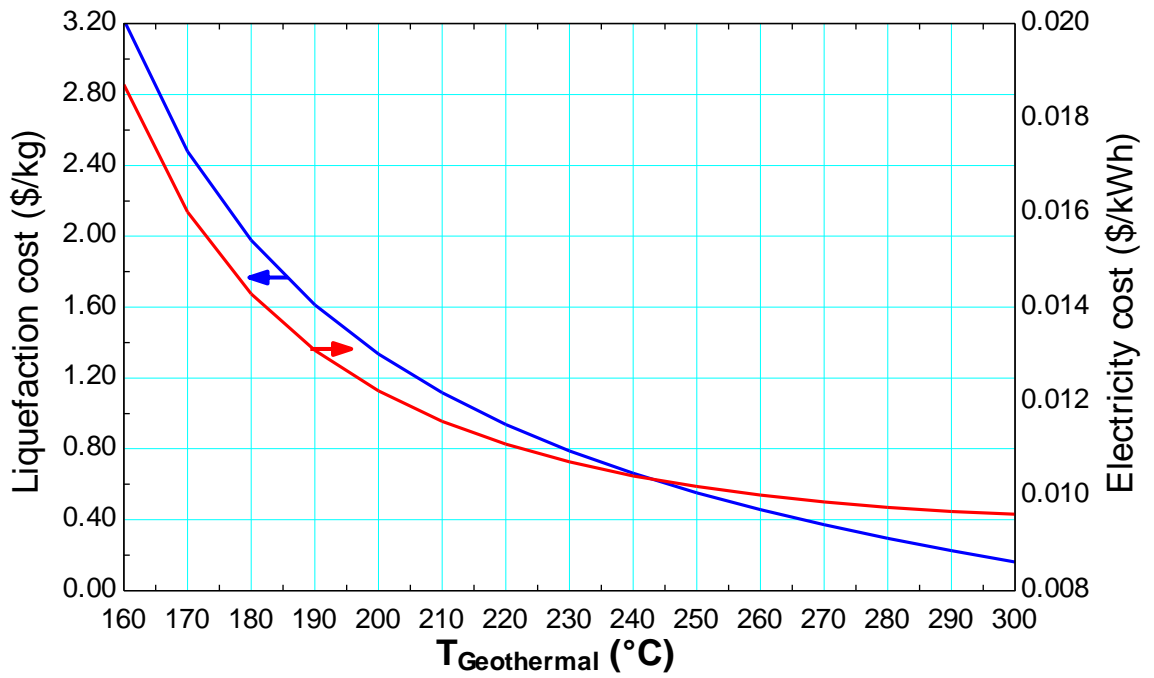


Figure 6.13. Variation of unit exergetic cost of electricity and hydrogen liquefaction with respect to geothermal water temperature in Model 5.

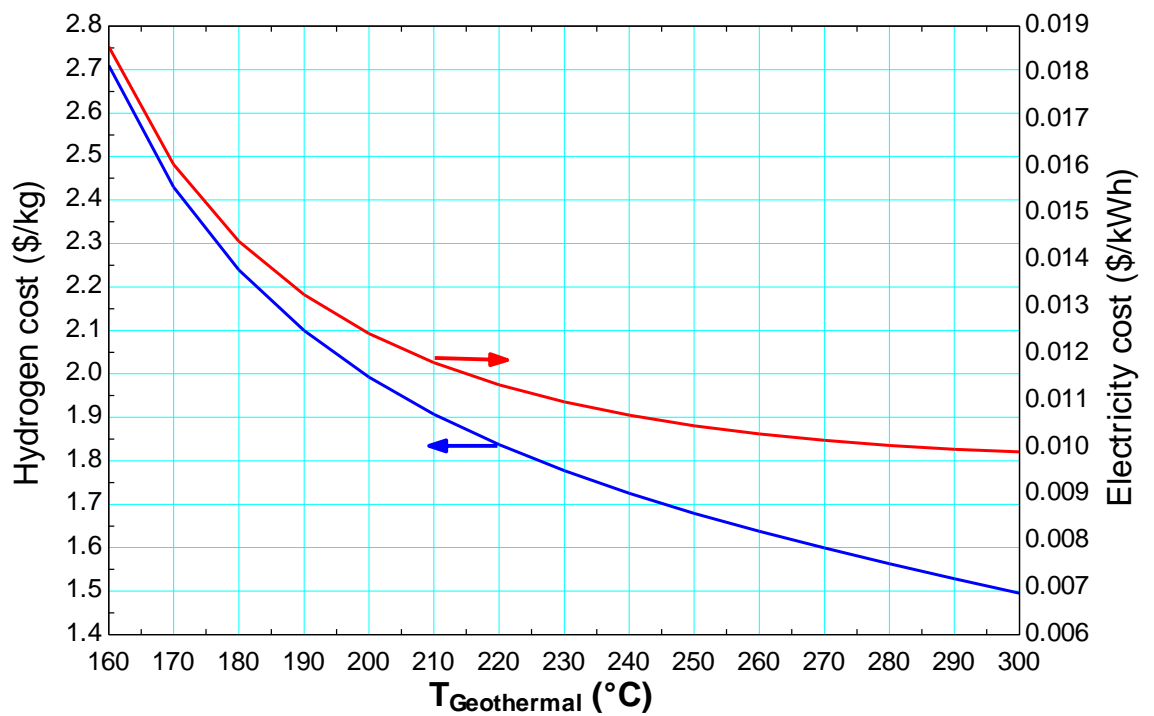


Figure 6.14. Variation of unit exergetic cost of hydrogen production and electricity with respect to geothermal water temperature in Model 6.

6.2 Results, Discussion, and Conclusions

In all models, we consider a geothermal resource at 200°C available at a rate of 100 kg/s. For the optimized Model 1, 8063 kW of net power is produced in the flash-binary geothermal power plant and 0.0514 kg/s hydrogen is produced in the electrolysis unit. Based on thermoeconomic optimization, the exergetic unit cost value of this produced hydrogen is calculated to be 1.119 \$/kg H₂ in Model 1. In Model 2, the rate of hydrogen production is 0.05278 kg/s, the power produced is 7992 kW, and the unit exergetic cost is 1.088 \$/kg H₂. As a result, the exergetic cost decreases by 2.8% in Model 2 with respect to Model 1. This decrease is due to using a preheater in Model 2.

In Model 3, the unit exergetic cost of hydrogen is 1.349 \$/kg H₂, but it decreases to 1.114 \$/kg H₂ in Model 4. This corresponds to a significant decrease of 17.4%. In Model 5, a flash binary geothermal power plant is used to produce power and this power is used for hydrogen liquefaction in Claude cycle. The unit exergetic cost of hydrogen liquefaction is calculated to be 1.335 \$/kg in Model 5 when hydrogen gas enters the Claude cycle at a room temperature of 25°C. This cost is 4.35% less than Model 3, and 16.5% higher than Model 4. Model 4 appears to be a more viable option when hydrogen liquefaction is desired.

Both production and liquefaction of hydrogen occur simultaneously in Model 6 where the unit exergetic cost of hydrogen is calculated to be 1.993 \$/kg H₂. Model 6 is more advantageous over other models when hydrogen needs to be produced and liquefied. In some applications, hydrogen production is sufficient and there is no need for liquefaction. In such cases, Model 1 and Model 2 should be considered. As a result of precooling of hydrogen gas, Model 4 is more appropriate when hydrogen needs liquefaction only.

Figure 6.15 shows the effect of geothermal water temperature on the exergetic unit cost of all six models. Except in Model 3, as the geothermal temperature increases the hydrogen cost decreases. This is due to higher thermodynamic performance at higher source temperatures. It turns out that geothermal source temperature is an important

parameter in the geothermal powered hydrogen production and liquefaction models and these systems have a higher application potential at higher geothermal temperatures.

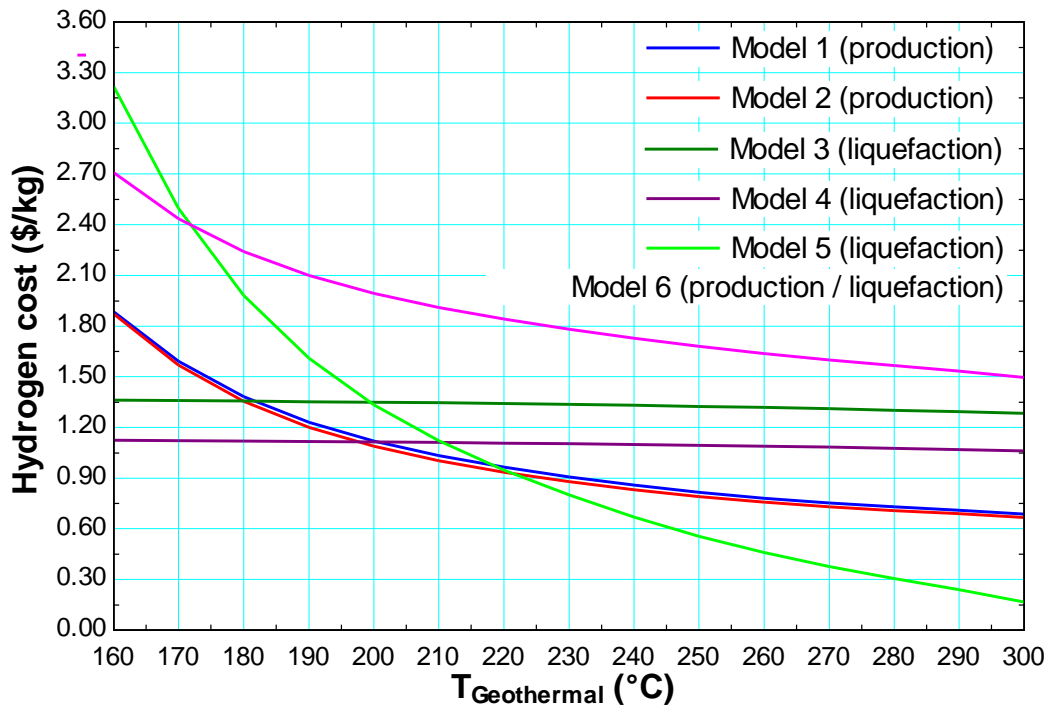


Figure 6.15. Variation of unit exergetic cost of hydrogen with geothermal water temperature in all models.

For the models considered, total investment cost, electricity cost, and unit exergetic cost of hydrogen are given in Table 6.1. Investment costs in hydrogen liquefaction models are higher compared to those in hydrogen production models. The total investment costs in Model 6 are \$61,392,397 and that in Model 4 are \$51,995,294, as compared to \$44,149,581 in Model 1 and \$45,015,379 in Model 2. Note that there are more equipments in hydrogen liquefaction models.

Table 6.1. Total investment costs and exergetic costs.

Model	Electricity work (kWh/kg H ₂)	Total cost of investment (TCI) (\$)	Unit exergetic cost of hydrogen (\$/kg H ₂)
1	43.50	44,149,581	1.119
2	42.20	45,015,379	1.088
3	10.22	48,658,120	1.349
4	10.06	51,995,294	1.114
5	15.08	42,358,129	1.335
6	15.08	61,392,397	1.993

6.3 Validation

Geothermal powered hydrogen production and liquefaction models that we considered in this study are analyzed from a thermoeconomic point of view. There has been no small or full scale application yet. Therefore, we will refer to literature for related studies.

Energy efficiency of the models for overall system is calculated between 6.7 and 8.9%, and exergy efficiency is calculated between 23.8 and 50%. It is reported for an ocean thermal energy conversion system coupled with PEM electrolysis that energy and exergy efficiencies are 3.6% and 22.7% respectively, and the exergy efficiency of the PEM electrolyzer is 56.5% [81].

Hydrogen can be produced at a rate of 0.0398, 0.0514, and 0.0527 kg/s using geothermal power in our hydrogen production models. In a study of PEM electrolyzer, hydrogen was produced at a rate of 5.4×10^{-6} kg/s at 6000 A/m² and 70°C under 876 W

of applied electrical power [82]. This system would produce hydrogen at a rate of 0.0235 kg/s if it used electricity at a rate of 7572 kW.

As part of the investigation, we studied the effect of electrolysis temperature on the energy and exergy efficiencies of the electrolysis process. Both efficiencies increase with electrolysis temperature. At a temperature of 70°C, the energy and exergy efficiencies are calculated to be 75.0% and 77.5%, respectively. In an experimental study conducted at the Industrial Engineering School of the University of Extremadura, Badajoz, Spain, exergy efficiency of the electrolyzer was obtained to be 68.8% while photovoltaic modules supplying electricity to the electrolyzer only had an exergy efficiency of 8.4% [83].

The COP of the liquefaction process is determined to be 0.2769 for Model 6, 0.4081 for Model 3, 0.4235 for Model 4, and 0.055 for Model 5. The exergy efficiencies are calculated to be 88.3% for Model 6, 69.4% for Model 3, 56.4% for Model 4, and 85.9% for Model 5 using the fuel-product approach. In a previous study [84], an absorption cooling technology was considered for a solar driven system. The COP of the system was calculated to be 0.57 for a generator temperature of 82°C. The COP value varied between 0.5 and 0.7 for generator temperatures of 82 to 122°C. Another study of ammonia water absorption refrigeration system gave a COP of 0.47 at a generator temperature of 121°C [85]. A solar driven absorption system operated at a COP of around 0.5 for a generator efficiency of 120°C. The discrepancy between theoretical model and experimental results were within 10% [86]. Thermodynamic results of an ammonia water absorption system at an evaporator temperature of -10°C with the heat exchangers and pumps having the same effectiveness and efficiencies show that the two stage system is more efficient, with a COP of 0.734 against 0.598 for the single stage system [87]. It appears that performance results of absorption refrigeration system of our model are in agreement with the results of similar systems.

Shimko [88] produced a pilot-scale liquefaction plant that demonstrates the ability to meet or exceed the efficiency targets. They modeled by scaling to larger plant sizes (50,000 kg/day). They originally proposed to use a modified Claude Cycle with the

Joule-Thompson Expansion Cycle. The second law efficiency of the first pilot plant of hydrogen liquefaction was calculated to be 22.1%. Ideal and actual work inputs of the pilot plant were calculated to be 3.89 and 17.6 kWh/kg H₂, respectively. These values are close to the ideal and actual work values obtained in our study (3.08 kWh/kg H₂ for ideal and 15.08 kWh/kg H₂ for actual liquefaction cycle).

Matsuda et al. [89] developed a large scale hydrogen liquefaction plant with high process efficiency. The Claude cycle was used. The liquefaction capacity of 300 t/day for one plant was estimated to be suitable and the target process efficiency was set to be more than 40% of the maximum efficiency. The feed gas was compressed to approximately 5 MPa, and then cooled down to -193°C in the cycle. The work input was determined to be 29.6 kWh/kg H₂ corresponding to a plant process efficiency of 46.4%. A higher efficiency in this plant was due to large capacity of liquefaction.

Stolzenburg et al. [90] developed the IDEALHY project for an efficient and cost-effective process for future large-scale plants. They showed that in a much improved process the specific electricity consumption would decrease from the current levels of 11 to 15 kWh/kg H₂ to about 6.4 kWh/kg H₂. Stang et al. [91] modeled a hydrogen liquefaction prototype laboratory unit. The work input was calculated to be 11.54 kWh/kg H₂. Staats et al. [92] analyzed numerically a supercritical hydrogen liquefaction cycle. Exergy efficiencies of 39 to 44% were predicted for the proposed cycle.

New geothermal plants generate electricity from \$0.03/kWh to \$0.07/kWh. Once capital costs for the plant are recovered, the price of power can go below \$0.05/kWh. In a theoretical study, the cost of producing a unit amount of electricity was calculated to be 0.0116 \$/kWh for double flash and Kalina cycles, 0.0165 \$/kWh for combined cycle and 0.0202 \$/kWh for binary cycle [93]. The levelized cost of electricity is calculated to be about 0.01223 \$/kWh in our study.

The unit average exergetic costs of hydrogen produced in the models are calculated to be 1.119 \$/kg, 1.088 \$/kg and 1.296 \$/kg in Model 1, Model 2, and 6, respectively. According to the study given in Ref. [94], every kg of hydrogen energy will cost around

\$0.8 when produced from natural gas, \$1.46 from coal, and \$2.85 from electrolysis of water. When grid electricity is used in a water electrolysis process, the unit hydrogen production cost is estimated to be between 2.0 and 3.5 \$/kg H₂. The base hydrogen cost ranges between 3.74 and 5.86 \$/kg H₂ when wind electricity is used in the electrolysis process [95]. It is estimated that high volume untaxed cost of hydrogen production from polymer electrolyte membrane (PEM) electrolysis ranges from 4.0 to 5.80 \$/kg H₂ [96].

The unit exergetic costs of hydrogen liquefaction models are calculated to be 1.349 \$/kg for Model 3, 1.114 \$/kg for Model 4, 1.335 \$/kg for Model 5 and 1.993\$/kg for Model 6. Syed et al. [97] presented an economic analysis of three hydrogen liquefaction systems with an associated cost comparison. The liquefaction cost was shown to reach a value of 0.63 \$/kg for the optimized large-scale type plant at a production rate of 30,000 kg/h when the cost of electricity was 0.04 \$/kWh. NREL et al. [98] presented an economic production and delivery cost of hydrogen. In industrial applications, hydrogen liquefaction cost varied between 2 \$/kg H₂ to 5 \$/kg H₂ depending on liquefaction plant capacities.

REFERENCES

- [1] Kanoglu, M., and Yilmaz, C. (2013). Thermal Design of Alkaline Water Electrolysis Assisted by Combined Flash Binary Geothermal Power Plant. In *ASME 2013 International Mechanical Engineering Congress and Exposition*. American Society of Mechanical Engineers. doi:10.1115/IMECE2013-62671.
- [2] Lund, H., and Mathiesen, B.V. (2009). Energy system analysis of 100% renewable energy systems. The case of Denmark in years 2030 and 2050. *Energy*, 34(5):524–531.
- [3] Midilli, A., and Dincer, I. (2007). Key strategies of hydrogen energy systems for sustainability. *International Journal of Hydrogen Energy*, 32:511–524.
- [4] Yilanci, A., Dincer, I., and Ozturk, H.K. (2009). A review on solar-hydrogen/fuel cell hybrid energy systems for stationary applications. *Progress in Energy and Combustion Science*, 35(3):231–244.
- [5] Berry, G.D., Pasternak, A.D., Rambach, G.D., Smith, J.R., Schocks, R.N. (1996). Hydrogen as a future transportation fuel. *Energy*, Vol. 21, No. 4, pp. 289-303.
- [6] Cohce, M.K., Dincer, I., Rosen, M.A. (2010). Thermodynamic analysis of hydrogen production from biomass gasification. *International Journal of Hydrogen Energy*, 35(10):4970–4980.
- [7] Momirlan, M., and Veziroglu, T.N. (2005). The properties of hydrogen as fuel tomorrow in sustainable energy system for a cleaner planet. *International Journal of Hydrogen Energy*, 30:795–802.
- [8] Lipman, T. E. (2004). *What Will Power the Hydrogen Economy?: Present and Future Sources of Hydrogen Energy* (No. UCD-ITS-RR-04-10). Institute of Transportation Studies, University of California, Davis.
- [9] Kanoglu, M., Bolatturk, A., and Yilmaz, C. (2010). Thermodynamic analysis of models used in hydrogen production by geothermal energy. *International Journal of Hydrogen Energy*, 35:8783-8791.
- [10] Bozoglan, E., Midilli, A., and Hepbasli, A. (2012). Sustainable assessment of solar hydrogen production techniques. *Energy*, 46:85-93.
- [11] Shapiro, D., Duffy, J., Kimble, M., and Pien, M. (2005). Solar-powered

- regenerative PEM electrolyzer/fuel cell system. *Solar Energy*, 79:544–550.
- [12] Grigoriev, S.A., Poremsky, V.I., and Fateev, V.N. (2006). Pure hydrogen production by PEM electrolysis for hydrogen energy. *International Journal of Hydrogen Energy*, 31:171–175.
- [13] Selamet, Ö. F., Becerikli, F., Mat, M. D., and Kaplan, Y. (2011). Development and testing of a highly efficient proton exchange membrane (PEM) electrolyzer stack. *International Journal of hydrogen energy*, 36(17), 11480-11487.
- [14] Hashimoto, A., Hashizaki, K., and Shimizu, K. (2002, June). Development of PEM water electrolysis type hydrogen production system for WE-NET. In *Proceedings of the 14th World Hydrogen Energy Conference on CD*.
- [15] <http://www.hpath.org>
- [16] Mirabal, S.T. (2003). *An Economic Analysis of Hydrogen Production Technologies Using Renewable Energy Resources* (Doctoral dissertation, University of Florida).
- [17] Kanoglu, M., Ayanoglu, A., and Abusoglu, A. (2011). Exergoeconomic assessment of a geothermal assisted high temperature steam electrolysis system. *Energy*, 36(7), 4422-4433.
- [18] Ahmadi, P., Dincer, I., and Rosen, M. A. (2013). Energy and exergy analyses of hydrogen production via solar-boosted ocean thermal energy conversion and PEM electrolysis. *International Journal of Hydrogen Energy*, 38(4), 1795-1805.
- [19] Esmaili, P., Dincer, I., and Naterer, G. F. (2012). Energy and exergy analyses of electrolytic hydrogen production with molybdenum-oxo catalysts. *International journal of hydrogen energy*, 37(9), 7365-7372.
- [20] Kanoglu, M., Dincer, I., and Cengel, Y. A. (2008). Investigation of geothermal energy use in gas liquefaction. *Heat Transfer Engineering*, 29(10), 885-892.
- [21] Kanoglu, M., Bolatturk, A., & Yilmaz, C. (2010). Thermodynamic analysis of models used in hydrogen production by geothermal energy. *International journal of hydrogen energy*, 35(16), 8783-8791.
- [22] Yilmaz, C. (2011). Thermodynamic and economic analysis of geothermal energy use in hydrogen production and liquefaction. *M.Sc. Thesis, University of Gaziantep, Turkey*.
- [23] Yilmaz, C., Kanoglu, M., Bolatturk, A., and Gadalla, M. (2012). Economics of hydrogen production and liquefaction by geothermal energy. *International journal*

of hydrogen energy, 37(2), 2058-2069.

- [24] Yilmaz, C., and Kanoglu, M. (2014). Thermodynamic evaluation of geothermal energy powered hydrogen production by PEM water electrolysis. *Energy*, 69, 592-602.
- [25] Balta, M. T., Dincer, I., and Hepbasli, A. (2010). Potential methods for geothermal-based hydrogen production. *International journal of hydrogen energy*, 35(10), 4949-4961.
- [26] Balta, M. T., Dincer, I., and Hepbasli, A. (2009). Thermodynamic assessment of geothermal energy use in hydrogen production. *International Journal of Hydrogen Energy*, 34(7), 2925-2939.
- [27] Ratlamwala, T. A. H., and Dincer, I. (2012). Comparative efficiency assessment of novel multi-flash integrated geothermal systems for power and hydrogen production. *Applied Thermal Engineering*, 48, 359-366.
- [28] Hand, T. W. (2008). *Hydrogen production using geothermal energy*. ProQuest.
- [29] Valdimar, K.J., Gunnarsson, R.L., Árnason, B., and Sigfússon, T.I. (1992). The feasibility of using geothermal energy in hydrogen production. *Geothermics*, 21(5-6), 673-681.
- [30] Árnason, B., and Sigfússon, I.T. (2000). Iceland a future hydrogen economy. *International Journal of Hydrogen Energy*, 25, 389-394.
- [31] Sigurvinsson, J., Mansilla, C., Arnason, B., Bontemps, A., Maréchal, A., Sigfusson, T.I., and Werkoff, F. (2006). Heat transfer problems for the production of hydrogen from geothermal energy. *Energy conversion and management*, 47(20), 3543-3551.
- [32] Scott, D. S. (2008). *Smelling land: the hydrogen defense against climate catastrophe*. Queen's Printer Publishing.
- [33] Timmerhaus, K.D., and Flynn, T.M. (2013). *Cryogenic process engineering*. Springer Science & Business Media.
- [34] Babadagli, A. (2005). Absorbsiyonlu Soğutma Sistemlerinin Termoeconomik Optimizasyonu, M.Sc., Thesis In Suleyman Demirel University, Isparta.
- [35] Brasz, J.J., Biederman, B.P., and Holdmann, G. (2005). Power production from a moderate-temperature geothermal resource. *GRC Trans*, 29, 729-733.

- [36] Kairouani, L. and Nehdi, E. (2006). Cooling performance and energy saving of a compression–absorption refrigeration system assisted by geothermal energy. *Applied Thermal Engineering*, 26(2) 288-294.
- [37] Adewusi, S.A., and Zubair, S.M. (2004). Second law based thermodynamic analysis of ammonia–water absorption systems, *Energy Conversion and Management*, 45(15), 2355-2369.
- [38] Best, R., Heard, C.L., Fernandez, H., and Siqueiros, J. (1986). Developments in geothermal energy in Mexico Part five: The commissioning of an ammonia/water absorption cooler operating on low enthalpy geothermal energy. *Journal of heat recovery systems*, 6(3) 209-216.
- [39] Nandi, T.K. and Sarangi, S. (1993). Performance and Optimization of Hydrogen Liquefaction Cycles, *International Journal of Hydrogen Energy*, 18, 131-139.
- [40] Staats, W.L. (2008). *Analysis of a supercritical hydrogen liquefaction cycle*. (Doctoral dissertation, Massachusetts Institute of Technology).
- [41] Krasae-in, S. Stang, J.H. and Petter, N.P. (2010). Development of large-scale hydrogen liquefaction processes from 1898 to 2009. *International Journal of Hydrogen Energy*, 35, 4524–4533.
- [42] Nandi, T.K. and Sarangi, S. (1991). Studies on production and storage of liquid, Ph.D., disseretation, Cryogenic Eneering Centre, IIT, Kharagpur.
- [43] Syed, M.T., Sherif, S.A., Veziroglu, T.N., and Sheffield, J.W. (2001). Second law analysis of hydrogen liquefiers operating on the modified Collins cycle. *Internal Journal of Energy Resources*, 25 (11) 961–978.
- [44] Berstad, D. O., Stang, J. H., & Neksa, P. (2009). Comparison criteria for large-scale hydrogen liquefaction processes. *international journal of hydrogen energy*, 34(3), 1560-1568.
- [45] Kanoglu, M., and Bolatturk, A., (2008) Performance and parametric investigation of a binary geothermal power plant by exergy. *Renewable Energy*, 33:2366–2374.
- [46] DiPippo, R., and Marcille, D.F. (1984). Exergy analysis of geothermal power plants. *Geothermal Resources Council Transactions*, 8:47-52.
- [47] Ganjehsarabi, H., Gungor, A., and Dincer, I. (2012). Exergetic performance analysis of Dora II geothermal power plant in Turkey. *Energy*, 46(1):101-108.
- [48] Cengel, Y.A., and Boles, M.A. (2011). *Thermodynamics: an engineering approach* (Vol. 7). M. Kanoğlu (Ed.). New York: McGraw-Hill.

- [49] Kanoglu, M. (2002). Exergy analysis of a dual-level binary geothermal power plant. *Geothermics*, 31:709–724.
- [50] Kanoglu, M., Dincer, I., and Rosen, M.A. (2007). Understanding energy and exergy efficiencies for improved energy management in power plants. *Energy Policy*, 35:3967–3978.
- [51] Kanoglu, M. and Cengel, Y.A. (1999). Improving the performance of an existing binary geothermal power plant: a case study. *Trans ASME, Journal Energy Resoucer Technology*, 121(3):196–202.
- [52] Ni, M., Leung, M.K.H., Leung, D.Y.C., and Sumathy, K. (2007). A review and recent developments in photocatalytic water splitting using TiO₂ for hydrogen production. *Renewable Sustainable Energy Reviews*, 11(3):401–425.
- [53] Chase, M.W. (1998). NIST-JANAF thermochemical tables. Fourth edition. American Chemical Society; *American Institute of Physics for the National Institute of Standards and Technology*.
- [54] LeRoy, R.L., and Bowen, C.T. (1980). The thermodynamics of aqueous water electrolysis. *Journal of Electrochemical Society*, 1954–1962.
- [55] Onda, K., Kyakuno, T., Hattori, K., and Ito, K. (2004). Prediction of production power for high pressure hydrogen by high-pressure water electrolysis. *Journal of Power Sources*, 132:64-70.
- [56] Poling, B. E., Prausnitz, J. M., and O'connell, J. P. (2001). *The properties of gases and liquids* (Vol. 5). New York: McGraw-Hill.
- [57] Kotas, T. J. (2013). *The exergy method of thermal plant analysis*. Elsevier.
- [58] Ni, M., Leung, M.K.H., and Leung, D.Y.C. (2008). Energy and exergy analysis of hydrogen production by a proton exchange membrane (PEM) electrolyzer plant. *Energy Conversion and Management*, 49:2748–2756.
- [59] Blasi, A.D., Andaloro, L., Siracusano, S., Briguglio, N., Brunaccini, G., Stassi, A., Arico, A.S., and Antonucci, A. (2013). Evaluation of materials and components degradation of a PEM electrolyzer for marine applications. *International Journal of Hydrogen Energy*, 38:7612-7615.
- [60] Caravaca, A., Sapountzi, F.M., Lucas-Consuegra, A., Molina-Mora, C., Dorado, F., Valverde, J.L. (2012). Electrochemical reforming of ethanolewater solutions for pure H₂ production in a PEM electrolysis cell. *International Journal of Hydrogen Energy*, 37:9504-9513.

- [61] Caldero'n, M., Caldero'n, A.J., Ramiro, A., Gonza'lez, J.Z., and Gonza'lez, I. (2011). Evaluation of a hybrid photovoltaic-wind system with hydrogen storage performance using exergy analysis. *International Journal of Hydrogen Energy*, 36:5751-62.
- [62] Dincer, I., and Kanoglu, M. (2010). *Refrigeration Systems and Applications*. 2nd. Ed., Wiley: June 14.
- [63] Timmerhaus, K.D., and Flynn, T.M. (1989). *Cryogenic process engineering*. The international cryogenic monographs series. New York: Plenum Press, USA.
- [64] Barron, R.F. (1985). *Cryogenic Systems*. Published by Oxford University Press, USA.
- [65] Auh, P.C. (1977). *A survey of absorption cooling technology in solar Applications*. Msc. Thesis, Department of Applied Science, Brookhaven National Laboratory, Upton, New York, October.
- [66] Clerx, M., and Trezck, G.J. (1987). Performance of an aqua-ammonia absorption solar refrigerator. *Solar Energy*, 39:379–388.
- [67] Lazzaretto, A., and Tsatsaronis, G., (1997). On the quest for objective equations in exergy costing, *In Proceedings of the ASME Advanced Energy Systems Division*, 37; 197-209.
- [68] Aspen Plus. Version 8.4 (2014). Aspen Technology Incorporated., Ten Canal Park, Cambridge, MA, USA. www.aspentech.com.
- [69] EES, Engineering Equations Solver - F-Chart Software, (2015). Box 44042, Madison, WI, USA. www.fchart.com.
- [70] Tsatsaronis, G., and Pisa, J. (1994). Exergoeconomic evaluation and optimization of energy systems – Application to the CGAM problem, *Energy*, 19; 287-321.
- [71] Lazzaretto, A., and Tsatsaronis, G. (2001). Comparison Between SPECO-Based and Functional Exergoeconomic Approaches, *In Proceedings of the ASME International Mechanical Engineering Congress and Exposition* in New York, 1-16.
- [72] Reini, M., Lazzaretto, A., and Macor, A. (1995). Average structural and marginal costs as a result of a unified formulation of the thermoeconomic problem, *In Proceedings of Second Law Analysis of Energy Systems: Towards the 21st Century*, Rome.

- [73] Bejan, A., Tsatsaronis, G., and Moran, M. J. (1996). *Thermal design and optimization*. John Wiley & Sons.
- [74] Tsatsaronis, G. and Moran, M.J. (1997). Exergy-aided cost minimization, *Energy Conversion and Management*, 38;1535-1542.
- [75] Tsatsaronis, G., and Czesla, F. (2002). Thermoeconomics, *Encyclopedia of Physical Science and Technology*, 3rd Edition, 16: 659-680.
- [76] Lazzaretto, A., and Tsatsaronis, G. (2006). SPECO: A systematic and general methodology for calculating efficiencies and costs in thermal systems. *Energy*, 31: 1257-1289.
- [77] Holladay, J.D., Hu, J., King, D. L., and Wang, Y. (2009). An overview of hydrogen production technologies. *Catalysis Today*, 139(4):244-260.
- [78] Ghaffarizadeh, A. (2006). Investigation on evolutionary algorithms emphasizing mass extinction. *Shiraz University of Technology, Shiraz, Iran*.
- [79] Charbonneau, P. (2002). Release notes for PIKAIA 1.2. NCAR technical note 451+STR. Boulder: National Center for Atmospheric Research.
- [80] Toffolo, A., and Lazzaretto, A. (2002). Evolutionary algorithms for multi-objective energetic and economic optimization in thermal system design, *Energy*, 27;549-567.
- [81] Chase, M.W. (1998). NIST-JANAF thermochemical tables. fourth ed. American Chemical Society; American Institute of Physics for the National Institute of Standards and Technology.
- [82] LeRoy, R.L., and Bowen, C.T. (1980). The thermodynamics of aqueous water electrolysis. *Journal of Electrochemical Society*, 127(9):1954–6192.
- [83] Onda, K., Kyakuno, T., Hattori, K., and Ito, K. (2004). Prediction of production power for high pressure hydrogen by high-pressure water electrolysis. *Journal of Power Sources*, 132(1):64-70.
- [84] Prausnitz, M., and O'Connell, J.P. (2004). *The properties of gases and liquids*. Fifth Edition, The McGraw-Hill Companies.
- [85] Blasi, A.D., Andaloro, L., Siracusano, S., Briguglio, N., Brunaccini, G., Stassi, A., Arico, A.S., and Antonucci, A. (2013). Evaluation of materials and components degradation of a PEM electrolyzer for marine applications. *International Journal of Hydrogen Energy*, 38(18):7612-15.

- [86] Caravaca, A., Sapountzi, F. M., de Lucas-Consuegra, A., Molina-Mora, C., Dorado, F., and Valverde, J. L. (2012). Electrochemical reforming of ethanol–water solutions for pure H₂ production in a PEM electrolysis cell. *international journal of hydrogen energy*, 37(12), 9504-9513.
- [87] Calderon, M., Calderon, A. J., Ramiro, A., Gonzalez, J. F., and Gonzalez, I. (2011). Evaluation of a hybrid photovoltaic-wind system with hydrogen storage performance using exergy analysis. *International journal of hydrogen energy*, 36(10), 5751-5762.
- [88] M.A. Shimko, Gas Equipment Engineering Corp., 1240 Oronoque Road Milford, CT 06460, Phone: (203) 874-6786; Fax: (203) 878-4123, E-mail: mas@gasequip.com DOE Technology Development Manager: Monterey R. Gardiner Phone: (202) 586-1758; Fax: (202) 586-9811 E-mail: Monterey.Gardiner@ee.doe.gov
- [89] Matsuda, H., and Nagami, M. (1997). Study of large hydrogen liquefaction process. *수소에너지*, 8(3), 175-175.
- [90] Seemann, I., Haberstroh, C., and Quack, H. (2013). Efficient Large Scale Hydrogen Liquefaction. In *European fuel cell forum*.
- [91] Stang, J., Neksa, P., and Brendeng, E. (2006). On the design of an efficient hydrogen liquefaction process.
- [92] Staats, W.L. (2008). *Analysis of a supercritical hydrogen liquefaction cycle* (Doctoral dissertation, Massachusetts Institute of Technology).
- [93] Coskun, A., Bolatturk, A., and Kanoglu, M. (2014). Thermodynamic and economic analysis and optimization of power cycles for a medium temperature geothermal resource. *Energy Conversion and Management*, 78, 39-49.
- [94] Millet, P., Mbemba, N., Grigoriev, S. A., Fateev, V. N., Aukauloo, A., and Etiévant, C. (2011). Electrochemical performances of PEM water electrolysis cells and perspectives. *International Journal of Hydrogen Energy*, 36(6), 4134-4142.
- [95] Saur, G., and Ainscough, C. (2011). US Geographic Analysis of the Cost of Hydrogen from Electrolysis. *Contract*, 303, 275-3000.
- [96] Bossel, U. (2006). Does a hydrogen economy make sense?. *Proceedings of the IEEE*, 94(10), 1826-1837.

- [97] Syed, M. T., Sherif, S. A., Veziroglu, T. N., and Sheffield, J. W. (1998). An economic analysis of three hydrogen liquefaction systems. *International Journal of Hydrogen Energy*, 23(7), 565-576.
- [98] Melaina, M. W., and Penev, M. (2013). *Hydrogen Station Cost Estimates: Comparing Hydrogen Station Cost Calculator Results with other Recent Estimates*.

BIOGRAPHICAL SKETCH

PERSONAL INFORMATION

Name: Ceyhun Yılmaz
Birth place and date: Kocaeli, 1987
Phone: +90342 317 2574
Fax: +90342 3601104
Email: ceyhunyilmaz@gantep.edu.tr

EDUCATION

M.Sc. Gaziantep University, Mechanical Engineering, 2011
B.S., Gaziantep University, Mechanical Engineering, 2009

WORK EXPERIENCE

2010-Present, Research Assistant, Gaziantep University

PROJECTS

1. TÜBİTAK, 113M207. “Jeotermal Enerjinin Hidrojen Üretimi ve Sıvılaştırılmasında Kullanımının Termoekonomik Analizi, Optimizasyonu ve Yaşam Döngü Maliyet Analizi”, 2013- 2015. Graduate student staff.
2. TÜBİTAK, 108M226. “Jeotermal Enerjinin Hidrojen Üretimi ve Sıvılaştırılmasında Kullanımının Termodinamik ve Ekonomik Analizi”, 2008-2010. Graduate student staff.

MEMBERSHIPS IN SCIENTIFIC ASSOCIATIONS

Türk Isı Bilimi ve Tekniği Derneği

REVIEWER FOR JOURNALS

International Journal of Exergy

PUBLICATIONS

International Journal Papers (SCI)

1. Yilmaz C, Kanoglu M, Abusoglu A. “Exergetic Cost Evaluation of Hydrogen Production Powered by Combined Flash-Binary Geothermal Power Plant” *International Journal of Hydrogen Energy*,40, 14021-14030 (2015).
2. Yilmaz C, Kanoglu M, Abusoglu A. “Thermoeconomic Cost Evaluation of Hydrogen Production Driven by Binary Geothermal Power Plant” *Geothermics* 57, 18–25 (2015).
3. Yilmaz C, Kanoglu M. “Thermodynamic evaluation of geothermal energy powered hydrogen production by PEM water electrolysis” *Energy* 69, 592-602 (2014).
4. Yilmaz C, Kanoglu M, Bolatturk A, Gadalla M. “Economics of hydrogen production and liquefaction by geothermal energy” *International Journal of Hydrogen Energy* 37(2), 2058-2069 (2012).
5. Kanoglu M, Bolatturk A, Yilmaz C. “Thermodynamic Analysis of Models Used In Hydrogen Production By Geothermal Energy” *International Journal of Hydrogen Energy* 35, 8783-8791 (2010).

Under Review

Kanoglu M, Yilmaz C, Abusoglu A. “Thermoeconomic Optimization of Hydrogen Liquefaction System Powered by Geothermal Energy” *Journal Of Thermal Science And Technology*, (Article No: 2015_o25, **Under Review**) (2015).

Kanoglu M, Yilmaz C, Abusoglu A. “Geothermal Energy Use in Absorption Precooling for Claude Hydrogen Liquefaction Cycle” *Renewable Energy*, (RENE-S-15-01895, **Under Review**) (2015).

Other International Journal Papers

1. Yilmaz C, Kanoglu M, Abusoglu A. “Geothermal Energy Use in Hydrogen Production” *Journal of Thermal Engineering* (Article in press) (2015)
2. Yilmaz C, Kanoglu M, Abusoglu A. “Thermodynamic And Thermoeconomic Analyses Of Hydrogen Liquefaction Cycle Assisted By Geothermal Energy” *Strojarsstvo Journal* (Article in press) (2015).

International Conference Papers

1. Yilmaz C, Kanoglu M, “Thermodynamic and Economic Investigation of Geothermal Powered Absorption Cooling System for Buildings” The 8th Mediterranean Congress of Heating Ventilation and Air-Conditioning (Climamed 2015), 9-11 September 2015, Paris, France.
2. Yilmaz C, Kanoglu M, Abusoglu A, “Thermoeconomic Optimization of

- Hydrogen Production by a Flash-Binary Geothermal Power Plant” International Conference on Advanced Technology & Sciences (ICAT'15), 4-7 August 2015, Antalya, Turkey.
3. Yilmaz C, Kanoglu M, Abusoglu A, “Geothermal Energy Use in Hydrogen Production” International Conference on Advances in Mechanical Engineering (ICAME-2015). İstanbul, Turkey.
 4. Yilmaz C, Kanoglu M, Abusoglu A, “Thermoeconomic Optimization of Hydrogen Production and Liquefaction by Geothermal Power” 7th International Exergy, Energy and Environment Symposium (IEEES'7-2015), UVHC, ENSIAME, Valenciennes, France (April 27-30, 2015).
 5. Yilmaz C, Kanoglu M, Abusoglu A, “Thermoeconomic Assessment of a Geothermal Powered Hydrogen Gas Liquefaction System”, Energy Technologies Conference ENTECH'14, 22-24 December 2014, Istanbul, Turkey.
 6. Yilmaz C, Kanoglu M, Abusoglu A, “Thermoeconomic Assessment of a Geothermal Powered Hydrogen Production System”, 2nd International Congress on Energy Efficiency and Energy Related Materials (ENEFM2014), October 16-19, 2014, Oludeniz, Turkey.
 7. Yilmaz C, Kanoglu M, Abusoglu A, “Jeotermal Güç Kullanan Bir Alkali Elektroliz Ünitesinden Hidrojen Üretiminin Termodinamik Analizi”, 11th International HVAC+R Technology Symposium, Proceedings: p. 231-239, May 8-10, 2014, Istanbul, Turkey.
 8. Yilmaz C, Kanoglu M, Abusoglu A, “Thermoeconomic Cost Evaluation of Hydrogen Production Driven by Binary Geothermal Power Plant”, The Second International Conference on Sustainable Systems and the Environment (ISSE 2014), February 12-13, 2014, American University of Sharjah, Sharjah, UAE.
 9. Kanoglu M, Yilmaz C, “Thermal Design of Alkaline Water Electrolysis Assisted by Combined Flash Binary Geothermal Power Plant”, Proceedings of the ASME, 2013 International Mechanical Engineering Congress & Exposition (IMECE 2013), November 13-21, 2013, San Diego, California, USA.
 10. Yilmaz C, Kanoglu M, “Thermodynamic Performance Analysis of Hydrogen Production by PEM Water Electrolysis Powered by Geothermal Energy”, The 2nd International Conference on Water, Energy and the Environment, Sep. 21-24, 2013, Kusadasi, Turkey.
 11. Yilmaz C, Demir S, Abusoglu A, “A Comparison of Exergoeconomic Methodologies for a Binary Geothermal Power Plant” Global Conference on Global Warming-2012 (GCGW-12), 8-12 July 2012, İstanbul, Turkey.
 12. Yilmaz C, Kanoglu M, “Energy and exergy analysis of hydrogen production by PEM water electrolysis powered by geothermal energy”, 6th International Ege Energy Symposium & Exhibition, IESE-12, June 28-30, 2012, Izmir, Turkey.
 13. Kanoglu M., Yilmaz C., Bolatturk A. “Economics of Hydrogen Production and Liquefaction by Geothermal Energy”, 10th International Conference on Clean Energy (ICCE-2010), September 15-17, 2010, Famagusta, N. Cyprus.
 14. Kanoglu M., Yilmaz C., Bolatturk A. “Thermodynamic Analysis of Models Used in Hydrogen Production by Geothermal Energy”, 5th International Ege Energy Symposium and Exhibition (IEESE-5), June 27-30, 2010, Denizli/Turkey.
 15. Kanoglu M., Yilmaz C., Bolatturk A. “Hydrogen Production and Liquefaction by

Geothermal Heat and Power”, International Conference on Hydrogen Production With Emphasis on Storage and Safety - ICH2P 2010, June 16 -18, Istanbul Technical University, Istanbul, Turkey.

National Journal Papers

1. Yilmaz C, Kanoglu M, Abusoglu A. "Jeotermal Destekli Amonyak Su Absorpsiyonlu Soğutma Sisteminin Bilgisayar Ortamında Modellenmesi", TTMD, Cilt 90, Mart-Nisan, 27-33 (2015)

National Conference Papers

1. Yilmaz C, Kanoglu M, Abusoglu A, Jeotermal Enerji ile Hidrojen Sıvılaştırma Sisteminin Termodinamik Analiz ve Optimizasyonu, 20. Ulusal Isı Bilimi Ve Tekniği Kongresi, 2-5 Eylül 2015 (ULIBTK'15), Balıkesir.
2. Yilmaz C, Kanoglu M, Abusoglu A, Jeotermal Destekli Hidrojen Sıvılaştırma Çevriminin Termodinamik Ve Termodinamik Analizi, 12. Ulusal Tesisat Mühendisliği Kongresi Ve Sodex, 8-11 Nisan 2015, İzmir.
3. Yilmaz C, Kanoglu M, Abusoglu A, Jeotermal Destekli Amonyak Su Absorpsiyonlu Soğutma Sisteminin Bilgisayar Ortamında Modellenmesi, 2. Ulusal İklimlendirme Soğutma Eğitimi Sempozyumu ve Sergisi, 23-25 Ekim 2014, Balıkesir.
4. Yilmaz C, Kanoglu M, Bolatturk A, Jeotermal Enerji ile Hidrojen Üretilmesi ve Sıvılaştırılması, Tesisat Kongresi TESKON 2011, 13-16 Nisan, 2011, İzmir.